TAMPEREEN TEKNILLINEN YLIOPISTO
TAMPERE UNIVERSITY OF TECHNOLOGY

Emmi Kantola

Development of High-Power VECSELs for Medical Applications

Julkaisu 1604 • Publication 1604

Tampere 2018

Tampereen teknillinen yliopisto. Julkaisu 1604
Tampere University of Technology. Publication 1604

Emmi Kantola

Development of High-Power VECSELs for Medical Applications

Thesis for the degree of Doctor of Science in Technology to be presented with due permission for public examination and criticism in Sähkötalo Building, Auditorium SA203, at Tampere University of Technology, on the 30th of November 2018, at 12 noon.

Tampereen teknillinen yliopisto - Tampere University of Technology
Tampere 2018

Doctoral candidate: Emmi Kantola, MPhys (Hons)
Optoelectronics Research Centre
Faculty of Natural Sciences
Tampere University of Technology
Finland

Supervisor: Mircea Guina, Prof.
Optoelectronics Research Centre
Faculty of Natural Sciences
Tampere University of Technology
Finland

Instructors: Mircea Guina, Prof.
Optoelectronics Research Centre
Faculty of Natural Sciences
Tampere University of Technology
Finland

2012–2016
Tomi Leinonen, D.Sc. (Tech.)
Optoelectronics Research Centre
Faculty of Natural Sciences
Tampere University of Technology
Finland

Pre-examiners: Vanderlei Bagnato, Prof.
São Carlos Institute of Physics
University of São Paulo
Brazil

Adrian Podoleanu, Prof.
School of Physical Sciences, Biomedical Optics
University of Kent
United Kingdom

Ronald Sroka, PD Dr.
Laser-Research-Laboratory (LFL) / LIFE-Center
Hospital of University of Munich
Germany

Opponent: Stefan Andersson-Engels, Prof.
Biophotonics
Tyndall National Institute
University College Cork
Ireland

ISBN 978-952-15-4270-1 (printed)
ISBN 978-952-15-4302-9 (PDF)
ISSN 1459-2045

Abstract

Vertical-external-cavity surface-emitting lasers (VECSELs) are versatile lasers sources that have become particularly appealing for different applications due to the unique features they can offer. They combine the wide wavelength coverage of semiconductor laser technology with the good beam quality and power scalability of solid-state thin-disk lasers. The external cavity architectures also allow for efficient frequency conversion from infrared to visible and UV wavelengths. In this way, VECSELs can provide high-power emission with good beam quality at the most challenging wavelengths, such as the yellow spectral region. Moreover, one of their major benefits is the compact design, which is particularly important for applications.

Potential applications for VECSELs are manifold and include fields such as medicine, astronomy and quantum optics research. This thesis is concerned with the medical applications, and particularly focuses on dermatologic applications requiring yellow lasers. The yellow spectral range is challenging for any laser technology, which is why not that many yellow lasers exist on the laser market. The first main objective of this thesis was to demonstrate frequency converted yellow-orange-red VECSELs in laboratory set-ups. This was followed by the development of a fully functional yellow laser based on VECSEL-technology and designed for medical use. Finally, the work was focused on performing a clinical trial designed to test the feasibility of VECSEL-technology in a dermatologic medical application.

As a result of this thesis work, we have demonstrated record high output powers from laboratory-based VECSELs: 20 W at 585 nm, 10 W at 615 nm and 72 W at 1180 nm. Moreover, the performed clinical trial showed that the developed yellow VECSEL system is at least as good as the traditionally used laser in the treatment of vascular lesions (specifically telangiectasia) in terms of the treatment efficacy. In addition, the treatment times were significantly shorter with the VECSEL system than with the traditional laser thanks to the fast scanning of the light application device.

With further improvements arising from the full exploitation of the laser’s power reserve, the system has the potential to be a breakthrough in the treatment of vascular-related skin conditions.

Acknowledgements

The work presented in this thesis was carried out at the Optoelectronics Research Centre (ORC), Tampere University of Technology (TUT) during the years 2012–2018. It was supported by the Finnish Funding Agency for Technology and Innovation (TEKES), Academy of Finland, TUT Rector's graduate school, Jenny and Antti Wihuri Foundation, Walter Ahlström Foundation, Finnish Foundation for Technology Promotion (TES) and Ulla Tuominen Foundation. Particularly, I would like to acknowledge TEKES FiDiPro project PhotoLase (#40152/14, with support funding provided by Modulight Oy, Nanofoot Oy, and Brighterwave Oy) for enabling to perform the first clinical trials with the lasers developed in ORC.

There have been few moments in my life in which I have considered myself the luckiest person alive, and starting my thesis work at ORC is one of them. A very special thanks goes to my supervisor Prof. Mircea Guina, whom I can still remember telling me in our first meeting how it will take three years to complete my thesis. Finally, after six years, I get to express my deepest admiration towards your work enthusiasm, efficiency, (gardening) and all the efforts you made to enable the completion of this thesis. I would also like to thank Dr. Tomi Leinonen who was also my supervisor from 2012–2016. The wisdom you shared (especially about coffee, which I still do not drink) was priceless, and thank you for letting me learn from the best.

An important part of this work was enabled by Dr. Antti Rantamäki, whom designed and built the yellow VECSEL system for the clinical trials. Your work was invaluable and I hope I get another chance to work with such a nice and talented person. Thank you also to Iiro Leino for designing the electronics and software to the yellow laser. It is to the merit of both of you that the system worked reliably throughout the clinical trials. Thank you also to Prof. Serge Mordon and his team at INSERM for helping to design the system and the clinical trials. I would also like to express my

sincere gratitude towards dermatologists Ari Karppinen and Toni Karppinen, who spend hours and hours of their own time in order to prepare, perform and analyse the clinical trials.

I am grateful to be part of the ORC community and want to thank the whole staff. In particular, I wish to thank Jussi-Pekka Penttinen and Dr. Ville-Markus Korpijärvi. Jussi-Pekka, I admire your dedication, (joke-telling) skills and entrepreneur-attitude that enable you to achieve any goals you set to yourself (eventually even that Dr. title); and Ville-Markus, I admire your hard-working attitude, comradery, (beard) and humour. It is due to these traits that you both also became very dear people to me. Thank you Dr. Antti Härkönen; you were always eager to help me in the lab and share your knowledge. Thank you also to Dr. Sanna Ranta and Miki Tavast for your excellent work with the MBE that enabled me to achieve the record-breaking output powers. Big thanks also to the supportive staff of ORC for all their help. I also acknowledge the solar cell team who always brightened up my day with their (somewhat) good jokes and stories.

Finally, I would like to thank my family and friends: especially my parents, my sister, Ringa and Helena, Glenn, Elli, Emmi, Lassi and Ella. You have supported me and shared your advices for more than just these six years (pains me to admit it but we are approaching three full decades with most of you). I cherish you all.

Tampere, November 2018
Emmi Kantola

Contents

List of Publications

The following publications are included in this thesis as appendices. In the text they are referred to as [P1]–[P5].

[P1] E. Kantola, T. Leinonen, S. Ranta, M. Tavast, and M. Guina, “High-efficiency 20 W yellow VECSEL,” *Optics Express*, vol. 22, no. 6, p. 6372–6380, 2014.

[P2] E. Kantola, T. Leinonen, J.-P. Penttinen, V.-M. Korpijärvi, and M. Guina, “615 nm GaInNAs VECSEL with output power above 10 W,” *Optics Express*, vol. 23, no. 16, p. 20280–20287, 2015.

[P3] E. Kantola, J.-P. Penttinen, S. Ranta, and M. Guina, “72-W VECSEL emitting at 1180 nm for laser guide star adaptive optics,” *Electronics Letters*, vol. 54, no. 19, p. 1135–1137, 2018.

[P4] E. Kantola, A. Rantamäki, I. Leino, J.-P. Penttinen, T. Karppinen, S. Mordon, and M. Guina, “VECSEL-based 590-nm laser system with 8 W of output power for the treatment of vascular lesions,” *Journal of Selected Topics in Quantum Electronics*, vol. 25, no. 1, 2019.

[P5] T. Karppinen, E. Kantola, A. Karppinen, A. Rantamäki, H. Kautiainen, S. Mordon, and M. Guina, “Treatment of telangiectasia on the cheeks with a compact yellow (585 nm) semiconductor laser and a green (532 nm) KTP laser: a randomized double-blinded split-face trial,” submitted to *Lasers in Medicine and Surgery* on 12.9.2018.

Author’s Contribution

[P1] The author designed and built the experimental setup for frequency doubling. She also carried out all the measurements and the analysis of the data. The paper was mainly written by the author. The gain mirror was designed, grown and processed by Tomi Leinonen and Miki Tavast. Sanna Ranta characterized the gain mirror in fundamental emission. Mircea Guina planned the experiments and coordinated the manuscript writing process.

[P2] The author designed the experimental setup for frequency doubling. The measurements were carried out together with Tomi Leinonen. The data was analysed by the author who was also the main writer of the paper. The gain mirror was processed by Jussi-Pekka Penttinen and grown by Ville-Markus Korpijärvi. Mircea Guina planned the experiments, participated in designing and development of the gain mirror, and coordinated the manuscript writing process.

[P3] The author designed and built the experimental setup and wrote most of the paper. Bonding of the heat spreader and gain mirror was done together with Jussi-Pekka Penttinen, who also processed the gain mirror. The structure was grown by Sanna Ranta. Mircea Guina coordinated the experiments and the manuscript writing process.

[P4] The author designed and built the table-top frequency-doubled yellow VECSEL and investigated nonlinear crystals of various length and from different suppliers. In addition, she also prepared the technical documentations needed to get authorization to perform the clinical trials. The author was also the main writer of the paper. Antti Rantamäki designed and built the yellow VECSEL module inside the laser system. The gain mirror for the module was designed and grown by Jussi-Pekka Penttinen and Sanna Ranta, respectively. The custom electronics inside the laser system were designed and fabricated by Iiro Leino. The outer casing of the system was designed in collaboration with the French National Institute of Health and Medical Research (INSERM Onco-Thai). Mircea Guina coordinated the development of the system, devising the parameter range of the laser together with Serge Mordon, and the integration steps.

[P5] The author prepared and wrote the technical documents required to start the clinical trial. Dermatologists Ari Karppinen and Toni Karppinen performed the treatments in the trial. They also helped to design and write the clinical protocol. The paper was co-written with Toni Karppinen. Antti Rantamäki built the yellow laser system used in the trial. The author and Antti Rantamäki acted as technical support during the trial treatments. Mircea Guina coordinated the project and contributed to the writing of the manuscript.

List of Abbreviations and Symbols

Abbreviations

Al	Aluminium
AlAs	Aluminium-arsenide
AlGaInAs	Aluminium-gallium-indium-arsenide
AR	Anti-reflective
BBO	Beta-Barium Borate nonlinear crystal
CPM	Critical phase matching
CW	Continuous wave
DBR	Distributed Bragg Reflector
DFG	Difference Frequency Generation
EMC	Electromagnetic compatibility
FSR	Free spectral range, frequency spacing of longitudinal laser modes
FWHM	Full-width-at-half-maximum
Ga	Gallium
GaAs	Gallium-arsenide
HR	High reflective
In	Indium
InGaAs	Indium-gallium-arsenide
InP	Indium-phosphide
INSERM	French National Institute of Health and Medical Research

ISO	International Organization for Standardization
KTP	Potassium titanyl phosphate nonlinear crystal
KTP laser	Frequency-doubled green (532 nm) solid-state laser
LBO	Lithium triborate nonlinear crystal
LD	Laser diode
MBE	Molecular beam epitaxy
MDD	Medical Device Directive
MECSEL	Membrane external-cavity surface-emitting laser
MOVPE	Metalorganic vapour phase epitaxy
N	Nitrogen
NCPM	Non-critical phase matching
NLO	Nonlinear crystal/optics
OC	Output coupler
ORC	Optoelectronics Research Centre
p	P-value (probability for the hypothesis to be true)
PDL	Pulsed Dye Laser
PDT	Photodynamic therapy
QW	Quantum well
QPM	Quasi phase matching
RoC	Radius of curvature
SD	Standard deviation
SDL	Semiconductor Disk Laser
SESAM	Semiconductor saturable absorber mirror
SFG	Sun Frequency Generation
SHG	Second Harmonic Generation
SNLO	Software for frequency conversion calculations
TEC	Thermoelectric cooler
TEM_{00}	Transverse Electromagnetic Mode of the lowest order (Fundamental transverse mode with Gaussian energy distribution)
TGS	Telangiectasia grading scale
UV	Ultaviolet
VCSEL	Vertical-Cavity Surface-Emitting Laser
VECSEL	Vertical-External-Cavity Surface-Emitting Laser
YAG	Yttrium aluminium garnet crystalline

Symbols, Greek alphabet

4σ	ISO standard for beam diameter. Four-times the standard deviation of an intensity distribution is obtained. For Gaussian beams, gives the same value as $1/e^2$.
Δk	Phase mismatch between two light waves
θ	Angle between the optic axis and the propagation direction k
φ	Angle between the projection of the light propagation, k, on to the XY plane and the X-axis in crystal coordinates.
ω_i	Optical angular frequency of incident beam
η	single-pass conversion efficiency of a nonlinear crystal

Symbols, Other

D_2	The second D line in the yellow region of the spectrum of neutral sodium. The D lines are emitted by electron transitions from the 3p to the 3s levels of sodium.
d_{eff}	The effective nonlinear coefficient of a nonlinear crystal
e	Extraordinary polarisation
e-ray	extraordinary ray, light that is polarised in the principle plane
k	Light propagation direction in a crystal
o	Ordinary polarisation
o-ray	Ordinary ray, light that is polarised orthogonally to the principle plane
T	Temperature
Z	Optic axis of a nonlinear crystal

Chapter 1

Introduction

1.1 Background and motivation

Lasers have been an important tool for many research, medical and industry fields since the first Ruby laser was constructed by T. H. Maiman in 1960. During the last six decades, several laser technologies have emerged and developed providing solutions for a variety of problems. Currently, the most common laser type is an electrically pumped semiconductor laser, also known as a laser diode (LD). They have a small footprint, low power consumption and a broad wavelength coverage and can be found in many devices such as DVD players and laser printers. However, they suffer from poor beam quality due to the slit geometry of the output surface, which leads to a large beam divergence. Moreover, the output power from a single laser diode is typically limited to some hundreds of milliwatts, though several can be stacked to reach multi-watt operation at the expense of the output beam quality.

Other laser technologies also include solid state, dye/gas and fibre lasers. They all have their advantages and disadvantages. Fibre lasers are known for high-power and easy delivery of light through the fibre, but are limited in the range of wavelengths. In turn, solid state lasers are mature and reliable, but the wavelength coverage is strictly limited to the ion transitions of the lasing material; they are also bulkier and more complex than fibre lasers. Dye and gas lasers were one of the first type lasers (along with solid state) to arrive in the market providing high-power continuous wave or pulsed laser light, but in addition to being complex they are also restricted in the wavelength coverage due to ion transition.

Overall, all the different laser technologies can offer a “colourful spectrum” of features and effective solutions for applications but (ironically) there appears to be a common challenge: high-power, short-pulse or continuous wave operation is achievable, but often at the expense of the spectral properties such as the emission wavelength. This is particularly true at the visible wavelength

range, which also is relevant for many applications in biophotonics. Moreover, laser development in general has always been largely driven by applications. So far, lasers have vastly penetrated industry, medicine, scientific research, military and entertainment. With such large variety of applications, it is practically impossible to develop an all-purpose laser system, which is why customizability has become an important feature for lasers. Different applications set quite different requirements for the light source in terms of size, operation mode, power and spectral features. For example, quantum optics research relies on the availability of narrow linewidth, resonantly tuned lasers to interrogate or change the state of atoms. Whereas, high-power yellow lasers emitting light pulses in the millisecond order are needed in dermatology to treat certain skin diseases. **To this end, the work presented in this thesis focuses on developing a particular type of semiconductor laser, which could bridge the gaps in the emission wavelength coverage of lasers, provide customised solutions for a variety of applications, and even enable the emergence of new applications.**

This type of semiconductor lasers, called vertical-external-cavity surface-emitting lasers (VECSELs) or Semiconductor Disk Lasers (SDLs), are recognized for their power scaling abilities, excellent beam quality, compact footprint and customizable spectral features. They combine the most beneficial characteristics of standard semiconductor and solid-state lasers: wavelength tailoring through material engineering and functionality enabled by external cavity architectures. These features allow for a broad coverage of lasing wavelengths in the infrared and, via second harmonic generation in nonlinear crystals, in the visible and UV spectral ranges [1]. Table 1.1 presents how VECSELs compare to other laser technologies in terms of general properties such as emission wavelength, output power, operation scheme etc.

Table 1.1. *List of main type of lasers and their general properties*

Laser type	Gain medium	Wavelength coverage	Power level	Beam quality	Operation schemes	Size
Solid-state lasers	Crystals (Nd:YAG, Ruby)	Limited (ion transitions)	Peak power in kW range	Good-excellent	CW and pulsed (down to fs)	Complex and bulky.
Fibre lasers	Optical fibre (Erbium, Ytterbium)	Limited	Peak power up to kW range	Good-excellent	CW and pulsed	Compact to large
Gas lasers	Gas (CO_2, Excimer, Copper vapour, Argon-ion)	Limited	Peak power in kW range	Good-excellent	Operate in pulsed mode (ns...ms)	Complex and bulky
Dye lasers	Dye (Rhodamine, Fluorescein)	Relatively broad, but limited	Up to kW range	Poor-good	Typically pulsed (ns), also CW	Complex and bulky
Laser diodes	Semiconductor material	Broad	< 10 W from single diode. > 100 W from stacked diodes	Poor	CW and pulsed	Compact
VCSELS	Semiconductor material	Narrow (DBR limited)	1–10 mW	Excellent	CW and pulsed	Compact
VECSELS	Semiconductor material	Very broad (efficient SHG)	< 100 W	Good-excellent	CW and pulse operation from ms down to fs	Compact

The development of the VECSELs in this thesis was mainly driven by medical applications. In fact, lasers and medical applications have a long history: only a year after the first demonstration of laser light (1960), a ruby laser was used to treat retinal lesions in rabbits [2], and in the past years, lasers have become important tools in many areas of healthcare and life sciences. Figure 1.1 illustrates the power and wavelength needs of different medical and life science applications. Apart from laser surgery, many applications fall on the visible spectral range. There already exists practical techniques to produce blue, green and red laser light, but the yellow-orange spectral range has proven to be challenging due to material restrictions. The golden standard for current

medical treatments requiring a yellow light source is the pulsed dye laser (PDL, for instance Candela V-Beam), which is known for its long wavelength (585–590 nm), adjustable pulse duration and integrated skin cooling for patient comfort and selective skin damage. However, it also has major disadvantages such as high initial cost, large size and circular beam profile. In addition, PDL lasers require annual maintenance to change the dye even if the laser has not been used, which is an added cost. For this reason there is still a need for a more compact, cost-effective and tailored yellow laser, which in the long run could increase the availability of yellow laser treatments and lower their cost for patients. Moreover, the availability of yellow-orange lasers with tailored or tunable wavelengths could also spark new application avenues that have been undiscovered so far due to the lack of available wavelengths in practical systems. Currently, the main medical applications for yellow lasers include eye surgery, dermatology and cell imaging, and it has already been shown that overall results can be improved and damage to healthy tissue decreased if lasers with tailored specifications are employed [3, 4, 5].

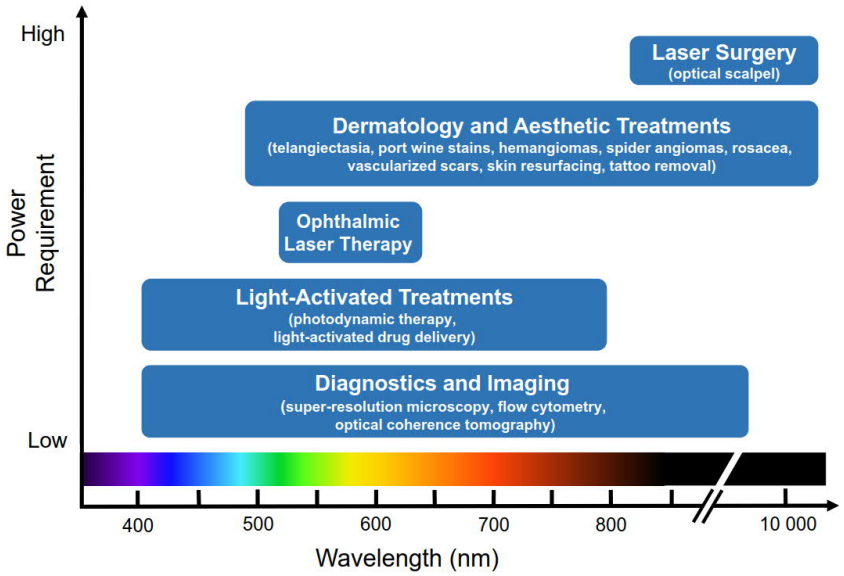

Figure 1.1. *Illustration of the laser wavelength and output power requirements for medical and other life science applications.*

In addition to medical applications, we also took into consideration other application areas that could benefit from high-power operation in the yellow-orange spectral region or from other visible and UV wavelengths that could be reach with similar frequency-doubling techniques as employed in this thesis to reach the yellow spectral range. For example, in astronomy, adaptive optics is often employed on earth-based telescopes to correct for the distortion of images caused by the

variations in the index of refraction of air. As part of the adaptive optics system, a reference object—a so-called guide star—is needed [6]. Unfortunately, there are not many naturally occurring guide stars in the sky, but one can be created artificially by exciting sodium atoms at ~80 km altitude with a yellow laser. The wavelength needs to match the sodium D_2 line and emit high-power radiation. In terms of laser specifications, this means over 20 W of continuous wave radiation at the challenging yellow wavelength of 589 nm with a narrow linewidth less than 250 MHz [7]. So far, these specifications have been matched only by expensive Raman fibre amplifier lasers employing single-frequency diode seed lasers [8].

Another field, which could benefit from tailored high-power VECSELs is quantum optics research. It has opened doors to ultra-fast computing, high bandwidth information transfer and other applications requiring precise knowledge of time or frequency. These developments rely on the manipulation of single quantum systems enabled by laser cooling of trapped atoms, first demonstrated by David Wineland in 1978 [9]. Furthermore, they could result in practical quantum optical devices such as atomic magnetometers, atomic clocks and, of course, a scalable quantum computer capable of solving problems not feasible for a classical computer [10, 11, 12]. These exciting developments depend on the availability of narrow-linewidth high-intensity lasers emitting at specific wavelengths in order to control quantum states. Narrow linewidth is essential, because the atoms need to be excited resonantly and the required wavelength is strictly determined by the atom in question. Quite often, the required wavelength is in the ultraviolet range, which can be achieved with VECSELs by first developing a visible laser and then frequency converting it to UV. In fact, this type of red VECSEL was used in manipulation of trapped magnesium ions by Burd et al. in 2016 [13].

1.2 Objectives

The general objective of the thesis was to develop VECSELs at challenging yellow-orange and red wavelengths where a high benefit could be expected in medical applications. This was achieved by first determining the prospective applications for yellow-orange lasers in medicine. Moreover, we also wanted to demonstrate the full development trajectory of a laser, from laboratory setup to a functional laser system, and perform a proof-of-concept clinical trial to validate the feasibility of using VECSELs in medical applications. The main objectives are listed in Table 1.2.

Table 1.2. *List of the main objectives of this thesis.*

1.	Identify prospective medical applications for yellow VECSELs.
2.	Develop high-power frequency-doubled VECSELs in research environment.
3.	Design and built a yellow VECSEL system for clinical use.
4.	Design and perform a clinical trial using the yellow VECSEL system in collaboration with local physicians.

1.3 Outline

This thesis is organised into six chapters. Chapter 2 introduces the prospective medical applications for VECSELs emitting yellow-orange radiation and generally explains the light-tissue interaction related to dermatologic treatments. Chapter 3 is devoted to presenting VECSEL technology including the operation principle and basic characteristics. This chapter will explain the benefits of the external cavity and the wavelength coverage enabled by material engineering. Particular emphasis is put on frequency-doubled VECSELs and on the choice of nonlinear crystal.

Chapter 4 reports the lasing features of the developed VECSELs and is divided into three sections, which present a high-power yellow, red and infrared VECSEL. These results correspond to publications P1, P2 and P3, respectively. This chapter also demonstrates a pulsing scheme for VECSELs, which is based on modulating the current of the pump laser. Chapter 5 discusses the needs for organizing a clinical trial for a research device. It will list all the mandatory preparations and documentations, as well as give an idea of the time schedule. Section 5.2 reports the technical specifications and other features of the developed yellow laser system. The end of chapter 5 is devoted to explaining the clinical protocol and the clinical results. It will include comments from the dermatologists on the usability and reliability of the yellow laser.

Chapter 6 concludes this thesis with a short summary of the laser results and the outcome of the clinical trial. The final words will give an outlook on the future of frequency converted VECSELs.

Chapter 2

Medical Applications for yellow lasers

This chapter reviews the basic laser-tissue interactions in section 2.1 and focuses on discussing the interaction most relevant for yellow lasers—*selective photothermolysis*—in section 2.2. Yellow lasers are mainly required by dermatology for the treatment of superficial blood vessels and thus the section 2.2 also identifies the ideal laser parameters for this treatment method. The chapter is concluded with a short review on the already existing commercial yellow lasers with their drawbacks that emphasise the need for more tailored lasers.

2.1 Basic concepts of laser-tissue interaction

The interaction of laser light with biological tissue is depended on the specific properties of the laser light and the targeted tissue. The main affecting properties of the laser light are wavelength, irradiance, power/energy and for pulsed irradiation pulse duration, energy per pulse and repetition rate. On the tissue side, these are the optical properties, heat transport and chemical composition, particularly the composition of the absorption molecules—so-called *chromophores*. The combination of these properties result in tissue specific reactions that are mainly based on the absorption of photons. To put it simply, when laser light enters tissue it is either absorbed or not. If it is not absorbed it can experience reflection, refraction, scattering, remission and/or transmission (as illustrated in Figure 2.1.), but these phenomena play less important roles in medical laser treatments based on the thermal effect (i.e. heat) induced by the absorption of photons [14, 15, 16]. Moreover, particular emphasis should be given to the wavelength of the

incident laser, because many of the optical properties of tissue (such as *absorption coefficient* and *scattering coefficient*) show wavelength dependence [17].

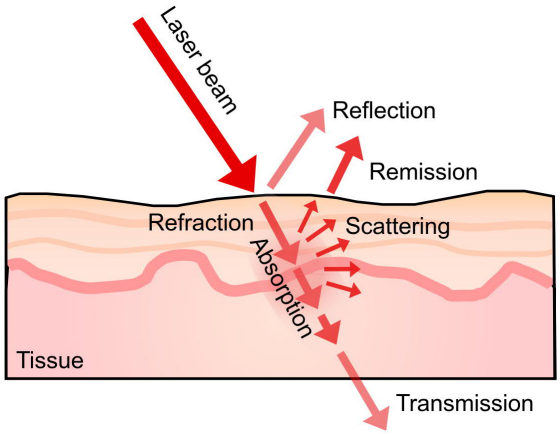

Figure 2.1. *Illustration of the phenomena that happen when light encounters biological tissue (or any media): reflection, remission, refraction, absorption, scattering, transmission.*

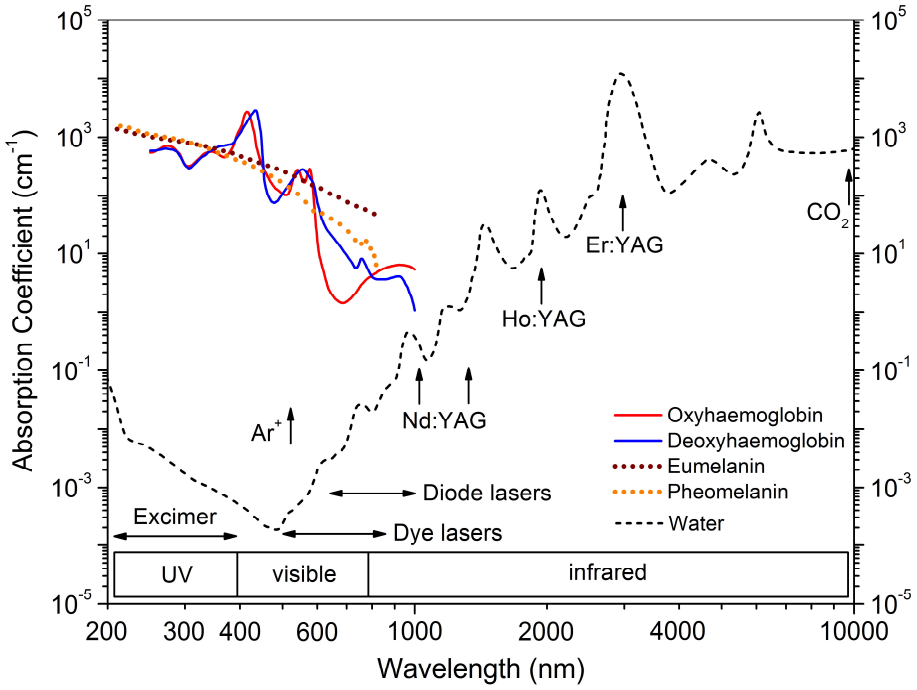

Figure 2.2. *Wavelength dependence of absorption coefficient for some of the main tissue components: water, melanin (14.26 mg/ml concentration) and haemoglobin. The figure was constructed using data from* [18, 19, 20].

The wavelength dependence of the absorption coefficients for some of the main tissue chromophores are given in Figure 2.2. The figure clearly shows water as the dominant absorber in the infrared range with the maximum water absorption at around 3 µm. In contrast, the visible spectral range from 400–800 nm is identified by minimal absorption by water and, instead, dominant absorption by melanin and two types of haemoglobin. Furthermore, if we also consider the wavelength dependence of the scattering coefficients of these chromophores we can estimate the wavelength dependent *optical penetration depth*. This estimation is based on the Beer-Lambert Law, which defines that the attenuation coefficient is a combination of the absorption and scattering coefficients. The optical penetration depth in tissue as a function of wavelength is presented in Figure 2.3. Although the spatial distribution of light induced heat is related to the optical penetration depth, there is also heat dissipation due to heat diffusion and heat transport by perfusion. The so-called *thermal heat reach* depends on the thermal conductivity of the tissue and the exposure time of the applied light. Table 2.1 lists some values of the thermal heat reach for typical exposure times. Thus the optical penetration depth and thermal heat reach define the spread of the laser induced tissue reaction. In case of short or pulsed laser exposure of the tissue the thermal reach is low compared to the optical penetration depth [21, 22, 23, 24].

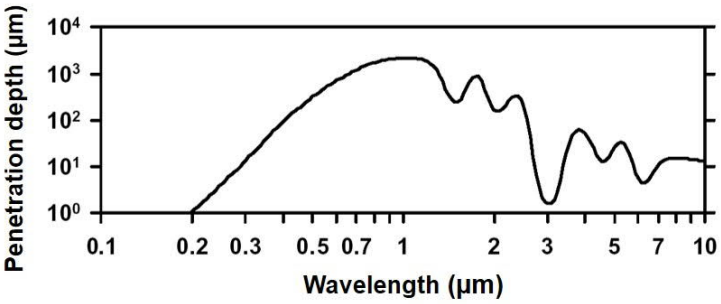

Figure 2.3. *Wavelength dependence of optical penetration depth in tissue. Courtesy of Dr. Ronald Sroka.*

Table 2.1. *Some values of thermal heat reach in tissue for certain exposure times. A mean thermal conductivity of 1.2 x 10^{-7} m^2/s was used.*

Exposure time	Thermal heat reach
10 s	2.3 mm
1 s	0.7 mm
1 ms	23 µm
1 µs	0.7 µm

2.1.1 Laser induced tissue reactions

The laser induced tissue reactions are plentiful, but can be divided into five main categories. These are *photochemical interactions*, *thermal interactions*, *photoablation*, *plasma-induced ablation* and *photodisruption*. The first three categories exhibit wavelength dependence and all, apart from the photochemical reactions, occur due to the absorbed laser light being transferred into heat. Figure 2.4 depicts how these reactions are related to the irradiance (y-axis) and the exposure time (x-axis) of the laser light. Following the diagonal drawn in the figure, we can see that the total energy density (fluence, J/cm^2) is within the same orders of magnitude for all the mechanisms. This indicates that the exposure time is the main defining parameter for a type of interaction [17]. Short definitions for each tissue reaction are provided in Table 2.3 along with their sub-types, some examples of clinical applications and typically used lasers. This thesis focuses on the thermal interactions and one particular sub-type of it, namely *coagulation*.

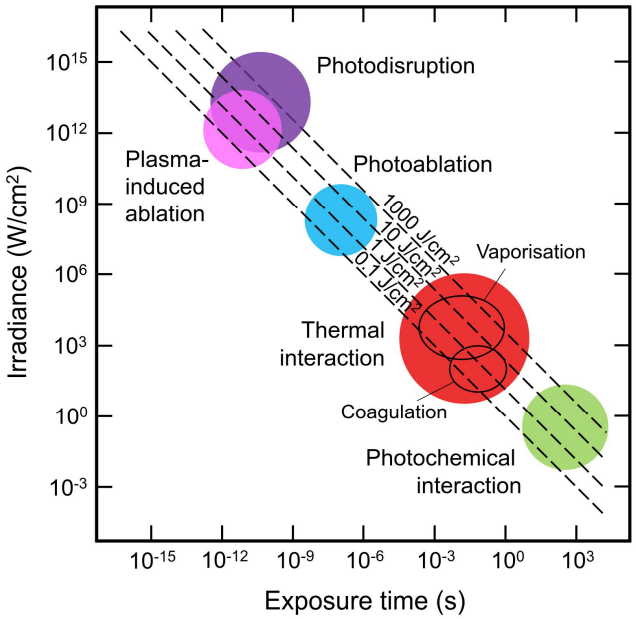

Figure 2.4. *Laser-tissue interaction map. The double-logarithmic graph shows irradiance on the y-axis and exposure time on the x-axis. The four diagonal lines represent lines of constant fluence. Each coloured circle represents a type of mechanism and gives a rough estimate of the associated laser parameters*. Adapted from [17] and [25].

Coagulation is defined as the denaturation of proteins, which occurs at temperatures around 60–65 °C. Optically the scattering coefficient increases thus more light is back-scattered from the tissue surface. Dependent on the surrounding chromophores, whitening or scattering induced colour change can be observed. The coagulation process is often used to occlude (close) vessel

structures during the laser treatment of vascular lesions (vascular = relating to blood vessels). In this case, the spread of the laser induced reaction correlates more with the thermal heat reach than with the optical penetration thickness due to the relative low penetration depth. Further increase of the temperature results in drying of the tissue as water starts to vaporise around 100 °C. This results in a reduction of the thermal conductivity of the tissue. Higher temperatures (150–300 °C) lead to burning and carbonisation. In this case the absorption coefficient increases and the tissue becomes black. All the light is then absorbed in this black area, hence there is no optical penetration, only heat diffusion into the tissue. At temperatures above 300 °C (can be reached by e.g. contact of fibre to the tissue) tissue is instantaneously vaporised and ablated. This process is useful for cutting tissue especially when bloodless incisions are of clinical interest. Furthermore, high-energy laser pulses can lead to plasma formation (e.g. ionisation), cavitation bubble induction and shockwaves which are used for destruction of hard tissue (e.g. kidney stone). The temperature induced reactions and their influence on the physical properties of tissue are listed in Table 2.2 [21, 22, 23, 24].

Table 2.2. *Temperature induced reactions in tissue.*

Temperature	Reaction	Optical/mechanical change
> 40 °C	Enzyme reaction, edema (swelling), membrane loosening	
45–65 °C	Tissue changes (reversible/irreversible depending on duration)	
> 65 °C	Coagulation, protein denaturation	Scattering coefficient increase
> 100 °C	Drying (water vaporisation)	Thermal conductivity decrease
> 150 °C	Carbonisation	Absorption coefficient increase
> 300 °C	Vaporisation, ablation, burn	Removal
1000 °C	Ionisation, plasma	Shockwave

As can be derived from Table 2.2, several of the described thermal reactions can be present in parallel and influence each other because of the induced changes in the physical properties of the tissue. However, in a specific application most often only one effect is wanted, which puts even more emphasis on the importance of choosing the right laser parameters. The next section

explains how coagulation is utilized in the dermatologic treatment concept called *selective photothermolysis*, and what is required from the laser source, particularly in terms of wavelength and pulse duration.

Table 2.3. *List of laser-tissue interaction mechanisms. Data for the table was collected from* [17] *and* [25]*, which also provide more detailed descriptions of the mechanisms.*

Photochemical		
Description	**Sub-types**	**Applications**
Light induces chemical reactions in tissue. Pulse duration: 1 s…CW Power density: 0.01–50 W/cm^2 Typical lasers: Red diode lasers, other visible lasers, also incoherent light sources	*Photodynamic therapy (PDT)*: administered photosensitizers (chromophores that cause light-induced reactions) are excited with light, inducing a reaction that creates reactive oxygen species or singlet oxygen which themselves induce cell death via different pathways. *Biomodulation*: energy of absorbed photons may affect cellular metabolism by inducing stimulative or inhibitive effects. Though, these effects are still under investigation.	Cancer treatment, wound healing, acupuncture
Thermal		
Description	**Sub-types**	**Applications**
Absorbed light generates heat. The temperature increase causes different effects on tissue depending on the duration and achieved peak temperature. Pulse duration: 1 µs…1 min Power density: 10–10^6 W/cm^2 Typical lasers: Visible and IR lasers (KTP, Argon, PDL, diode lasers, CO_2, Nd:YAG, Er:YAG)	Coagulation: tissue that reaches 60–65 °C starts to coagulate (protein denaturation, blood clotting) and a change in colour can be observed. Vaporisation: around 100 °C, water in tissue vaporises creating pressure that leads to microexplosions. Carbonization: at higher temperatures than 100 °C, tissue starts to release carbon and blackens.	Vessel treatment, eye-vessel closure, endovenous laser treatment, laser-induced interstitial thermotherapy, laser incision with sealing of the small vessels

Photoablation

Description	Applications
"Etching" of tissue with minimal thermal damage. High-energy photons directly break molecular bonds causing ablation. Pulse duration: 10…100 ns Power density: 10^7–10^{10} W/cm^2 Typical lasers: Excimer lasers, fs-lasers	Offers precise and clean "cutting" and, hence, is used in refractive corneal surgery, cutting without sealing

Plasma-induced ablation

Description	Applications
Also known as *plasma-mediated ablation*. Part of a phenomenon called *optical breakdown*. High-energy light pulses ionize molecules in tissue. The created plasma bubble ablates tissue with negligible thermal effects. This mechanism also neglects secondary effects of plasma, which are included in the next mechanism. Pulse duration: 100 fs…500 ps Power density: 10^{11}–10^{13} W/cm^2 Typical lasers: Nd:YAG, Ti:Sapphire, fs-lasers	Refractive corneal surgery, dental caries removal, neurovascular studies [26]

Photodisruption

Description	Applications
In addition to plasma formation, also shock waves are generated as part of the optical breakdown phenomena. In tissue, this can also lead to cavitation and jet formation. These phenomena cause mechanical forces that "rupture" or "cut" tissue. Typical pulse duration: 100 fs…1 ms Typical power density: 10^{11}–10^{16} W/cm^2 Typical lasers: Nd:YAG, Ti:Sapphire	Lens fragmentation, lithotripsy (destruction of kidney/gall stones)

2.2 Laser light treatment of cutaneous vascular lesions

Lasers have been used in dermatology to treat cutaneous vascular lesions (unwanted superficial blood vessels on the skin), such as telangiectasia, hemangiomas and naevus, for over three decades. In fact, laser treatment of facial telangiectasia (dilated blood vessels) is one of the most frequently requested laser treatments in dermatology. The current treatment modalities are based on the technique of *selective photothermolysis* published by Anderson and Parrish in 1983 [27]. In the paper, they explain how microvessels—or indeed any other tissue target—can be selectively targeted and thermal damage to the surrounding tissue minimized by choosing an appropriate wavelength of light. In the treatment of vascular lesions, the aim is to destroy unwanted microvessels by selectively targeting *oxyhaemoglobin*, a chromophore abundant in blood. Oxyhaemoglobin absorbs the light energy (particularly that of 418, 542 and 577 nm as shown later) and converts it to heat, which spreads to the rest of the vessel structure causing the desired thermal damage [28] i.e. destruction of the vessel. At the same time, absorption by other main chromophores in skin, most notably melanin and water, should be minimized in order to only target the microvessels [29].

Figure 2.5 shows the absorptions curves for haemoglobin, melanin and water with emphasis around the visible spectrum. As indicated in the figure with arrows, oxyhaemoglobin has high absorption peaks at 418, 542 and 577 nm. The absorption is highest around 418 nm, but this region also has high absorption in melanin (dotted brown and orange curves) than the 542-nm and 577-nm regions. Melanin absorption continues to decrease towards the longer wavelengths of light, which makes longer yellow wavelengths, such as 585–590 nm, better suited for the treatment of deeper vessels, as the laser light is absorbed less by the upper layers of the skin [30]. In fact, the absorption in different chromophores in different skin layers largely determine the optical penetration depth of a laser wavelength (earlier shown in Figure 2.3). The wavelength dependence of optical penetration depth is additionally illustrated in Figure 2.6 giving emphasis to the currently commercially available laser wavelengths.

The main absorbers in the upper layer of skin (*epidermis*) are different types of melanin (eumelanin, pheomelanin), which have increasing absorption towards the blue-green spectral range. For this reason, blue-green laser light only penetrates some hundreds of micrometres into skin and is, therefore, mainly good for the treatment of very superficial vessels. In the deeper layers of skin (*dermis*), both types of haemoglobin as well as water start to play a larger role. Absorption of haemoglobin is the dominant reason why longer visible wavelengths (such as yellow-orange-red)

only reach optical penetration depth up to few millimetres. Although haemoglobin absorption decreases for red and infrared wavelengths, the increasing absorption of water (which is present in all layers of skin) from 600 nm onwards limits the overall practical penetration depth of lasers to some millimetres. Deeper penetration can in principle be achieved with higher fluence, but it is accompanied by the reduction of selective absorption and the increased risk of collateral damage due to unspecific heating.

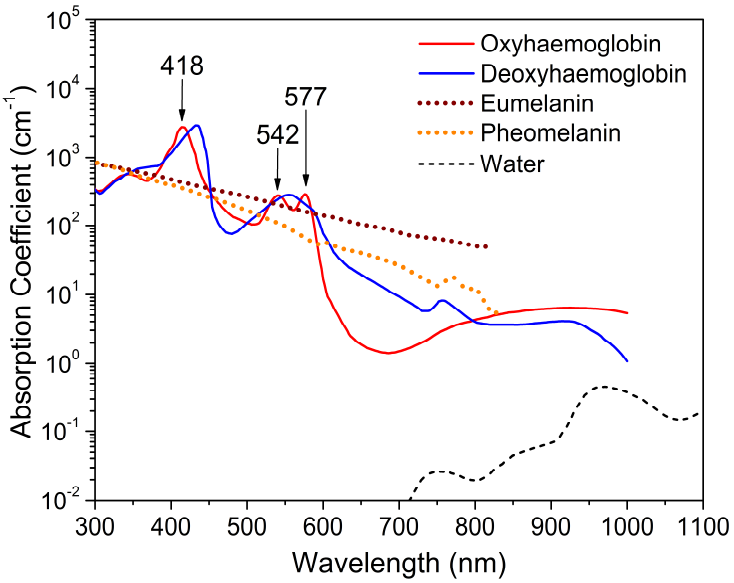

Figure 2.5. *Absorption curves for the main skin constituents (melanin, haemoglobin and water) as functions of wavelength. The figure was constructed using data from* [18, 19, 20].

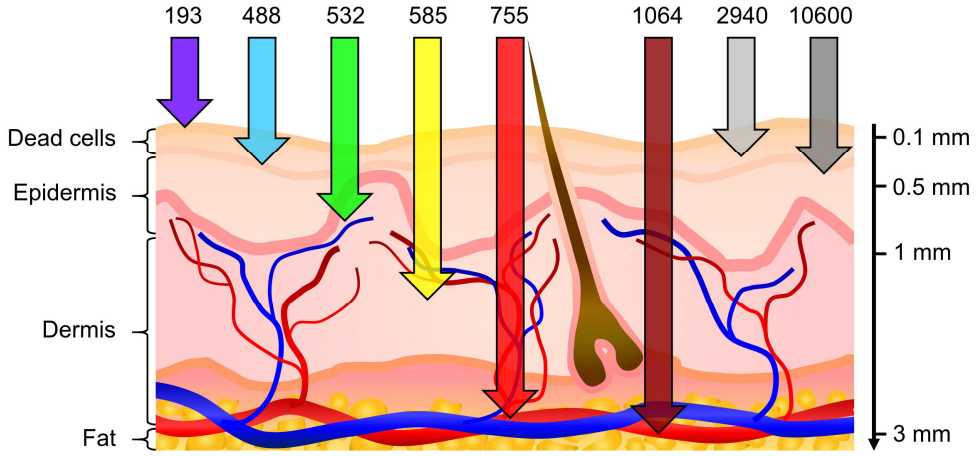

Figure 2.6. *Wavelength dependence of the penetration depth of dermatologic lasers. Wavelengths are indicated in nanometers on the top of the illustration.*

In addition to wavelength, the pulse duration of the laser light also needs to be optimised according to the target chromophore. The determination of the appropriate pulse duration relies on the concept of *thermal relaxation time* (TRT). TRT is the time needed for a chromophore to dissipate half of its heat gained from the laser light, and ideally the pulse duration should match the TRT of the chromophore. If the pulse is shorter than the TRT it might not produce enough heat for effective treatment, whereas, very short pulses can cause vessel rupture that leads to visible purpura [31]. Laser pulses that are longer than the TRT produce excessive heat at the target resulting in collateral damage on the surrounding tissue due to increased heat diffusion (see Table 2.1). TRT is longer for larger vessels and, hence, longer pulse durations should be used for larger vessels. As a rule of thumb, the pulse durations for 0.1–1 mm thick vessels should be in the range of 1–100 ms [32].

In summary, microvessels can be destroyed with laser light through transfer of energy from light into heat. Furthermore, the process can be made more selective by targeting only certain chromophores (in this case haemoglobin) with a specific wavelength. In addition, the pulse duration of the light should also be adjusted according to the vessel diameter. The wavelength selection minimizes absorption by other chromophores and the correct pulse duration assures effective treatment without subjecting the surrounding tissue to excessive heat. These two concepts set the targets for the laser sources in dermatology. The high haemoglobin absorption peak at 577 nm makes it a tempting choice for the treatment of cutaneous vascular lesions. However, currently used yellow lasers, such as pulsed dye lasers (PDLs), have opted for a longer wavelength of 585–590 nm in order to increase the penetration and decrease the melanin absorption while still maintaining high haemoglobin absorption. In terms of fluence, the typical values used in the treatment of vascular lesions by a yellow laser range between 5 and 20 J/cm^2 [30].

2.3 Existing laser systems for the treatment of vascular lesions

Table 2.4 lists the currently commercially available lasers studied for treating vascular lesions, also indicating their emission wavelength and pulse length [32, 33]. The current golden standard for the treatment of vascular lesions is the pulsed dye laser (PDL, e.g. Cynergy Cynosure and Candela Vbeam). It has been used to treat vascular lesions since 1985 and offers a versatile solution for a variety of conditions [30]. The main features include a typical emission wavelength of 585 or 595 nm, pulse durations in the 10–40 ms range and spot sizes ranging from 3 mm up to

about 12 mm. In addition, a dynamic skin cooling device is often used in parallel to reduce discomfort and to allow the use of higher fluence. Earlier versions of the PDL had a much shorter pulse duration of ~0.45 ms but a longer pulse was later employed to reduce purpura and vessel rupture. The PDL is the first laser that has been designed according to the theory of selective photothermolysis and, therefore, is not associated with severe adverse effects [30]. However, the drawbacks of the PDL system include large size and high acquisition and maintenance costs. Furthermore, the system delivers the laser light in a circular beam pattern, which makes it difficult to cover treatment areas uniformly.

Table 2.4. *List of currently available commercial lasers for the treatment of vascular lesions [P4].*

Laser	Technology	Wavelength (nm)	Pulse length (ms)
KTP	Frequency-doubled solid-state laser	532	1–200
Copper vapour	Metal-vapour laser	578	50–200
Pulsed Dye Laser (PDL)	Dye laser	585, 590, 595, 600	0.45–40
Alexandrite	Solid-state laser	755	3
Diode	Semiconductor laser	800, 810, 930	1–250
Nd:YAG	Solid-state laser	1064	1–100

Other commercially available and traditional options for the treatment of vascular lesions include the green-light emitting KTP laser and the yellow-light emitting copper bromide laser. The KTP laser operates at 532 nm and, therefore, has a high absorption by melanin, which leads to an increased risk of dyspigmentation [34]. The yellow copper bromide laser, on the other hand, is commonly associated with adverse side effects, such as scarring and hypo- and hyperpigmentation [35]. In the 1980s, the blue-green emitting argon laser (along with the red-light emitting ruby laser) was the most frequently used laser to treat vascular lesions, but since then it has been replaced with lasers emitting in the longer wavelength range. Lasers emitting beyond the yellow spectral region, i.e. in the red and near-infrared, have also been considered due to their ability to penetrate deeper in the skin. Such lasers (the red Alexandrite, diode lasers and Nd:YAG) are used only to target large vessels, deeply located in the skin. In their case, the selectivity of the treatment is more determined by the TRT than the wavelength of the laser.

In addition, new types of yellow lasers are emerging in the medical market as fully functional medical systems [36, 37, 38]. This suggests that laser technology is finally catching up with the

demands of the medical field, and it is now possible to tailor laser features to specific medical applications, for example, with VECSEL technology, which is reviewed in the next chapter.

Chapter 3

VECSEL Technology

This Chapter provides an overview on the basic operation principles and characteristics of VECSELs. The structure of a VECSEL gain mirror, pumping scheme, thermal management and cavity configurations are described. The chapter will also present the concept of frequency doubling and how it was applied to the lasers in this thesis.

3.1 General concept

Optically-pumped vertical-external-cavity surface-emitting lasers (VECSELs) are high-brightness light sources that convert higher energy (low wavelength) laser light into lower energy (high wavelength) laser light via a semiconductor gain mirror. Historically, the concept of a VECSEL dates back to 1966 when Basov et al. published a paper describing lasers with radiating mirrors [39], but it took another three decades before the proposed concept was fully acknowledged and the first working devices were demonstrated [40, 41]. Several more years were then needed before the benefits of the technology were fully proven and a surge of new developments were triggered [42, 43].

Figure 3.1 illustrates a typical VECSEL setup. Similarly to any other laser, VECSELs are comprised of the three main laser components: the gain material, the cavity, and the pump source. In VECSELs the gain is provided by the semiconductor gain mirror and the resonator cavity is formed between the gain mirror and one (or more) external dielectric mirrors. In comparison, the cavity for edge-emitting laser diodes (LDs) is formed between two cleaved surfaces of a semiconductor waveguide. The LD waveguide is typically some hundreds of nanometres thick, whereas the width is in the micrometre range. This large difference between the thickness and width of the laser output aperture leads to beam asymmetry and, hence, poor beam quality in high-

power operation. However, surface emitting lasers such as VCSELs (Vertical-cavity surface-emitting lasers) and VECSELs avoid the issue of asymmetric beams by emitting vertically from the surface of the semiconductor gain mirror through a symmetrical aperture. But a distinct difference between a VCSEL and a VECSEL arises from the pumping scheme. VCSELs are electrically pumped via metallic contacts, whereas VECSELs usually employ optical pumping which enables larger active volume and higher output power. These two features (optical pumping combined with surface emitting geometry) enable VECSELs to produce high-power emission while still maintaining good beam quality.

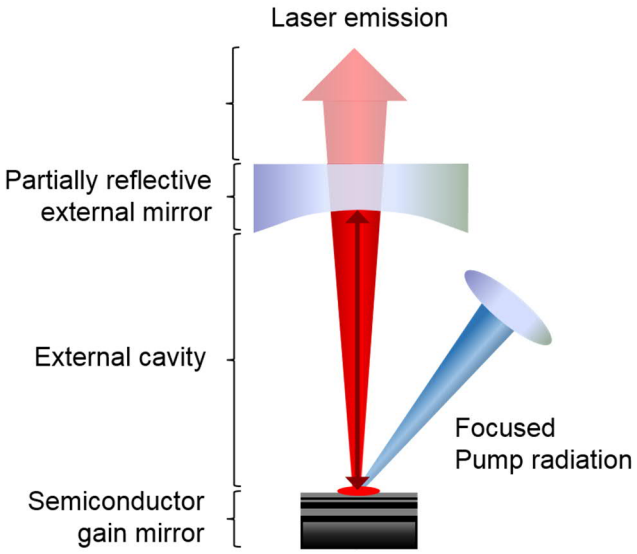

Figure 3.1. *Schematic illustration of a VECSEL depicting the basic properties. Not to scale (semiconductor gain mirrors are typically only some hundreds of micrometres thick). Due to the intrinsic low gain of VECSEL gain mirrors, only a few percent of the cavity power is coupled out with the partially reflecting mirror.*

In addition, the external cavity (further discussed in section 3.2) allows for the inclusion of intracavity elements [44]. Typically, VECSEL cavities are in the order of centimetres or tens of centimetres long, which makes it possible to insert nonlinear crystals for frequency conversion [45] or wavelength selective elements, such as birefringent filters and etalons, to reach narrow linewidth operation [46]. The external cavity also allows for the inclusion of a semiconductor saturable absorber mirror (SESAM) leading to the generation of ultrashort pulses [47]. Another significant advantage of VECSELs compared to laser technologies that use bulk lasing media (e.g. solid state lasers) arises from semiconductor material engineering. Through careful design and growth of the gain mirror, VECSELs can be tailored to emit at a specific wavelength needed in an

application. Although, there are certain material limitations and challenges regarding some wavelength ranges, which are shortly discussed in section 3.6.

3.2 Gain mirror structure

A VECSEL gain mirror is comprised of two main components: a highly reflective mirror and a semiconductor gain region. Often, they are both epitaxially grown on top of a semiconductor wafer/substrate using either molecular beam epitaxy (MBE) or metalorganic vapour phase epitaxy (MOVPE). A typical mirror structure is a so-called Distributed Bragg Reflector (DBR) mirror, which is composed of a periodic stack of semiconductor material layers with alternating high and low refractive indices. Roughly 20–25 pairs of low and high index layers are grown to achieve >99% reflectivity for the VECSEL emission wavelength. In some specific cases, other types, such as dielectric DBRs, metallic or hybrid mirrors have also been used [48, 49]. Moreover, DBR-free gain structures (a so-called MECSEL) have also been realised, where the mirror section is replaced by an external cavity mirror [50, 51].

The gain region usually includes several quantum well (QW) or quantum dot (QD) layers separated by barrier layers. The purpose of the barrier layers is three-fold; they absorb the pump light, confine the pump-generated carriers to the QWs for efficient recombination and in some cases compensate for the strain imposed by the QWs on the structure. Whereas, the QWs determine the emission wavelength of the VECSEL, which corresponds to the QW energy.

The total thickness of the gain mirror structure is usually less than 10 µm and the thickness of the gain region even less (~2 µm) with each QW typically having a thickness of 4–12 nm [52]. Due to this short interaction length between the laser mode and the gain material, the QWs are placed at the antinodes of the optical field. This configuration is called a resonant periodic gain (RPG) structure. In this way, the relatively low gain can be increased by maximising the coupling with the QWs [1]. Moreover, if the QWs introduce a large strain to the gain structure, additional strain compensation layers can be added in the active region [52]. A thin window layer concludes the gain mirror structure and prevents non-radiative recombination at the surface. Figure 3.2 shows a schematic example of a gain mirror structure. As a general rule, the centre of the DBR reflection bandwidth, the QW material gain peak and the RPG resonance should coincide at the target operation wavelength at the operation temperature for optimal performance.

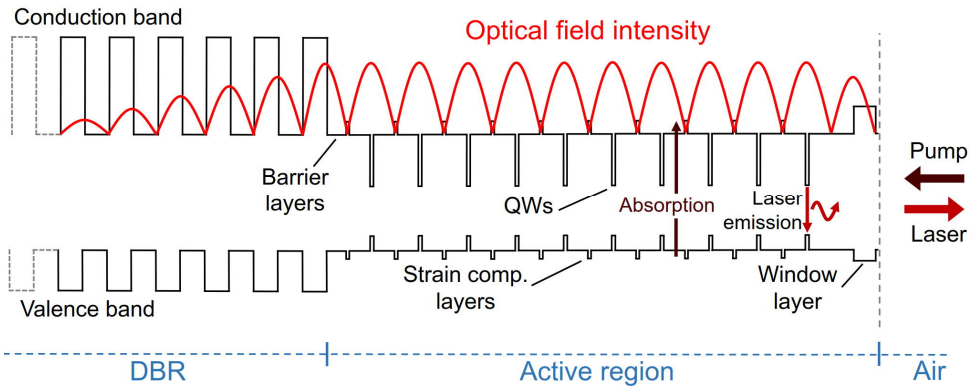

Figure 3.2. *Schematic illustration of a VECSEL gain mirror band structure. Adapted from [P1].*

3.3 Optical pumping

Fibre-coupled multi-mode diode lasers are typically used to optically pump VECSELs. They are low-cost, produce tens of watts of power and are readily available at several wavelengths thanks to solid-state laser needs. However, in contrast to solid-state lasers, VECSELs are not so particular with the pump laser wavelength. They absorb pump radiation in a broad wavelength range; the energy of the pump laser photons just need to be higher than the VECSEL's bandgap energy, which is determined by the material composition. Usually, the gain structure is designed to absorb most of the pump radiation in the barrier layers; the number of QWs and barrier layers are chosen so that ~80% of the pump radiation is absorbed throughout the thickness of the gain region (QWs placed beyond this point are unlikely to receive enough pumping for inversion). This ensures that single-pass pump passage is sufficient to meet lasing condition. In another scheme, only the QWs are designed to absorb the pump radiation, in which case the quantum defect (defined in the next section) can be very low [53].

3.4 Thermal management

VECSELs are sensitive to temperature rise and in the early experiments, high-power operation was limited due to inadequate heat extraction techniques. The heating of the gain structure arises from three main sources: 1) the quantum defect, 2) non-radiative recombination, and 3) pump radiation that passes through the gain region un-absorbed (~20%) and is absorbed in the DBR instead and transferred to heat [54]. The quantum defect is defined as the difference in energy

between the pump laser photon and the VECSEL emission photon; this energy is lost to heat when the high energy pump photons convert to the lower energy emission photons in the gain structure. The main mechanism for non-radiative recombination is Auger recombination, which has a positive feedback loop i.e. the probability of it increases with increasing temperature [55]. Excessive heating caused by these three mechanisms leads to reduced efficiency via increased non-radiative recombination and carrier leakage, which is further worsened when the pump power is increased due to the positive feedback loop. Moreover, the increased temperature also red-shifts the emission wavelength of the QWs, which can then lead to a mismatch between the emission wavelength and the RPG resonance wavelength (which red-shifts slower than the emission wavelength) [56]. This mismatch reduces gain, but can be compensated by designing the QWs to emit at a shorter wavelength so that it matches the RPG resonance at high pump power [57, 58], i.e. *detune* the emission and cavity wavelengths. If the pump-induced heating is not addressed efficiently, a VECSEL's output power will eventually exhibit so-called *thermal rollover* i.e there is a point after which the output power only continues to decrease even if the pump power is increased due to the negative temperature effects described above.

There are two general approaches to extracting heat from the gain mirror: the so-called *intracavity heat spreader* and *flip-chip* approach, shown schematically in Figure 3.3. Both of them include bonding a heat spreader element with high thermal conductivity to the gain mirror and further extracting the heat with a water- or TEC-cooled heatsink. In the intracavity heat spreader approach, a transparent heat spreader (such as diamond or other material with high thermal conductivity) is capillary bonded [59] to the emitting surface of the gain mirror. The shortcomings of this approach arise from the bonding process and the intracavity configuration. The bonding process is prone to failure because small dirt/dust particles can easily prevent successful bonding if they get in between the gain mirror and the heat spreader during the process. The elimination of such particles is difficult even in cleanroom environment, and they often originate from the edges of the cut gain mirror. Furthermore, the fact that the heat spreader is inside the cavity requires the material to have low-absorption at the lasing wavelength and to be of high optical-grade quality, which often leads to high cost. In addition, the heat spreader introduces intracavity losses and can act as an etalon inside the cavity, thus, affecting the spectral features. In principle, the etalon effect can be suppressed by employing a wedged heat spreader, but in this case an anti-reflective (AR) coating is necessary to keep the reflection losses as small as possible [60].

In the flip-chip approach, the gain mirror structure is grown in reverse order so that the active region is grown first on the substrate/wafer and the DBR mirror second. Next, the structure is bonded to a heat spreader from the DBR side and the substrate is removed with wet-etching [42]. The benefit of this approach is that lower-cost diamond heat spreaders can be employed, because

the heat spreader is not inside the cavity. However, the main difference to the intracavity approach is that since the heat is removed through the DBR, the thermal resistance of the DBR has to be as low as possible. This is challenging for some material systems that require thick DBR structures (due to longer operation wavelength or poor index contrast of materials) or are made of materials with high thermal resistance [61]. Other challenges in this approach also arise from the etching and bonding processes. The gain mirror structure is very fragile without the support of the substrate and the bonding process usually requires the use of temperatures exceeding 150 °C. If there is a large difference in the coefficients of thermal expansions of the gain structure and of the heat spreader, the fragile gain can experience detrimental mechanical stress as the bonding solder cools down and hardens [61]. This is especially critical for hard solders, but the issue can be alleviated by using soft solders, such as indium, or even alternative bonding methods [62, 63, 64].

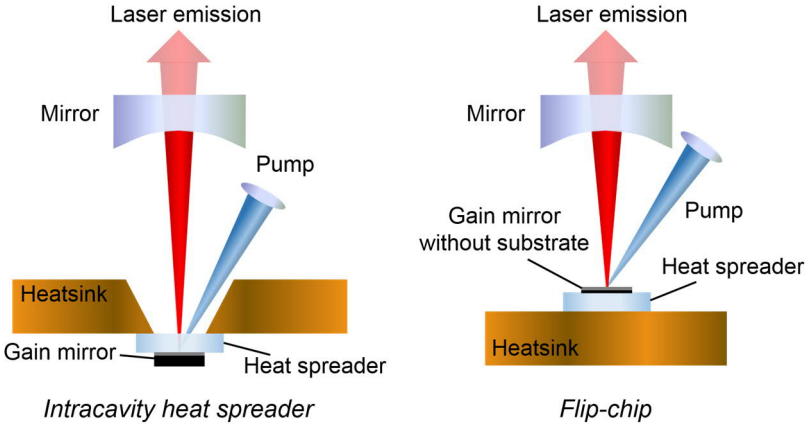

Figure 3.3. *Illustration of the two main heat extraction approaches: intracavity heat spreader and flip-chip.*

Both of the two heat extraction approaches have proved successful in enabling output powers in excess of tens of watts. The highest output power measured to date, that is 106 W, is with the flip-chip approach at a wavelength of 1028 nm [65]. The highest power recorded (72 W) with the intracavity approach is presented in this thesis for a longer, more challenging wavelength of 1180 nm [P3]. In addition to the choice of heat extraction, one should also pay attention to minimising non-radiative recombination by reducing defects in the gain structure and quantum defect optimization by a proper choice of pump wavelength and barrier layer material. Yet another approach to reduce the thermal load on a gain mirror is to pump with a pulsed laser. In this case, more modest cooling assemblies and heatsink temperatures can be employed while still reaching high peak powers [66].

Finally, even more advanced cooling approach involves sandwiching the gain structure between two heat spreaders [51] preceded by a total removal of the substrate, or even of the DBR as well [50]. This *membrane* technology (referred to as MECSEL in section 3.2) could also provide a solution to the problem of finding suitable material systems for direct emission at visible wavelengths by eliminating the need of a monolithic DBR. Furthermore, stacking of these membrane-heat spreader pairs could provide the means for further power scaling in the future.

3.5 External cavity

The external cavity allows for the inclusion of additional cavity elements, such as nonlinear crystals for frequency conversions, filters and etalons for linewidth narrowing and SESAMs for mode locking. To this end, it enables VECSELs to offer a wide range of functionalities by extending the wavelength coverage from IR to visible and UV, operation mode from high-power CW to ultrashort pulses and spectral characteristics from multi-mode to single-frequency emission. The cavity design is usually dependent on the desired functionality and in the simplest form resembles a letter I in shape with only one external mirror deployed. Such a cavity is favoured in reaching record output powers, and also for single-frequency operation due to larger spacing of longitudinal modes i.e. larger free-spectral range (FSR) associated with shorter cavities [65, 46]. For frequency doubling and mode locking with SESAMs, V- and Z-shaped cavities are preferred in order to accommodate for the additional components and to provide a small mode waist or tight focusing of the cavity beam. For power scaling purposes, it is also possible to employ multiple gain elements in a single cavity [67, 68].

Laser light is coupled out of the cavity through one (or more) of the cavity mirrors, which has a partially reflecting coating on it. These particular external mirrors are called output couplers (OCs). The intrinsic low gain of VECSELs makes them vulnerable to high losses; hence, the transmissivity of the output couplers is usually only a few percent. Typically, the VECSEL gain mirror acts as one of the cavity mirrors, but it is also possible to include a DBR-free gain structure in between external mirrors [50, 51]. This approach is particularly interesting for emission wavelengths that lack good material to grow high-reflective DBRs. The common VECSEL cavity architectures are illustrated in Figure 3.4.

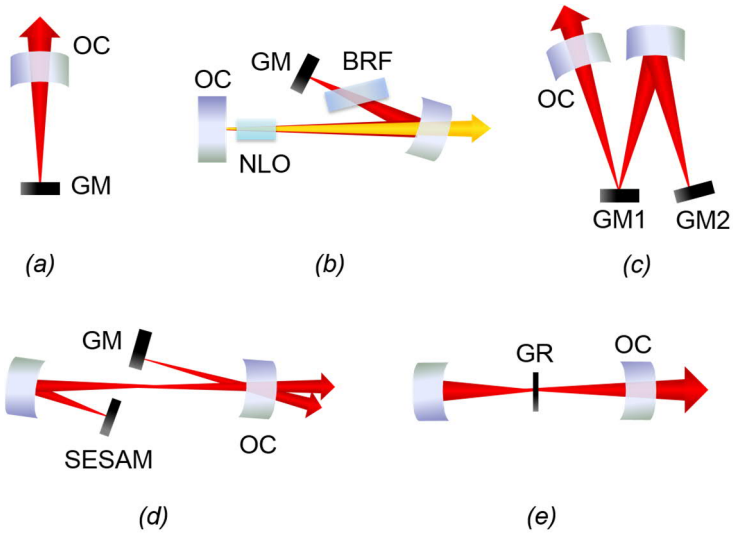

Figure 3.4. *Common VECSEL cavities: (a) straight I-cavity formed between a gain mirror (GM) and an output coupler (OC), (b) V-cavity with frequency doubling with a nonlinear crystal (NLO). The birefringent filter (BRF) fixes the polarization for the crystal and narrows spectrum, (c) cavity with two gain mirrors, (d) Z-shaped cavity with SESAM for passive modelocking, (e) DBR-free gain region (GR) in between two external mirrors. Note that pump laser optics are not illustrated for simplicity.*

In addition to frequency conversion and pulsing schemes, the external cavity also enables high-power emission with good beam quality. The cavity design determines the size of the fundamental mode on the gain mirror, which can be relatively easy to match with the pump spot to favour single transverse mode operation (TEM_{00}), i.e. Gaussian beam distribution. With power scaling in mind, the mode size on the gain mirror can be designed to have a large diameter for larger gain volume, and at the same time the matching large pump spot distributes the pump-induced heating to a greater area. Single-frequency operation requires further suppression of longitudinal cavity modes with filters and etalons.

3.6 Wavelength coverage

The development of VECSELs has evolved along three main directions: i) **power scaling**, ii) **generation of ultrashort pulses (not covered in this thesis)**, and iii) **wavelength coverage** [61]. To date, the wavelength range of directly emitting VECSELs spans from 665 nm to 5260 nm, though not without gaps. This range is further extended to visible and UV wavelengths and beyond 5260 nm with frequency conversion via nonlinear crystals (discussed in the next section). Such a

wide wavelength coverage, illustrated in Figure 3.5, is enabled by different material systems. The gaps in the coverage are also bridged by the tuning capability of VECSELs. For example, tuning ranges as broad as 43 nm at 1µm [69], 156 nm at 1.96 µm [70], and 900 nm at 5 µm [71] have been demonstrated using intracavity filters.

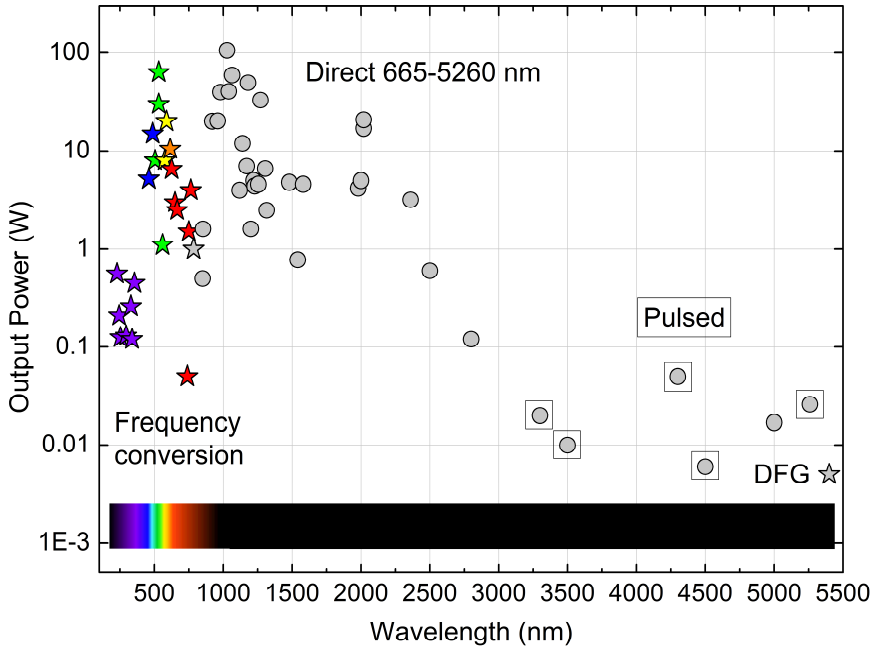

Figure 3.5. *Wavelength coverage of (mainly CW) VECSELs in relation to their output power. Circles signify direct emission and stars frequency converted emission (2nd, 3rd or 4th harmonic or difference frequency generation (DFG)). The boxed circles are pulsed VECSELs, but ultrashort modelocked VECSELs are omitted from this illustration.*

Most of the developments have focused on GaAs structures employing InGaAs QWs i.e. near 1 µm wavelength range, and, not surprisingly, the highest power [65] and shortest pulses [72, 73] has been measured from VECSELs with ~1 µm emission. The advantage of this material system is high reliability and high thermal conductivity [74, 75]. Moreover, GaAs/AlAs layers can be used to fabricate high refractive index contrast DBRs with good optical properties. Material systems for shorter wavelengths (360–920 nm) suffer from high strain and poor performance DBRs. Particularly, there is a green-yellow wavelength gap that cannot be reached with direct emission [1]. However, this material problem is circumvented by fabricating VECSELs in the 900–1300 nm range and employing intracavity frequency doubling. Another approach could be to use a DBR-free gain structures (MECSELs), but so far, the lowest wavelength reached with this method is 608 nm [76].

It should be noted that wavelengths above 1100 nm are challenging to produce due to the strain introduced by the multiple InGaAs QWs, which can lead to misfit dislocations and poor performance. This problem is tackled by introducing strain compensation layers to the structure [52] or incorporating small amounts of nitrogen into the QWs [77, 78]. The strain compensation technique was used to obtain the 72 W at 1180 nm presented in this thesis [P3]. Whereas, the dilute nitride method has resulted in the demonstration of a VECSEL emitting all the way at 1550 nm [79] and was used in the structure of the frequency-doubled red VECSEL included in this thesis [P2]. The drawback of nitrogen incorporation is that it is associated with the formation of point defects.

Typically, VECSELs emitting in the 1.25–1.6 range utilize InP structures with AlGaInAs QWs. However, this material system suffers from low refractive index InP-based DBRs. Therefore, instead of monolithic gain mirror structures, InP-based VECSELs often employ wafer bonded GaAs-based DBRs [80, 81]. VECSELs emitting above 1.6 µm have been realised with GaInAsSb, PbSe or PbTe QWs [82, 83]. These rather peculiar material systems benefit from high refractive index contrast DBRs, but usually require low operating temperatures. Figure 3.6 illustrates the wavelength coverage of VECSELs in connection to the material systems.

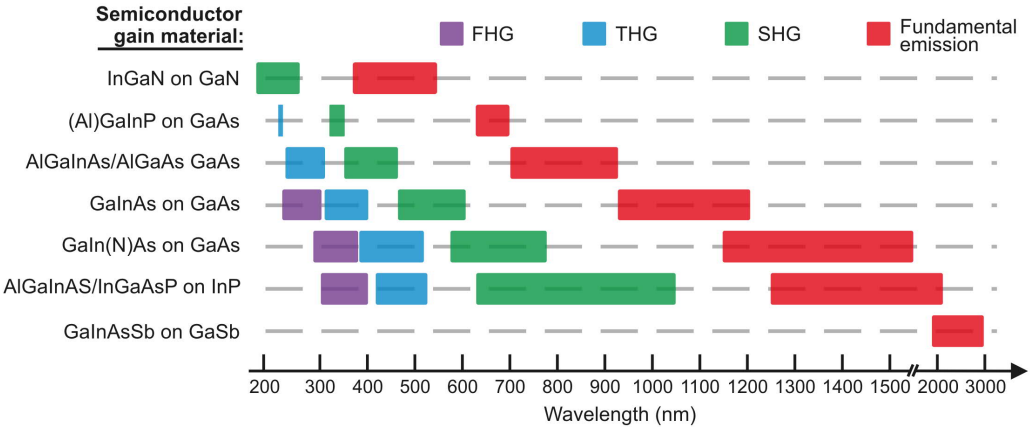

Figure 3.6. Wavelength coverage of VECSEs in relation to the used semiconductor gain materials. Adapted from [1].

3.7 Intracavity frequency-doubling in VECSELs

Nonlinear behaviour and frequency doubling, also known as second harmonic generation (SHG), are already well established concepts and explained extensively in several textbooks [84, 85, 86,

87]. Therefore, this thesis will only focus on the most important considerations needed to understand the phenomenon and on what factors affect the conversion efficiency.

3.7.1 Basic concept

As mentioned in the previous sections, the green-yellow spectral range is challenging to achieve with direct emission. For this reason, intracavity frequency doubling of 1–1.3 µm VECSELs has gained a lot of attention. It involves inserting a nonlinear crystal near the mode waist of a VECSEL cavity. VECSELs are particularly suitable for intracavity doubling due to their high intracavity power that can reach values in the order of 1000 W. Another advantage is that the infrared radiation is circulated in the cavity, hence, the part that is not converted will travel through the nonlinear crystal again. In other words, only a small fraction of the intracavity power needs to be converted per round trip to achieve sufficient conversion. Typical optimum output coupling ratios for VECSELs vary in the 1–5% range and, thus, similar 1–5% frequency conversion efficiency would be ideal for the laser operation and still translate into tens of watts of frequency-converted light. In comparison, to reach these values in external frequency doubling, one would have to achieve 100% conversion efficiency, which is practically unattainable, especially for bulk crystals and with CW operation.

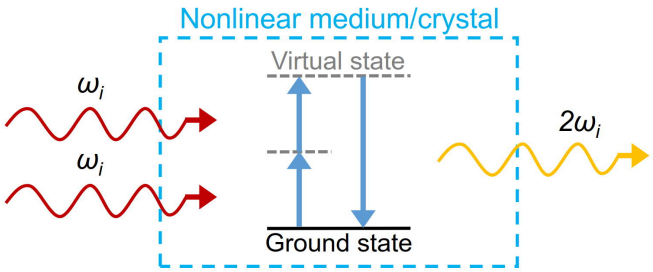

Figure 3.7. *Illustration of the phenomenon of second harmonic generation (also known as frequency doubling) in a nonlinear medium.*

In simple terms, the phenomenon of frequency doubling can be described as light with frequency ω_i entering a crystal with nonlinear properties that converts it to light with frequency $2\omega_i$, i.e. twice the frequency of the incident light (illustrated in Figure 3.7). In physical terms, it can be described as two-photon absorption in a medium, which shifts the carriers to a higher energy level, after which photons with twice the energy of the absorbed photons are emitted as the carriers return to ground state. However, certain conditions need to be met before this process can occur efficiently; these are addressed below.

3.7.2 Phase matching, the effective nonlinear coefficient and selection of a nonlinear crystal

There are two major factors to consider to achieve high-efficiency frequency conversion: phase matching and the effective nonlinear coefficient, d_{eff}, of a crystal. The choice of an appropriate crystal for a certain application is usually a compromise between these two. The effective nonlinear coefficient describes the strength of the nonlinear interaction in a specific material. In general, one should of course aim for as high d_{eff} value as possible, but this is sometimes not practical or possible due to the phase matching constraints. The concept of phase matching relies on matching the relative phases of the fundamental and the frequency converted light throughout the propagation length inside a crystal. However, this is challenging to achieve in practice, because the refractive index of a crystal material depends on the wavelength. Therefore, quite often we encounter a phase mismatch, Δk, between the two light beams. This mismatch can be minimized through careful consideration of different phase matching methods.

Phase matching methods are simpler to explain for uniaxial crystals, such as Beta-Barium Borate (BBO). However, in this thesis we mainly used a biaxial crystal called Lithium triborate (LBO). The difference in these two crystal types is the number of optic axes; uniaxial has one and biaxial two. Biaxial crystals have a more complex function for light propagation, but we will confine ourselves to the principle planes of XY, YZ and XZ, in which case a biaxial crystal acts as a uniaxial crystal [87]. In practice, only these three principle planes are utilised for phase matching anyway.

In uniaxial crystals, the optic axis is usually denoted with *Z* and together with the light propagation direction *k* it defines the principle plane. Light that is polarized orthogonally to the principle plane is known as an ordinary ray, denoted with *o*, and its refractive index does not depend on the propagation direction. Whereas, light that is polarised in the principle plane is called an extraordinary ray, *e*, and its refractive index depends on the propagation direction. This difference between the refractive indices is known as *birefringence* and it is one of the two basic methods to achieve phase matching; if the fundamental and the frequency-converted rays have different polarisations it is possible to match their refractive indices [85].

The dependence of the *e*-ray on the propagation direction is a function of the angle θ, which is the angle between the optic axis and the propagation direction *k*. To achieve phase matching in a uniaxial crystal, it should have a certain orientation defined by θ. This type of phase matching, which relies on angle tuning, is called *critical phase matching* (CPM). For biaxial crystals, there is also a second defining angle, φ. This is the angle between the projection of the light propagation, *k*, on to the XY plane and the X-axis (shown in Figure 3.8). The drawback in this CPM method is that the light does not propagate on the optic axis anymore. Consequently, the *o*- and the *e*-ray

propagate at slightly different directions, which is referred to as spatial walk-off [87]. It can result in elliptical output beams and reduced conversion efficiency. In addition, d_{eff} is affected by the propagation direction which is determined by the angles θ and φ.

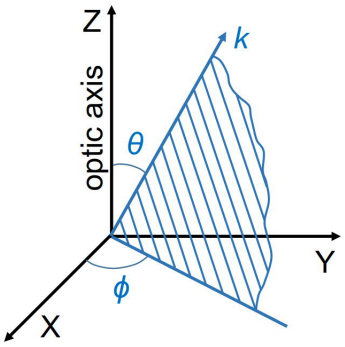

Figure 3.8. *Polar angles that define the propagation direction of light, k, in the crystal to achieve phase matching in the birefringence phase matching method. Adapted from* [87].

Spatial walk-off can be avoided in the special case of birefringent phase matching, called *non-critical phase matching* (NCPM). In this case, the angle θ is set to 90°, which places the light propagation on the optic axis. The refractive indices are then matched by temperature tuning the crystal. The drawback for NCPM is simply the fact that it is not possible for all crystal materials and wavelengths and sometime it requires very high or very low operating temperatures.

Some crystals do not exhibit birefringence, hence, another method is used to achieve phase matching, called quasi phase matching (QPM) [84]. In this method, a nonzero phase mismatch is allowed for a certain propagation length, but the d_{eff} is inverted after each coherence length (defined as the distance where the conversion efficiency reaches its first maximum, inversely proportional to Δk) so that the two waves converge back to the same phase. This periodically poled structure can be established with various techniques, for example by applying an intensive electric field through periodically patterned contacts [88]. Compared to birefringence phase matching, QPM offers much larger d_{eff} and a wider wavelength coverage, since the poling period can be adjusted to almost any wavelength (UV range is challenging for any crystal due to absorption). Moreover, it does not require for the fundamental and the frequency converted light to be of different polarisation, like in the case of CPM and NCPM. The drawbacks include higher cost, fabrication challenges regarding the poling periods and they are more susceptible to damage (e.g. via photorefractive effect) [89].

Another way to categorise phase matching is to use the notations Type 0, Type I, Type II. They are defined by the polarisation of the interaction rays. For instance, Type I phase matching is

achieved when two o-rays interact to produce one e-ray i.e. the fundamental and the frequency-converted rays have different polarisations. Whereas, in Type II the two fundamental rays have opposite polarisations. Type 0 is used to denote QPM in which all the interaction rays have the same polarisation. Type I and II are covered in CPM and NCPM and further divided into minus and plus interactions depending whether the crystal acts as a negative or positive crystal [87]. Table 3.1 attempts to summarize all the phase matching types and methods, and how they relate to the polarisation of the interaction rays.

It should also be noted that there are higher harmonic generations than just SHG, such as third harmonic and fourth harmonic, but they are seldom used directly due to the low third and fourth order nonlinearity in materials. Typically, cascaded processes with two crystals of second order nonlinearity are employed [90]. In fact, second order nonlinearity is divided into sum-frequency generation (SFG) and difference-frequency generation (DFG), and SHG is simply a special case of SFG. Although, it is the most used type because it employs only one pump laser.

Table 3.1. *Phase matching types and methods.*

Type	**Polarisations of the Interaction rays (Principle plane for biaxial crystals)**	**Method**
Type 0	e + e → e	QPM
Type I	o + o → e (XY) e + e → o (XZ)	CPM (NCPM for certain crystals if $\theta = 90°$ and $\varphi = 0°$)
Type II	e + o → e (XZ) o + e → o (YZ)	CPM

To summarize, understanding frequency conversion in nonlinear crystals and choosing a suitable crystal is not a trivial matter. Phase matching (or rather phase mismatch) and d_{eff} are the main factors that affect the efficiency of the conversion, but other factors such as the length of the crystal and power density of the laser light also play a role. The choice of a suitable crystal usually starts with finding a material, which is transparent for the laser wavelength and has a high enough d_{eff} for a suitable type of phase matching. For this purpose, one can use a software, such as SNLO [91], to find phase matching solutions and their d_{eff} for various cases. Another major factor that affects the experimental conversion efficiency values is the crystal quality. The facets of nonlinear crystals are also often anti-reflection coated for the pump and frequency converted wavelengths. The quality of the coatings can also significantly affect the conversion efficiency, particularly in an intra-cavity configuration. LBO crystals are known for a wide transparency, high damage threshold,

high d_{eff} and NCPM option, which is why it was the material of choice for the doubling crystals in this thesis.

Chapter 4

Laser Results

This chapter reviews the laboratory-environment laser demonstrations in this thesis. The first section reports the results for a CW frequency-doubled yellow VECSEL including a tuning experiment and pulsed operation. The second section presents the output characteristics of a frequency-doubled red VECSEL in CW and pulsed mode with further investigations on the conversion efficiency of the doubling crystal. The third and final section reports the record power for a VECSEL emitting in the 1.2-µm range. All the gain structures in this thesis were grown by molecular beam epitaxy (MBE).

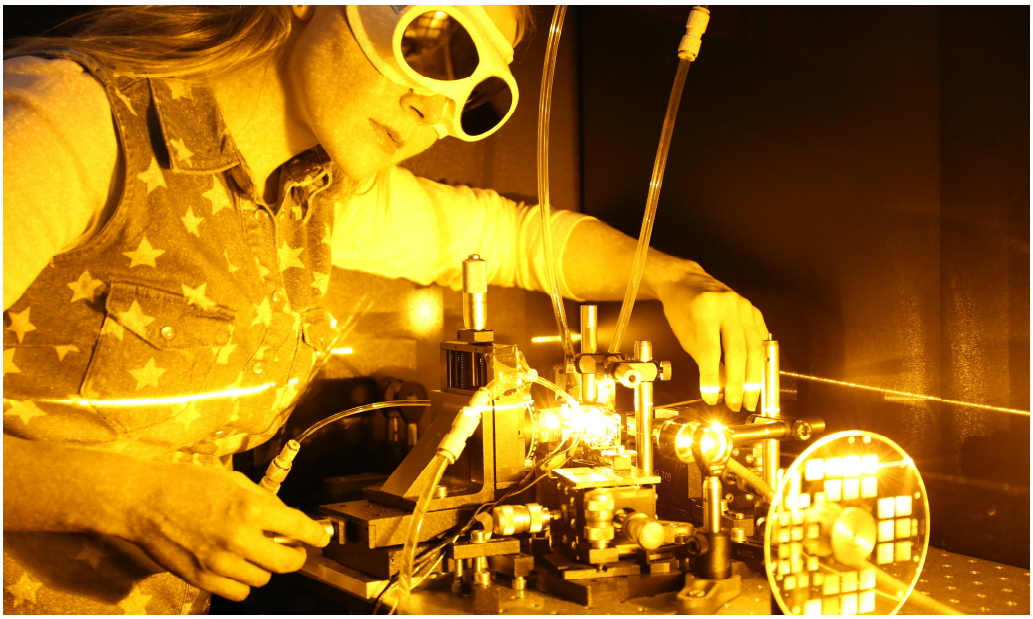

Figure 4.1. *Frequency-doubled yellow VECSEL in operation. Results presented in section 4.4.*

4.1 Frequency-doubled yellow VECSEL (20 W)

The 1180-nm gain mirror presented in [P1] was designed and grown for frequency doubling to the yellow spectral range. As discussed in Chapter 2, there is a need for high-power yellow lasers in medical and life science applications, as well as in other fields, such as astronomy.

4.1.1 Experimental set-up

The gain mirror structure was designed to emit 1180-nm emission. A 25.5-pair AlAs/GaAs DBR was grown on top of a GaAs substrate followed by the gain region, which incorporated 10 InGaAs QWs sandwiched in between GaAs barrier layers and GaAsP strain compensation layers. The intracavity heat spreader approach was employed for efficient thermal management. This included capillary bonding a diced 2.5 mm x 2.5 mm VESCEL chip onto a 300-µm-thick intracavity diamond heat spreader. Moreover, the diamond was attached to a water-cooled copper mount via indium foil.

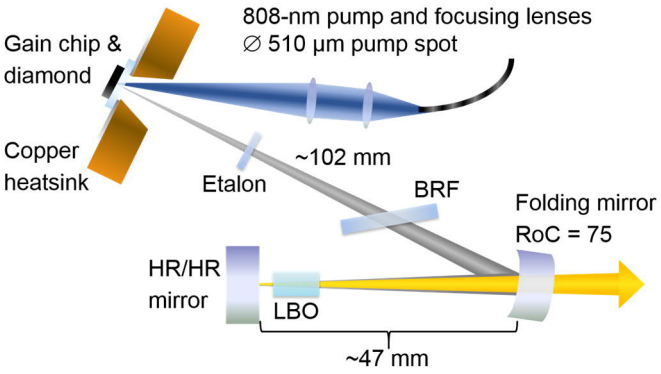

Figure 4.2. *Cavity configuration for the frequency-doubled yellow VECSEL [P1].*

The cavity was designed for frequency-doubling and employed two external mirrors forming a V-shape along with the gain mirror, shown in Figure 4.2. The flat end-mirror had HR coating for both the fundamental and the yellow wavelengths, whereas, the folding mirror was highly transmissive for the yellow and HR for the fundamental. This enabled us to have high intracavity power for the fundamental emission and to measure the frequency-doubled output from one direction.

A 1.5-mm-thick birefringent filter (BRF) was placed at a Brewster's angle in the first arm of the cavity in order to fix the polarization of the fundamental emission, to narrow the spectrum and enable wavelength tuning. A 100-µm-thick etalon was placed next to it to further narrow the

spectrum. The gain mirror was pumped with an 808-nm diode laser. The pump radiation was focused to a spot with a diameter of 510 µm ($1/e^2$). The fundamental mode size on the gain mirror was slightly smaller than the pump spot. It is easier to obtain fundamental transverse mode operation if the pump and the mode size are matched, but a compromise was made to produce a favourable mode waist for the doubling crystal.

The doubling crystal was chosen to be a 10-mm-long NCPM lithium triborate (LBO), because of its high d_{eff}, high damage threshold, and absence of walk-off. The facets of the crystal were flat and AR-coated for the fundamental and the yellow radiation. Phase matching was achieved by temperature tuning the crystal around 38°C. This was achieved by enclosing it in a TEC-stabilised copper oven. We noticed some damage on the AR-coatings after the CW measurements, which is why we employed a 10-mm-long CPM LBO for further experiments with a pulsed pump laser. The damage was visible to the eye and further investigations with an optical microscope convinced us that only the coating was damaged and not the crystal itself. We attributed this damage to the high intracavity power incident on the crystal facet (~3 MW/cm^2). It could have also started from a burnt dust particle and escalated as the pump power was increased.

4.1.2 Continuous wave operation

A record output power of 20 W of yellow radiation was measured behind the folding mirror. This corresponded to an estimated absorbed pump power (reflected power from the crystal surface subtracted from the incident pump power) of 75 W and a mount temperature of 8.3°C. The highest optical-to-optical conversion efficiency of ~28% (from absorbed pump power to yellow output) was recorded for 16 W of output power. The emission spectrum was centred at 588.1 nm with a FWHM of <0.2 nm. The output power characteristics along with the spectral features are shown in Figure 4.3 (*Left*). The beam profile for the yellow radiation was preserved circular with some distortions as seen in Figure 4.3 inset (partly caused by dust specs on the CCD camera). In addition, the tuning range of the frequency-doubled VECSEL was determined by rotating the BRF around its axis. For this experiment, the pump power was kept constant at 55 W and the temperature of the LBO oven was optimised for each wavelength separately[*]. This resulted in a tuning bandwidth of ~26 nm ranging from 576 nm up to 602 nm (Figure 4.3 *Right*). The 20 W of yellow is to date the highest power achieved at this wavelength range for this type of laser and it is also among the best results in the visible range alongside with the 30-W result at 532 nm reported by Coherent Inc. [45].

[*] The temperature dependence of NCPM LBO is well-known and the phase matching temperature can be calculated using Sellmeier's equations [119].

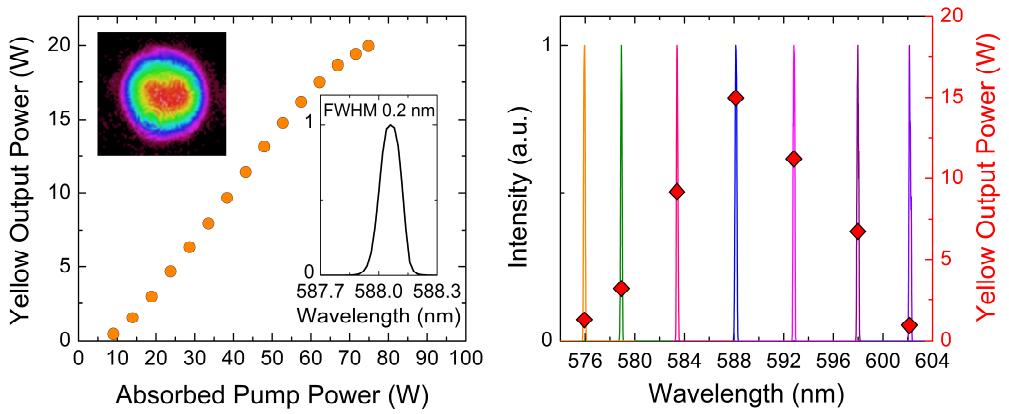

Figure 4.3. *Left: Output power characteristics for the frequency-doubled yellow VECSEL. Beam profile and spectrum at maximum power as insets. Right: Tuning curve and the corresponding output powers (right y-axis) [P1].*

4.1.3 Pulsed operation

Pump-induced heating of the gain structure causes thermal rollover and limits the CW operation. In addition, certain (medical) applications require pulsed laser light. In order to study the thermal effects and improve the conversion efficiency, a pulsed pump laser was employed. The same cavity configuration was used as with the CW measurements, however, the NCPM crystal was substituted with a CPM crystal due to damaged AR-coating. The temperature of the CPM LBO was kept near room temperature and the gain mirror mount temperature stayed at 21°C throughout the pulsed operation experiments corresponded to a water coolant temperature of 20°C.

The pump laser was driven with a driver capable of producing pulse widths up to ~1.5 µs. Two Si-based detectors were deployed to monitor the light pulse shapes generated by the VECSEL and the pump laser, shown in Figure 4.4 (*Left*). First, the driver was set to produce 1.5 µs pulses and then to 1.0 µs while keeping the repetition rate constant at 10 kHz. These pulse settings produced 1.08 and 0.57 µs pulse widths (FWHM) for the yellow radiation. For a reliable comparison with CW operation, we also measured the power characteristics generated by the new CPM crystal with a CW pump for a coolant temperature of 20°C.

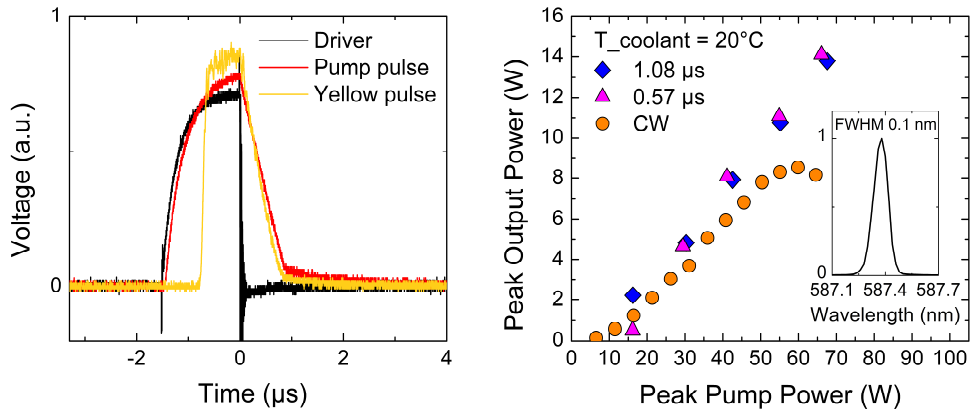

Figure 4.4. *Left: Pulse shapes for the pump laser driver (black trace), pump laser output (red trace), and frequency-doubled VECSEL output (yellow trace) for 1.5 µs pulse width setting. Right: Output power characteristics for CW (average power) and pulsed operation at two different pulse width settings. Output spectrum for 0.57-µs pulse width at maximum power as an inset [P1].*

Figure 4.4 shows clear thermal rollover behaviour for the CW measurement, whereas, pulsed operation shows linearly increasing trend, limited by the available peak pump power (70 W). Moreover, the optical-to-optical conversion efficiency of the CW operation at maximum output power was 15%, whereas, for the pulsed operation the conversion efficiencies were 20% and 21%, for the 1.08 µs and 0.57 µs pulses respectively. The maximum output power reached in CW operation was 8.5 W compared to the maximum peak powers of 13.8 W for the 1.08 µs pulse and 14.1 W for the 0.57 µs pulse. The output characteristics of the pulsed operation experiments are shown in Figure 4.4 (*Right*) with yellow spectrum for the 0.57 µs pulse as an inset. The FWHM of the spectrum for each pulse width were almost equal: 0.119 nm for 1.08 µs pulse and 0.113 nm for 0.57 µs pulse.

4.2 Frequency-doubled red VECSEL (10 W)

The 1230-nm gain mirror presented in [P2] was designed and grown for frequency doubling to the red spectral range. As discussed in Chapter 2, there is a need for high-power red lasers in medicine and life sciences, and potentially also in laser display technology; with further conversion to the UV range, red VECSELs also find applications in quantum optics.

4.2.1 Experimental set-up

The resonant gain mirror structure was designed to emit in the 1230-nm range and incorporated dilute nitride to enable the longer infrared emission. The gain region was comprised of 10 GaInNAs QWs surrounded by GaAs barriers. The nitrogen composition in the QWs was 0.5% and the whole structure was annealed after the growth to improve the material quality. Similar thermal management configuration was employed as with the 1180-nm material. A diced 3 mm x 3 mm chip was capillary bonded to a 300-µm-thick diamond heat spreader, which was attached to a water-cooled copper heatsink.

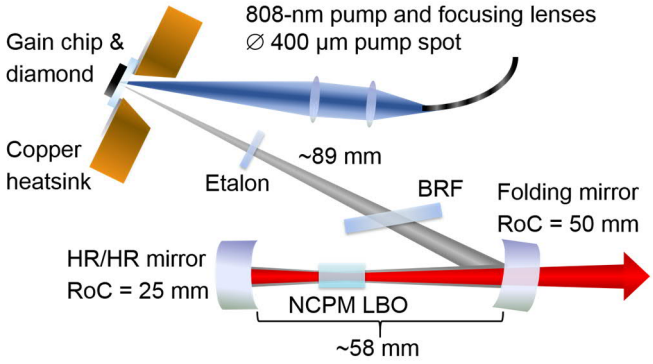

Figure 4.5. *Cavity configuration for the frequency-doubled red VECSEL [P2].*

The VECSEL was built into a V-shaped cavity formed by the gain mirror and two curved dielectric mirrors, shown in Figure 4.5. The gain mirror was pumped with an 808-nm diode laser, which was focused to a spot size of ~400 µm ($1/e^2$). The total length of the cavity was ~147 mm and the mode diameter on the gain mirror was ~240–300 µm (elliptical due to the folded cavity architecture). All the cavity mirrors were highly reflective for the fundamental emission and the curved end-mirror was also HR for the red emission. The folding mirror had high transmission for the red emission. We measured the reflectivities of the mirrors experimentally in order to estimate the intracavity power of the fundamental emission from the leakage of the HR mirrors. This included measuring the laser beam before and after the mirrors at different wavelengths in order to calculate the transmitted/reflected part of the beam.

A 1.0-mm-thick BRF and a 100-µm-thick etalon were placed in the first arm of the cavity to fix the polarization and narrow the linewidth of the laser. In addition, the same 10-mm-long NCPM LBO that was used with the yellow VECSEL was placed near the cavity mode waist for efficient frequency doubling. Phase matching was achieved by tuning the crystal's temperature to ~20°C. The temperature was first estimated with Sellmeier's equations and then adjusted experimentally

to produce the highest output power. CPM crystals were also tested, but even with the damaged AR-coating the NCPM LBO generated the highest conversion. This could be expected, since the NCPM LBO has higher d_{eff} than CPM LBO.

4.2.2 Continuous wave operation

The red emission was measured behind the folding mirror. The VECSEL reached a maximum of 10.5 W for an absorbed pump power of 59.7 W. This corresponded to an optical-to-optical conversion efficiency of 17.5% and was achieved for a mount temperature of 5–8°C. The emission wavelength was centred at 615 with a FWHM of 0.4 nm. The beam profile shows an elliptical shape, which might be consequence of the multi-transversal mode operation potentially caused by the difference between the pump spot diameter and the mode size on the gain mirror. The output power characteristic are shown in Figure 4.6 (*Left*). The beam profile and the output spectrum are shown as insets and were recorded at 7 W of output power.

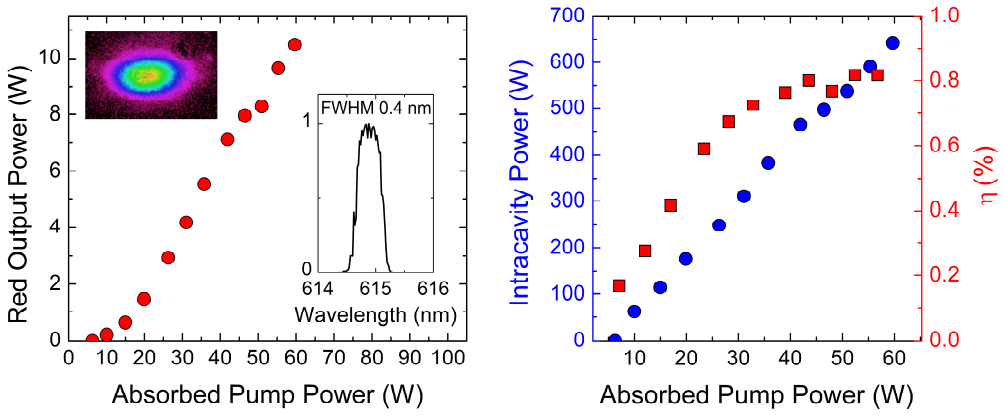

Figure 4.6. *Left: Output power characteristics for the frequency-doubled red VECSEL. Beam profile and spectrum as insets, recorded at 7 W of output power. Right: Intracavity power (blue circles, left y-axis) and single-pass conversion efficiency, η, (red squares, right y-axis) of the NCPM LBO crystal [P2].*

Figure 4.6 (*Right*) shows the calculated intracavity powers as a function of the absorbed pump power. The single-pass conversion efficiency (optical-to-optical), η, of the crystal was calculated by using the intracavity power together with the measured red output power and is also displayed in Figure 4.6 (*Right*). The intracavity power was estimated by measuring the leakage of IR radiation from the HR flat end-mirror. The small drop visible on the single-pass conversion curve is due to the small power drop in the red output power. This was probably caused by a wavelength jump, which we have often observed in frequency-doubled VECSELs that are not perfectly temperature

stabilised. The same drop is not observable on the intracavity power curve probably because the IR leakage value might have been recorded right before the wavelength jump. The maximum single-pass conversion efficiency of 0.8% corresponds well to the optimal output coupling of the 1230-nm gain material, which was determined to be 1.5% by experimentally testing different output couplers. In the intracavity configuration, the fundamental emission travels to both directions inside the crystal hence the total conversion efficiency was 1.6%.

4.2.3 Pulsed operation

The red VECSEL was also tested in pulsed operation in order to achieve higher conversion efficiencies. The cavity was kept as it was; only the pump laser was changed to the pulsed 808-nm diode laser. The pump laser driver was set to produce 1.5-µs pulse widths, in which case the red output had a pulse width of 1.16 µs (FWHM). The pulse waveforms measured at the maximum output power are shown in Figure 4.7 (*Left*). During the measurements the mount temperature stayed at 20°C. For comparison, a power curve in CW mode was also measured for a mount temperature of ~20°C. Figure 4.7 (*Right*) shows the recorded output characteristics for both operation modes. The maximum output power achieved in CW mode was 8.0 W, whereas, in pulsed mode the maximum peak output power was 13.8 W. Furthermore, thermal rollover was reached in the CW operation, but the pulsed operation was pump power limited. The maximum optical-to-optical conversion efficiency in pulsed operation was 20.4%, which is approximately 3 percentage points more than in CW operation.

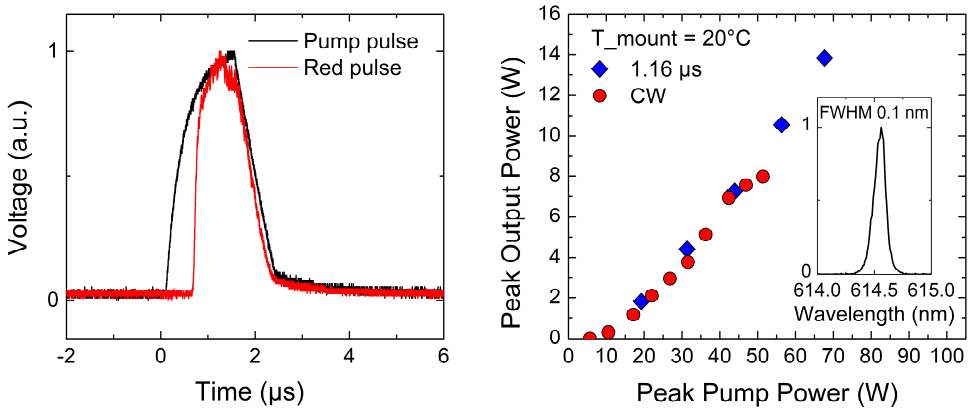

Figure 4.7. *Left: Pulse shapes for the pump laser output (black trace), and frequency-doubled VECSEL output (red trace) Right: Output power characteristics for CW (average power) and pulsed operation at two different pulse width settings. Output spectrum for 1.16-µs pulse width at maximum power as an inset [P2].*

4.3 High-power 1180-nm VECSEL (72 W)

A new gain structure was fabricated for 1180-nm emission in [P3] in order to provide chips for a yellow VECSEL system designed for medical use. In addition, the structure aims at satisfying the challenging narrow-linewidth requirements set by the laser guide star adaptive optics.

4.3.1 Experimental set-up

The gain mirror was comprised of an active region with 10 GaInAs QWs grown on top of a 26-pair AlAs/GaAs DBR. The strained QWs were embedded between GaAs barrier layers and GaAsP strain compensation layers. The structure was terminated with a GInP window layer to prevent surface recombination, and the active region thickness was matched to make the gain mirror microcavity resonant at the fundamental wavelength. This resonant structure along with carefully optimised detuning, provided the increased gain for the new 1180-nm gain mirror as compared to the one used in section 4.1.

In addition to the new improved gain mirror, heat extraction from the gain mirror was also improved by using a thicker, 2-mm intracavity diamond heat spreader. Furthermore, instead of a compact water-cooled copper mount, a 200-mm-thick copper plate cooled with four 200-W thermoelectric coolers (TECs) was employed to further extract the heat away from the gain mirror. The new high-gain material and the advanced cooling assembly enabled to reach much higher powers than before.

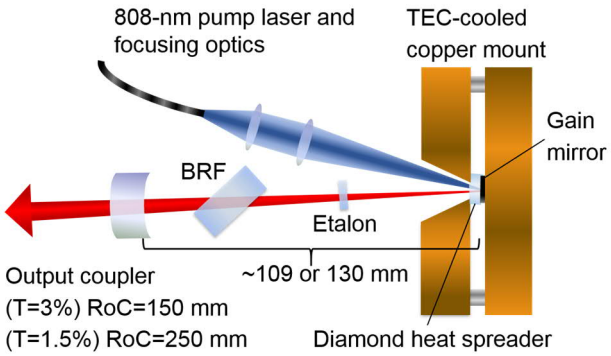

Figure 4.8. *Cavity configuration for the high-power 1180-nm VECSEL. The BRF and etalon were employed only in the longer cavity (l = 130 mm, RoC = 250 mm) for narrowing the spectrum [P3].*

This time a simpler cavity configuration was designed, since there was no need to fit a nonlinear crystal inside the cavity. Only one external mirror was employed forming a 109-mm-long I-shaped

cavity with the gain mirror, illustrated in Figure 4.8. The 808-nm pump light was supplied by a 200-W diode laser. The light was focused to a rather large top-hat spot size of 950-µm in diameter (4σ value) to provide lateral power scaling. The VECSEL was first measured in free-running, but a longer I-cavity (130 mm) was built to demonstrate the feasibility of the laser for narrow-linewidth operation.

4.3.2 Continuous wave operation

Different output coupling ratios were tested with the free-running cavity and the highest power was yielded with a 3%-coupler. Output power curves were measured at three different heatsink temperatures of 0, 10 and 20°C and plotted as a function of the incident pump power in Figure 4.9 (*Left*). The incident pump power is defined as the total power incident on the diamond surface and does not take into account the reflections from the diamond surfaces (estimated to be 5% with the AR-coating). The VECSEL reached a maximum of 72 W at a heatsink temperature of 0°C. This corresponded to 257 W of incident pump power, 29% optical-to-optical conversion efficiency and 38% slope efficiency. To date, this is the all-time second highest power reported from a VECSEL, only surpassed by the 106-W VECSEL at 1 µm, which is based on the more mature InGaAs/GaAs material system [65]. Thus, further merit is given to the result with the more challenging wavelength range of ~1.2 µm. During the 72-W operation, the spectrum of the laser was centred at 1185.5 nm and the FWHM was measured to be 5.5 nm, shown as an inset in Figure 4.9 (*Left*). At heatsink temperatures of 10 and 20°C, the maximum output powers were 62 and 53 W, respectively.

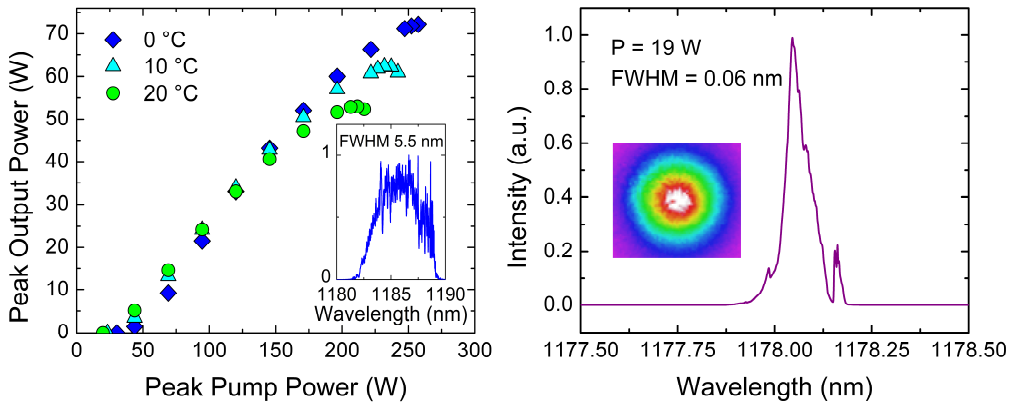

Figure 4.9. *Left: Output power curves for heatsink temperatures for 0, 10, 20°C. Lasing spectrum recorded at 72 W of output power is shown as an inset. Right: Normalised linear lasing spectrum at the maximum power (19 W) from the cavity including a 5-mm-thick BRF and a 250-µm-thick YAG etalon. Beam profile measured at 19 W of output power shown as an inset [P3].*

4.3.3 Narrowing the spectrum

The cavity was extended to make room for the intracavity filters. For reference, the output power of the longer cavity was first measured with a 3% output coupler. A maximum of 25 W was measured for a heatsink temperature of 20°C. Next, a 1.5% coupler was employed to compensate for the losses produced by the added intracavity filters. In this setup, a 5-mm-thick quartz BRF and a 250-µm-thick YAG etalon were inserted into the cavity and the lasing wavelength was fixed to ~1178 nm. A maximum of 19 W of output power was measured at 20°C, and the FWHM linewidth of the uncovered table-top laser was 0.06 nm (Figure 4.9 (*Right*)). The beam profile showed fundamental transverse mode operation (shown as an inset in Figure 4.9 (*Right*)).

The purpose of this wavelength narrowing was to demonstrate that high-power single-frequency operation would be possible in future with appropriate mechanical design. In the future work, a thicker BRF might be beneficial to further damp the unwanted cavity modes. In an earlier demonstration by Zhang et al. single-frequency operation was reached with a 10-mm-thick BRF [46]. This thesis work was confined to the existing stock in the lab.

Chapter 5

Clinical Trials

As a final step in this thesis, the developed yellow VECSEL was applied in a clinical trial for a proof-of-concept demonstration [P5]. This included first developing the laboratory laser into a fully functional system that can be operated by physicians, presented in [P4]. This chapter reviews the preparations required to perform clinical trials regarding the laser system, as well as regulatory considerations. Sections 5.1 and 5.2 present the design consideration and the operation features of the yellow VECSEL system. Documentation and permit requirements are listed in section 5.3. Finally, the design of the clinical protocol and the results of the trial are reported in sections 5.4 and 5.5.

5.1 General consideration in designing a device for clinical use

Safety is the most important consideration when designing a medical device for commercial or for investigational purposes. International Organization for Standardization (ISO) has set specific safety standards for electrical medical devices in their document ISO/IEC 60601-1. Other ISO standards to consider are risk management for medical devices (ISO 14971) and ISO 14155, which addresses the good clinical practice for the design, conduct, recording and reporting of clinical trials [92]. European Union also has its own directive, namely Medical Device Directive (MDD), whose main purpose is to standardize the laws relating to medical devices within the European Union. Devices that comply with these standards are given a CE-mark and can enter the commercial market [93].

It is necessary to have a good understanding of these standards before starting the design process of a medical device. For example, electrical connections in the device must comply with the ISO 60601-1 standards to ensure the safety of the user and the patient. Some of this workload can be reduced by using already CE-marked power sources and drivers. Electromagnetic compatibility (EMC) is also an important factor to consider. Treatment rooms are often scattered with various electrical equipment (some of which can be vital to the patient health), hence, it is important that the new medical device does not interfere with the surrounding electrical devices, or vice versa. It is also important to make sure that the materials, such as used optics and outer casings, do not pose hazards to the patient, particularly if they are in contact with the patient.

In addition to safety, it is important to design the laser features to match the needs of the application. Chapter 2 reviewed the light-tissue interactions in the context of dermatologic applications and the laser parameters that affect the outcome of a laser treatment. In general, the most important features are the lasing wavelength and the delivered energy, which is determined by the pulse duration and the intensity of the laser beam. It was also shown that there is a need for a yellow laser in the field of dermatology for the treatment of superficial unwanted blood vessels. For this purpose, ideally a laser should operate in the 580–590 nm wavelength range, produce 1–100 ms second pulses and deliver fluences in the order of 5–20 J/cm^2. The reliability and stability of these operation parameters is also a safety issue, since the treating physician needs to be able to trust that the laser produces the parameters he intends to treat the patient with.

5.2 Yellow VECSEL system

The yellow VECSEL system was designed and built in the Optoelectronics Research Centre (ORC), Tampere University of Technology, in collaboration with the French National Institute of Health and Medical Research (INSERM). It was based on the work done with frequency-doubled VECSELs and the system features were tailored to match the needs of dermatology applications.

5.2.1 Laser module

The laboratory setup of the frequency-doubled yellow VECSEL presented in section 4.1. was developed into a compact laser module. The VECSEL employed the gain mirror structure presented in section 4.3 and a LBO crystal for frequency doubling. A commercial 808-nm diode laser was used to pump the gain mirror. The VECSEL cavity (similar to the one shown in Figure 4.2) was assembled and sealed inside an airtight aluminium housing, shown in Figure 5.1 (*Left*). All the cavity components were glued on a baseplate for a robust finish. The baseplate was

temperature stabilized, but the most critical cavity components, such as the LBO crystal, also had their own temperature control. Dielectric mirrors were used to steer the yellow output beam through a collimation lens and towards a fibre port. The dielectric mirrors also act as wavelength filters to remove residual fundamental radiation from the output beam. In addition, a beam pick-off was placed in front of the fibre port to direct a small portion of the output beam into a photodiode for monitoring the output power. The collimated output beam was then coupled into a multimode fibre with a core diameter of 200 µm. In case we needed to change the fibre, the photodiode was calibrated again since the coupling efficiency is sensitive to even small alignment deviations. We observed a maximum of 10% change in output power, but most often it was far less.

The output power delivered by the module as a function of the incident 808-pump power is shown in Figure 5.1 (*Right*). The VECSEL operated in CW mode and a maximum output power of 8.6 W was achieved at an emission wavelength of 588 nm. CW operation was chosen, rather than pulsed, because it is relatively easy to mechanically pulse the laser light to produce 1–100 ms light pulses. This was achieved by utilising a fibre port and a handheld scanner presented in section 5.2.2. Power stability is also an important factor in medicine so that physicians can be certain of how much light energy they are using per treatment. The module was tested by measuring the output power of the system through the optical fibre for 15 minutes (shown in Figure 5.2), which corresponds to a typical treatment time. The laser was set to emit ~4 W (typical treatment output power) and the corresponding standard deviation of the output power was only 2.6 mW.

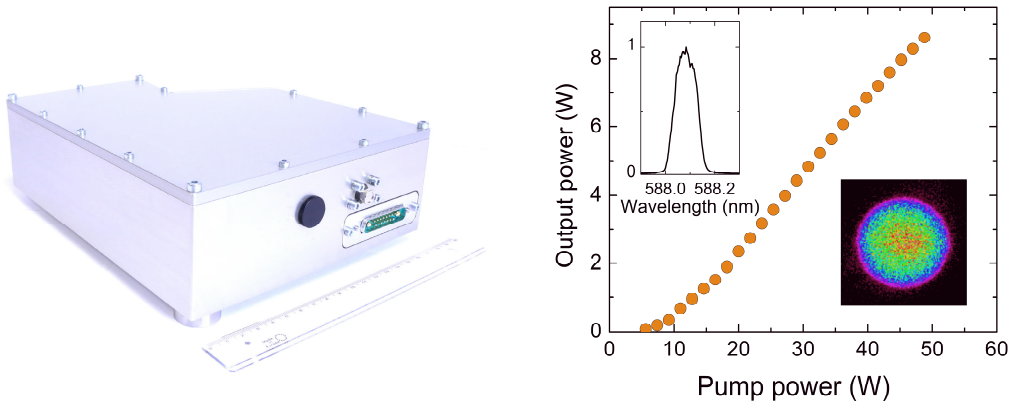

Figure 5.1. *Left: Photo of the VECSEL module accompanied by a 20-cm ruler. Right: Output power characteristics along with the beam profile (measured at the focus of the handheld scanner) and lasing spectrum shown as insets [P4].*

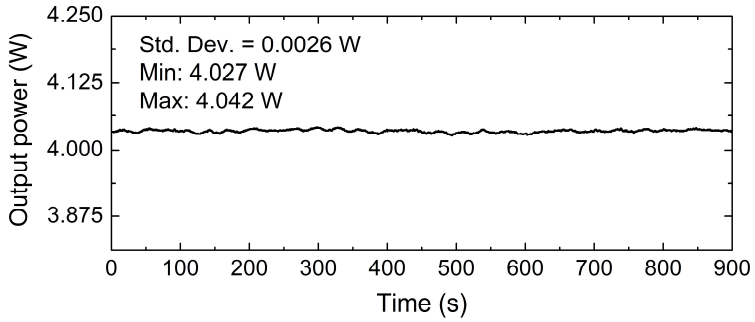

Figure 5.2. *Output power stability of the VECSEL module shown as a function of time. The yellow laser was set to emit ~4 W and a power meter was used to collect data for 15 minutes [P4].*

5.2.2 System features

The VECSEL module was integrated into a laser system resembling a table-top computer in size, shown in Figure 5.3a. The system encloses the VECSEL module, the pump laser and custom-built electronics. It is powered-up with a mains switch in the back panel and a turn-key switch in the front panel. The key switch enables the system usage and activates a 30-second warm-up period, after which the laser is in *Standby*-state and can be ramped up to a wanted power level.

The treatment parameters are controlled using a touch screen on top of the system, shown in Figure 5.3b. The varied parameters are laser power and pulse length with typical ranges of 0–7 W and 10–100 ms, respectively. These parameters, along with the spot size of the output beam, determine the treatment fluence, which is automatically calculated and displayed on the touch screen. The system produces a spot size of 1.4 mm in diameter (Gaussian intensity distribution) allowing to reach treatment fluences up to 52 J/cm^2, which is sufficient for treating superficial blood vessels. Compared to the pulsed dye laser (PDL), the 1.4-mm spot size is relatively small meaning that more spots are needed to cover the same area as with a PDL. In the VECSEL system, this shortcoming is overcome by employing a handheld scanner (shown in Figure 5.3c), which directs the fibre-coupled light onto skin in a pre-defined pattern. Using such a scheme with a typical pulse duration of 25 ms (i.e. 25 ms dwell time on each treatment spot), an area of about 1 cm^2 can be covered in less than a second. The smaller spot size also sets lower power requirements for the laser light, since the necessary fluences can be reached with lower output powers. In addition, the use of a scanner also brings flexibility enabling a diverse choice for treatment areas via programming. It should be noted that the1.4-mm spot size was determined by the optics inside the scanner, hence other spot sizes could be made available with different hand pieces. However, the current programming and fibre connections only support the used handheld scanner, which was supplied by MedArt A/S (Denmark).

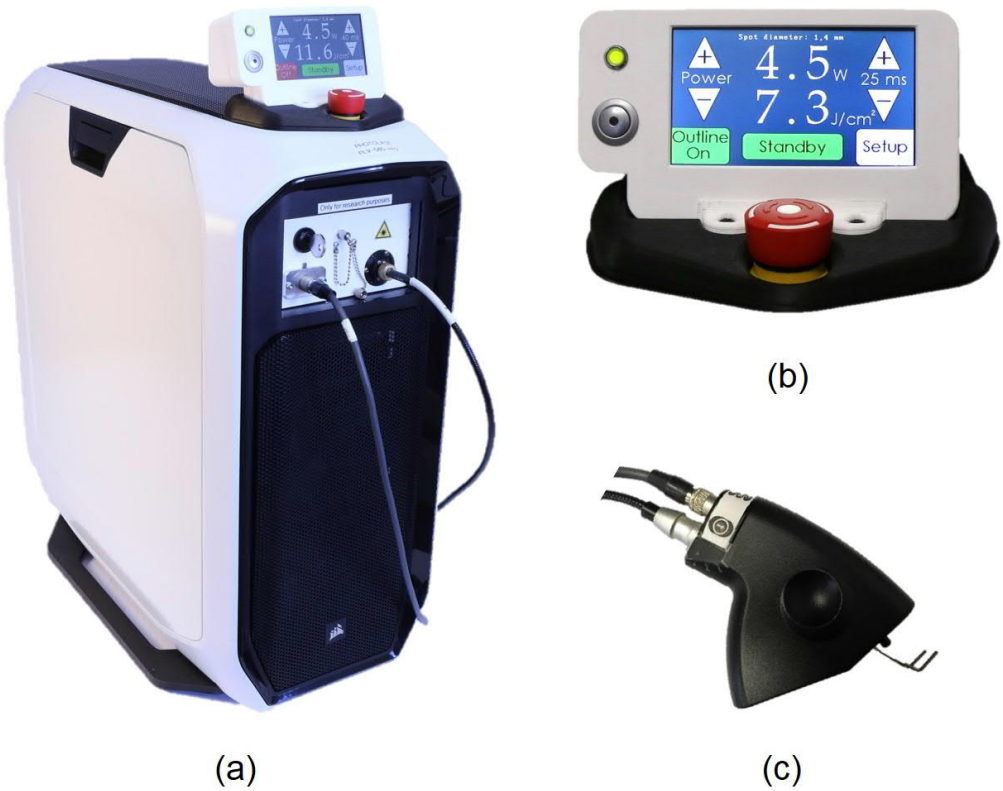

Figure 5.3. *Photo of the yellow VECSEL system (a), the touch screen (b) and the handheld scanner (c) [P4].*

The scanner has three different settings that can be varied by pressing the buttons on the side of it: scan pattern, scan area size and spot density. The available scan patterns include a single spot, line, square and hexagon profiles. Compared to the pulsed dye laser, which usually provides only circular beam spot profiles, these settings offer the user the freedom to select the most appropriate pattern for each situation and in principal avoids the problem of overlapping and un-treated areas caused by a circular spot. The scanner also includes a metallic distance piece attached to the front to indicate the correct treatment distance of 27 mm. The scan patterns are listed in Table 5.1 and illustrated in Figure 5.4. The delivery of laser light is activated by pressing a foot pedal connected to the back panel of the device; the foot pedal opens a shutter blocking the yellow beam and initiates the operation of the laser scanner. Once the scanner has covered the predetermined treatment area, the shutter is automatically closed.

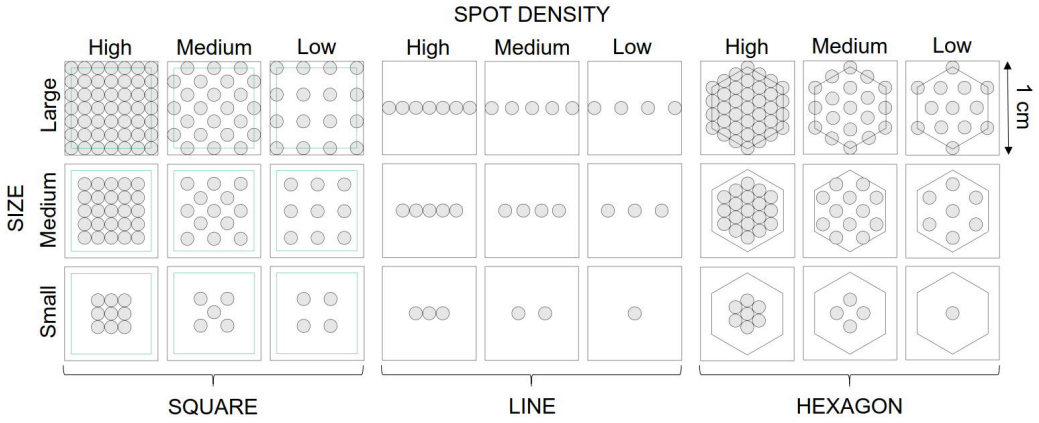

Figure 5.4. *Illustration of the scanning patterns (courtesy of MedArt A/S) [P4].*

Several safety measures have been implemented to the system in order to prevent any accidental light emission when the system is on. These features require that the handheld scanner and the output fibre are connected to the system before the shutter can be opened by the foot pedal. Moreover, the system also has to be at the target power level to enable light emission; if the output power is not within 0.1 W of the target, light is not emitted even if the foot pedal is pressed. Finally, the system is also equipped with an interlock that can be connected to a trigger signal, which turns the laser off if unauthorized personnel enter the treatment area.

Altogether, the air-cooled system weighs about 30 kg and is portable. The system does not have wheels, but for easier transfers it could be enclosed inside a wheeled suitcase. The technical specifications of the system are listed in Table 5.1.

Table 5.1. *Technical specifications of the yellow VECSEL system [P4].*

Technical Specifications	
Basic features	
Wavelength	585 ±5 nm
Power	up to 8.6 W in CW
Size	64 x 26 x 60 cm^3
Weight	approx. 30 kg
Treatment parameters	
Spot size	1.4 mm diameter
Pulse length	10–100 ms
Fluence	0–52 J/cm^2
Scan patterns	Line, square, hexagon
Scan area	From single spot up to 1 cm^2
Spot spacing	Low, medium and high density

5.3 Documentation and regulatory requirements

It is essential to document the technical data of the investigational medical device, as well as other considerations, such as risk management and various tests. They are important to keep for own records, but they are also required when applying for a permit to commence a clinical trial. In Finland, a favourable statement is required from the local ethical committee and the final permit is given by the National Supervisory Authority for Welfare and Health (Valvira). Figure 5.5 lists most of the documents prepared for the clinical trial. The main document packages were Risk Management, Investigator's Brochure and Clinical Protocol. The documentation process is rather long and it is further extended by the waiting time for the permit applications. It took approximately one year from the start of the documentation process to reach the start of the trial.

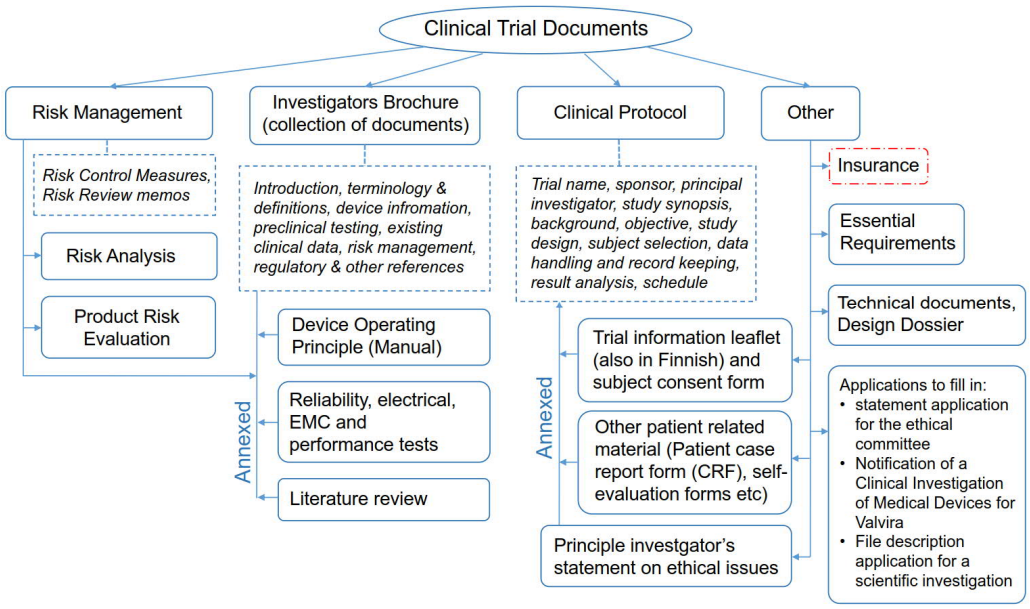

Figure 5.5. *Flowchart of the documents required for a clinical trial.*

5.3.1 Risk management

Risk management is an important process in developing a device, which aims at minimizing the probability of unfortunate and harmful events. It involves identifying, classifying and controlling all potential events associated to the device that may cause harm to people, the environment, the equipment, or to the device itself. These events may originate from various sources such as manufacturing or users.

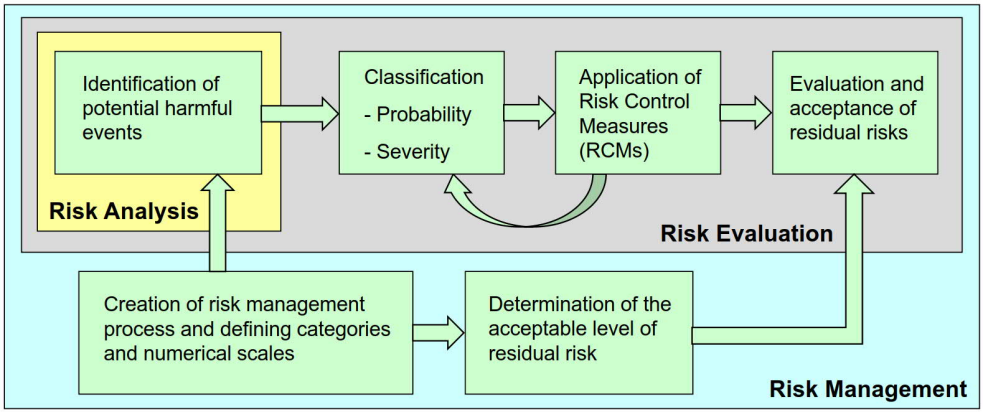

Figure 5.6. *Flow chart of the Risk Management process.*

The potential risks of the yellow VECSEL system were divided into four categories: risks specific to treatment, risks specific to use of lasers, risks specific to programmable electrical medical systems and risks specific to medical devices. Each risk was also given a numeric value (1–5) to represent the probability and severity of the risk. The multiplication product of these values gives the overall level of risk and places each risk into one of the three categories: Acceptable (1–6), ALARP (as low as reasonably practicable) region (7–14), Intolerable (15–25). All risks located in Intolerable-class were then reduced by preventive Risk Control Measures (RCM's) to either ALARP-area or acceptable area. A final evaluation of the residual risks was performed after the implementation of RCMs. Figure 5.6 illustrates the risk management process and the main risks and their control measures identified for the yellow VECSEL system are listed in Table 5.2.

Table 5.2 *Main risks identified for the yellow VECSEL system and their control measures.*

Description	Probability	Severity	Risk Rate	Risk Control Measure (RCM)	Probability	Risk Rate
Overdose of light (too high optical output power), produced by the laser	3	4	12	Maximum output power is limited to 6-10 W (depending on the module) Display fluence of the light dose clearly on the device If output power is not within the error limits (±200 mW) the foot pedal is disabled	1	4
Handheld scanner malfunction (wrong pattern, too large/small spot size, does not produce any light etc.)	4	4	16	Verify the scanner functionality and compatibility with the main unit Follow the scanner's test procedure before treatment (see MedArt scanner manual)	1	4
Ocular exposure to laser radiation	3	5	15	Prevent unintentional launch of laser light by integrating proximity sensor to fibre port and interlock functionality. Systematic wearing of protective goggles with appropriate specifications (at least OD 5+ at 580–590 nm)	1	5
Software malfunction	5	5	25	Test and verify software	1	5
Servicing electric shock	3	5	15	Warning that unit to be serviced only by trained/authorized personnel	1	5
Use by untrained physician/other	2	5	10	Warning caution in instruction manual	1	5

5.3.2 Investigator's brochure

The Investigator's Brochure (IB) is a so-called umbrella document, which collects and summarizes main information from the other documents. It is intended to provide the clinical investigators' a comprehensive but compact information package of the investigational device. It lists the device features and specifications and presents the results of risk management and preclinical tests. Other larger documents that are prepared in conjunction with the IB are Operation Manual, Preclinical Tests and Literature Review. In particular, the preparation of the Literature Review was a time consuming process that involved going through many lists of literature (mainly journal articles) given by chosen search databases (such as Google scholar and PubMed) for predetermined search terms. This review provided the basis for the justification to perform the designed clinical trial. Preclinical Tests included mechanical, electrical and EMC testing. Moreover, the reliability of the system was also tested by measuring the repeatability (and stability) of the system in terms of the scanner operation, shutter operation and laser output.

5.3.3 Clinical protocol

The design of the clinical protocol is especially important: it should be justified, clear and yield meaningful results. The protocol is usually designed with the clinical investigators and includes the preparation of many practical and compulsory patient related documents, such as information leaflet, subject consent form and self-evaluation forms. Ethicality of the protocol also needs to be explicitly considered in a separate statement by the clinical investigators. The next section gives a summary of the clinical protocol designed to test the efficacy of the yellow VECSEL system.

5.4 Clinical trial protocol

5.4.1 Objectives and background

The primary objective of the study was to compare the clinical outcome and adverse events of treating facial telangiectasias (dialated blood vessels) with traditional KTP-laser and the new investigational yellow VECSEL system, namely PhotoLase[†] laser, in a double-blinded randomized split-face trial. Both devices are Class 4 lasers with slightly different wavelengths, 532 nm for KTP and 585 ± 5 nm for PhotoLase. The secondary objective was to assess the usability, reliability and treatment characteristics of the PhotoLase laser from the perspective of the user. The hypothesis

[†] not trademarked, working-name during the project/trial

was that the new investigational device PhotoLase is as good or better in treating facial telangiectasia as the conventional KTP laser and does not produce more adverse/side effects.

5.4.2 Subject selection

Volunteering adults with Fitzpatrick's skin phototype I-IV and symmetrical facial telangiectasia were included in the trial. Ordinary laser exclusion criteria, such as pregnancy, lactation, haemophilic conditions, drug/alcohol abuse and significant tanning (less than 6 weeks prior to treatment) was also applied.

5.4.3 Trial design and methods

The study was a split-face comparative double-blinded study without a separate control group. It enabled a comparison between two lasers: the KTP laser and the investigational PhotoLase laser. The split-face design eliminated the individual biases and the randomization of the side of the face eliminated the possible small variations in the symmetry of the telangiectases on the face. The double-blind assessment eliminated the two investigators' and the subjects' subjective and objective bias. This means that the subjects were not aware which side was treated with which laser, and even though the two investigators also performed the treatments, their efficacy assessments can be regarded blinded, since the before-and-after images did not show information about which device was used in either side of the face. The subjects had 1–2 treatments depending on the investigator's assessment.

Both lasers were equipped with a scanner that produced a hexagon pattern and covered an area roughly 1 cm^2 in size. The KTP laser (Aura XP, Laserscope) employed Laserscope Smartscan and PhotoLase the MedArt scanner, presented in section 5.2.2. The spot diameter was 1.0 mm in KTP and 1.4 mm in PhotoLase.

The primary endpoints of the trial were the 7-point Telangiectasia Grading Scale (TGS) value and self-assessment of possible adverse effects using Visual Analogue Scale (VAS) for pain and a 4-point scale (0=absent, 1=mild, 2=moderate, 3=severe) for erythema, edema, crusting, purpura and blisters. The TGS value assessment was performed by comparing baseline and post-treatment split-face images after 1–2 months from the treatment. Both the subjects and the investigators performed the TGS assessment. However, the subjects only used a mirror and their own memory of the before-situation to give an evaluation. Whereas, the investigators performed the comparison using the before-and-after images and made a consensus decision on the TGS value. Canfield Visia facial imaging system was employed to ensure comparable images with standardized light

and facial positioning. The system also offers multi-spectral images with different filters, such as erythema-weighted images.

Assessment of adverse effects was conducted through self-assessment forms given to the subjects. The amount of experienced pain was monitored using VAS (visual analogue scale, scale from 0 (no pain) to 100 (worst possible pain)) and evaluated by the subjects right after each laser treatment. The subjects also evaluated the observed adverse effects such as erythema (redness), oedema (swelling), purpura (bruising), crusting and blisters 48–72 hours after the treatment. Additionally, the treating investigator assessed the adverse events right after each treatment.

The TGS has the following scores: -1 = condition worsened; 0 = no change; 1 = some improvement (<25%); 2 = intermediate improvement (25–50%), 3 = significant improvement (50–75%); 4 = very significant improvement (>75%); 5 = complete resolution of telangiectasia. The subject's self-assessment for the adverse effects was performed immediately after each treatment and then again after 48–72 hours. The patient flow in the trial is illustrated in Figure 5.7.

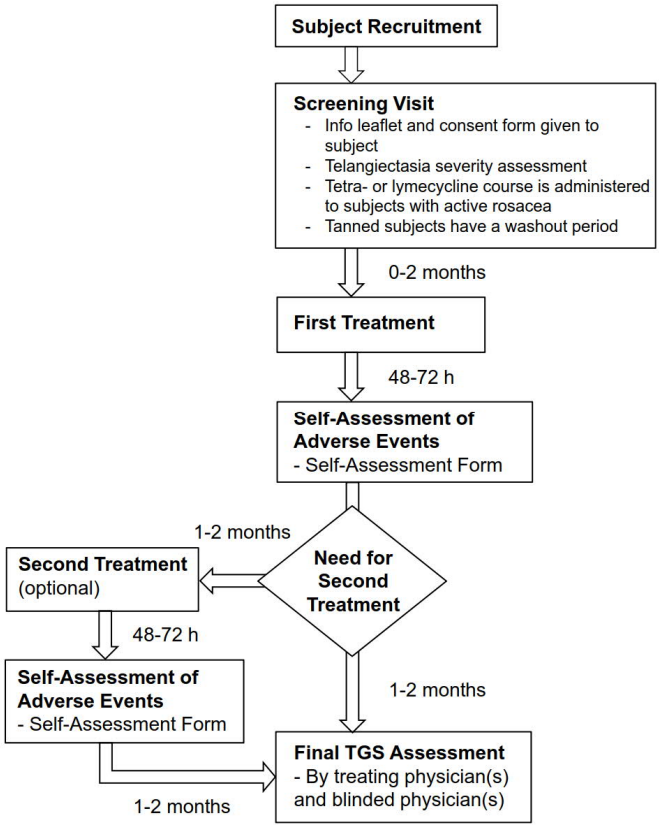

Figure 5.7. *Flow chart of the trial process [P5].*

5.5 Clinical Results

5.5.1 General

Twenty-four volunteers participated in the trial, but six of them were excluded from the analysis, because their telangiectasia could not be assessed from the Visia images. The mean age of the remaining 18 subjects was 48 years and the gender ratio was 16 females and two males. Nine subjects received KTP on the left cheek and PhotoLase on the right cheek, and nine subjects vice versa. Second treatment was performed on thirteen subjects. The Fitzpatrick's skin phototypes were I, II or III in 6/8/4 subjects, respectively. The baseline telangiectasia grades were I, II, or III in 4/9/5 subjects, respectively, and the grades were practically symmetrical in all of the subjects.

Treatment parameters were selected to achieve the same clinical end-point of vessel disappearance or clot formation within the vessel. This end-point was based on the subjective perception of the two investigators, whom together have more than 27 years of experience in treating dermatologic conditions. Double passes were performed when needed. KTP settings were 20–30 J/cm^2 at 10 ms pulse duration and PhotoLase settings were 5.6–8.1 J/cm^2 at 25 ms pulse duration. The pulse duration of each device was determined by the investigators. They chose to use a higher pulse duration for PhotoLase, since it was the minimum duration that produced the end-point they were looking for. No topical anesthesia or cooling was used, which proved to be an issue with PhotoLase laser.

5.5.2 Efficacy

Figure 5.8 illustrates the distribution of TGS scores assessed by the subjects and the blinded investigators after one treatment. According to the blinded investigators, fifteen subjects (83%) had a TGS value of 3 or larger, indicating at least 50% improvement after the first PhotoLase treatment, and a similar result was observed for KTP (p=0.29). The subjects' assessment favoured KTP; seven subjects had at least 50% improvement with PhotoLase after first treatment, whereas for KTP it was 10 subjects (p-value of 0.008[‡]).

The subjects and the investigators also assessed the potential benefit of the second treatment. According to the subjects, 11/13 benefited from the second KTP treatments and 10/13 from the second PhotoLase treatment, however the difference in the treatment efficacy was statistically insignificant (p=0.54). According to the investigators, 9/13 subjects benefited from the second KTP

[‡]Result is statistically significant if $p < 0.05$, whereas, a high p-value indicates that the result (in this case the difference between the TGS values) is statistically insignificant.

treatment and 8/13 from the second PhotoLase treatment. In this case also, the difference between the devices was statistically insignificant (p=0.81).

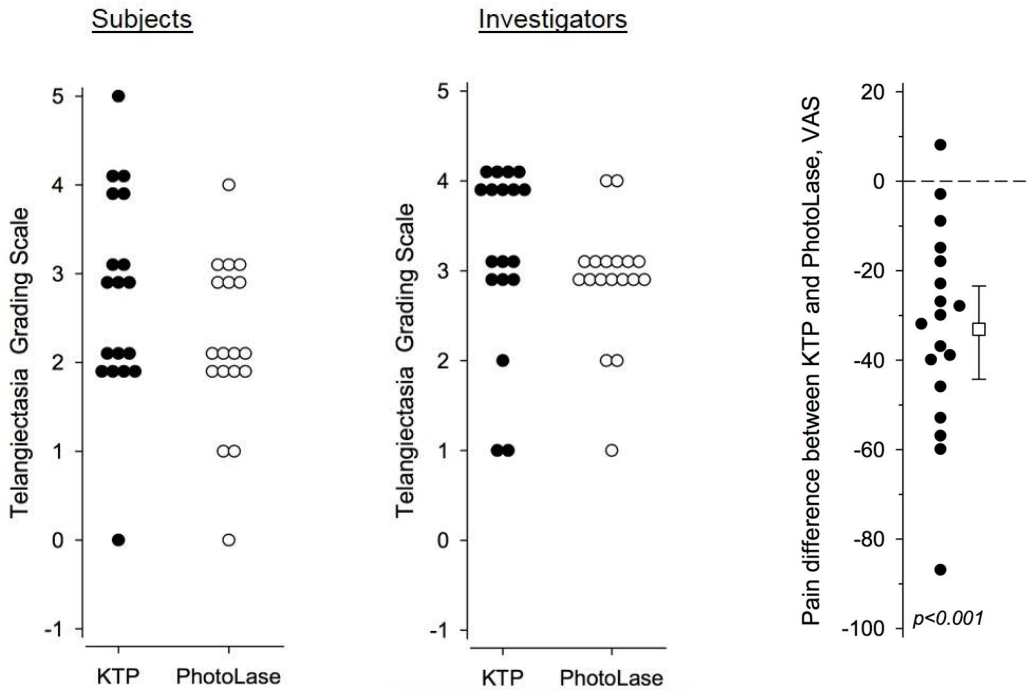

Figure 5.8. *Telangiectasia Grading Scale values assessed by the subjects (left) and the blinded investigators (middle) after one treatment. The difference of pain between KTP and PhotoLase treatments assessed by the subjects using the Visual Analogue Scale (0–100) is illustrated on the right. It shows that more pain was reported with PhotoLase treatment [P5].*

Figure 5.9 shows the before and after Visia images of a female subject with moderate telangiectasia. The left side was treated with KTP laser and the right side with PhotoLase laser. In this case, the assessed TGS values were 4 on the KTP side and 3 on the PhotoLase side after the first treatment, and 4 in both sides after the second treatment, according to the blinded investigators. In this case, the female subject assessed equal amount of improvement on both sides after both treatments. Figure 5.10 also shows the erythema-weighted Visia images.

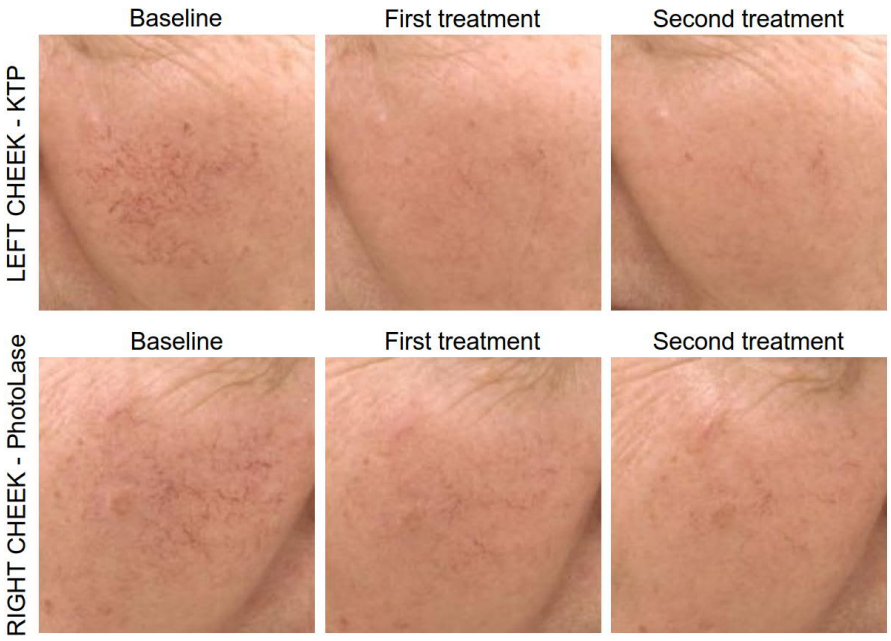

Figure 5.9. *Regular Visia images of a female subject with moderate baseline telangiectasia. More than 75% clearance of telangiectasia was observed on both cheeks after the second treatment [P5].*

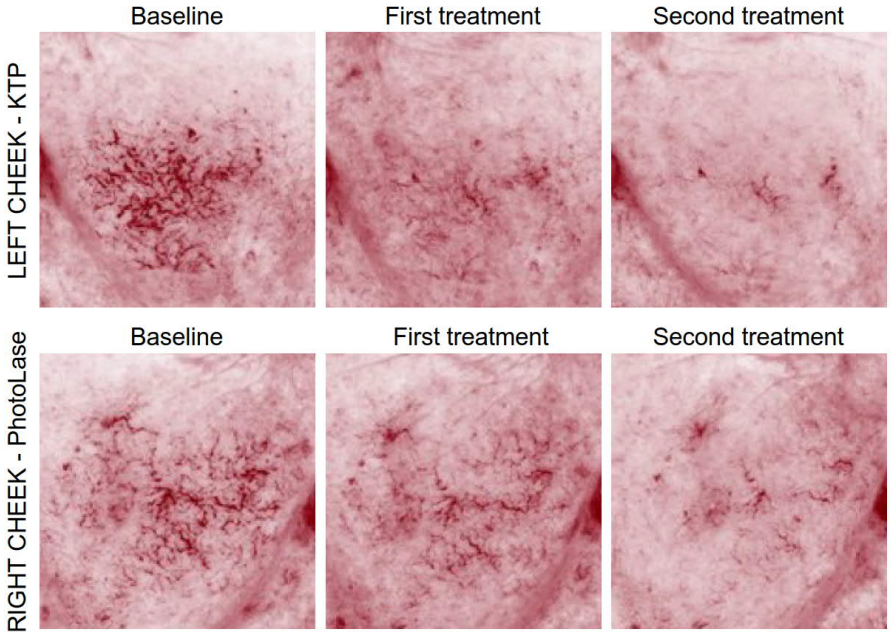

Figure 5.10. *Erythema-weighted Visia images of the same female subject. Note the added benefit of the second treatment [P5].*

5.5.3 Adverse effects

The subjects evaluated that PhotoLase treatment causes more pain than the KTP treatment. The mean VAS-value for PhotoLase was 67.6 (SD[§] 22.9) and 34.6 (SD 16.9) for KTP (shown in Figure 5.8 (*Right*)). There was no difference in the frequency of erythema, crusting or purpura between KTP and PhotoLase, as assessed using a 0–3 scale, 2-3 days after the treatments. More blistering and less edema were seen after PhotoLase treatment ($p < 0.05$, Table 5.3). A small superficial atrophic scar was noted in two subjects on the PhotoLase side.

Table 5.3. *The frequency of adverse effects 2–3 days after the first treatment with KTP and PhotoLase. The intensity of the reactions was scaled: 0=absent, 1=mild, 2=moderate, 3=severe [P5].*

Adverse effect	Treatment reactions 2–3 days after KTP treatment (%)	Treatment reactions 2–3 days after PhotoLase treatment (%)	P-value
Erythema			0.87
0	1 (6)	2 (11)	
1	7 (39)	7 (39)	
2	8 (44)	6 (33)	
3	2 (11)	3 (17)	
Crusting			0.55
0	11 (61)	9 (50)	
1	4 (22)	5 (28)	
2	3 (17)	3 (17)	
3	0 (0)	1 (6)	
Edema			0.007
0	2 (11)	3 (17)	
1	1 (6)	7 (39)	
2	5 (28)	6 (33)	
3	10 (56)	2 (11)	
Purpura			0.12
0	11 (61)	14 (78)	
1	3 (17)	3 (17)	
2	1 (6)	1 (6)	
3	1 (6)	0 (0)	

[§] Standard deviation

Blistering			0.023
0	15 (83)	10 (56)	
1	3 (17)	3 (17)	
2	0 (0)	3 (17)	
3	0 (0)	2 (11)	

5.5.4 Functionality of the yellow VECSEL system

As a secondary objective, the investigators also assessed the functionality and user-friendliness of the yellow VESCEL system. The investigators reported that the most obvious difference between the two laser systems was scanning speed. With KTP one scan of ~1 cm^2 area took 17.5 seconds, whereas with PhotoLase less than 1 second. If we assume and average of 3 seconds between treatment scans, this yields a 4.7-fold difference in treatment speed favouring PhotoLase. The Smartscan scanner was also larger, bulkier and heavier. It should be noted though that the Smartscan is older technology than the MedArt scanner and essentially both lasers could accommodate different scanners or hand pieces after some technical and software changes. The Smartscan scanner was operated using a button integrated in the scanning unit, whereas the MedArt scanner was used with a foot pedal. The investigators favoured the hand-button for easier administration of the pulses. The foot pedal employed by PhotoLase also had to be pushed very gently in order to initiate the scanning, which we deemed to be a design fault in the commercially bought foot pedal. In future designs of PhotoLase a more robust foot pedal is warranted. Both laser systems were stable during the trial period and no significant malfunctions were noted, apart from the difficulty of initiating a scan with PhotoLase foot pedal. The investigators were pleased with the touch screen control of PhotoLase, but did not find it better or worse than the KTP-laser's control panel. KTP-laser was equipped with an aiming beam, whereas this feature was missing from PhotoLase; the position of the scan pattern was only indicated by physical grooves on the distance piece. Investigators would prefer to have an aiming beam. The investigators also thought that PhotoLase was more compact, narrower, lighter and easier to carry compared to the KTP-laser.

5.5.5 Discussion and conclusions

The strengths of the study were the randomised split-face design, high-quality Visia images, and excellent subject compliance. It is also, to our knowledge, the first head-to-head study that compares a yellow (585 nm) VECSEL laser to the traditional green KTP laser in the treatment of facial telangiectasia. No serious adverse effects were reported during the study; only two

superficial non-permanent scars that resulted from blisters were noted on the PhotoLase sides. The weaknesses of the study, in retrospect, were the absence of tissue cooling which prevented the usage of higher fluences with PhotoLase, milder occurrence of facial telangiectasia on subjects, the relatively large grading steps in the TGS grading scale and older generation KTP-laser.

Other recent studies that have utilised a yellow laser (PDL or other) in the treatment of telangiectasia have reported higher as well as slightly lower cure rates than were achieved in our study (50% cure rate in 83.3% of treated areas with PhotoLase or KTP). In a study by Kapicioglu et al., the used laser parameters for a 577-nm SDL laser were a 6-mm spot size and a fluence range of 16–22 J/cm^2 [94]. The reported cure rate was 76.6% for telangiectasia after the first treatment. In another study by Tanghetti, the used laser parameters for a 595-nm PDL (V-Star, Cynosure) were a 10- to 40-ms pulse duration and a fluence range of 8.1–14.5 J/cm^2 [95]. The study also utilized Zimmer air cooling. About 80% of the subjects reached a 50% or higher cure rate with 1–2 treatments. We also found another split-face study that compared a different KTP-laser (Gemini, Laserscope) and a 595-nm PDL (Candela VBeam) in the treatment of facial telangiectasia [96]. In the study, the PDL settings were a 10-mm spot, a fluence of 7.5 J/cm2, a 10-ms pulse duration, optional pulse stacking, and dynamic nitrogen cooling spray. The KTP settings were mostly 10 J/cm^2 at 18 ms and 9 J/cm2 at 23 ms with 5- and 10-mm spot sizes, respectively, and a sapphire contact cooling. The cure rates were 62% with KTP, and 49% with PDL after the first treatment.

There are probably two main reasons for the different cure rates. Firstly, more pronounced treatment outcomes could have been obtained if the subjects in the trial had had more severe facial telangiectasia. However, our trial was conducted in the private sector, where typically also milder presentations of telangiectasia are treated compared to hospital conditions. Secondly, we did not use any cooling or topical anaesthesia to prevent possible vasoconstriction in the treatment area. The pain experienced by the subjects limited the use of higher fluences with PhotoLase, which is capable of producing fluences up to 52 J/cm^2. This pain could be alleviated with a tissue cooling device allowing us to use higher fluences (such as in other studies), which can be expected to lead even better clinical outcomes. To this end, a tissue cooling device will be added to the next design of the system and we will also consider increasing the spot size. In addition, two other technical issues will be addressed in the next design: missing aiming beam and the troublesome foot pedal.

Moreover, the third weakness arises from the insensitivity of the TGS assessment tool. We believe it explains the discrepancy in the subjects' and the investigators' assessment. Subjects might easily give different TGS scores, if they notice even a slight difference in the erythema between

face sides. Experienced clinicians, then again, will not let too small differences distract the overall assessment. In addition, the subjects' assessment was based on their memory, whereas the blinded investigators had high-quality standard and erythema-weighted images to compare the results very systematically. Finally, we acknowledge that the present study would be stronger, if the PhotoLase system had been compared to a modern PDL or large spot size KTP. The functionality and speed of modern devices are on a different level than that of Aura XP with SmartScan. Newer KTP devices with large spot size can also treat telangiectases with lower fluencies due to deeper penetration and even distribution of energy, reducing the cooling effect of blood flow [97]. On the other hand, we still considered it fair to compare the clinical outcome of the present devices, since the scanning patterns were similar and the spots sizes were close to each other in terms of diameter.

In conclusion, the yellow VESCEL system PhotoLase produced similar clinical outcome as the traditional green KTP laser. A major benefit of the PhotoLase system is the significant decrease of treatment time, which could be even further decreased by enlarging the scanning area for single illumination. The main downfall was the higher pain experienced by the subjects, which can be addressed with integrated tissue cooling. According to the investigators, the PhotoLase system can also be considered more user-friendly in the present setting. However, larger studies with optimized cooling and laser parameters are warranted to gain evidence of superiority compared to other systems. To this end, we are designing a clinical study in cooperation with INSERM and Lille Hospital (France) to be commenced in the following months. It will also be a split-face study comparing PhotoLase and KTP laser in the treatment of facial telangiectasia. The main differences to the already performed trial are the hospital setting (most likely subjects have more severe telangiectasia), the addition of a tissue cooling device (which will enable to use higher fluences with PhotoLase), larger subject group and newer KTP laser (Excel V, Cutera).

Chapter 6

Conclusions

The general objective of this thesis was to develop VECSELs at challenging wavelengths, which was fulfilled by demonstrating 20 W at 588 nm, 10 W at 615 nm and 72 W at 1178 nm. The main characteristics and results from these VECSELs are listed in Table 6.1. More specifically, the goal was to proof the potential of VECSEL-technology in medical applications. This was achieved by developing a yellow VECSEL system designed to be used in the treatment of vessel-related skin conditions, such as dilated blood vessels (telangiectasia). The system produces continuous wave yellow emission up to 8 W at a wavelength of 585 ± 5 nm. It is equipped with a handheld scanner that delivers the laser light onto skin in a desired pattern. The most important treatment parameters, fluence and pulse duration, are adjustable from the touch-screen display.

The yellow VECSEL system was tested as part of a clinical trial, which compared the efficacy of the new system to the traditional green KTP laser in the treatment of facial telangiectasia. According to the trial, there was no statistically significant difference between the efficacies of the two lasers. Over 50% cure rate was achieved with the yellow VECSEL system in 83% of the treatment areas after first treatment, and even better results were seen after two treatments. A benefit of the yellow VECSEL system was fast scanning of treatment areas provided by the scanner technology. Treatments were somewhat more painful with the yellow laser, but this could be addressed by integrating a cooling device to the system and will be tested as part of another clinical trial. No serious adverse effects were reported during the trial and the clinical investigators reported that they considered the yellow VECSEL system to be user-friendly, but would prefer to have an aiming beam and a button for light-activation rather than a foot pedal.

Table 6.1. *Summary of results from the laboratory set-up VECSELs in this thesis.*

Wavelength (nm)	Doubling crystal	Operation mode	Output power (W)	Heatsink temp. (°C)	FWHM (nm)	Opt.-to-opt. conversion efficiency
588	NCPM LBO	CW	20.0	8.3	0.2	27%
588	CPM LBO	CW	8.5	20		15%
588	CPM LBO	Pulsed, ~1 µs	14.1 (peak)	20	0.1	21%
615	NCPM LBO	CW	10.5	8	0.4	17.5%
615	NCPM LBO	CW	8.0	20		
615	NCPM LBO	Pulsed, ~1 µs	13.8 (peak)	20	0.1	20.4%
1180		CW	72	0	5.5	29%
1178		CW	19	20	0.06	14%

6.1 Prospective medical applications of VECSELs

VECSEL technology is quite mature. It has already entered the laser market providing compact solutions at various wavelengths for a wide range of applications. However, there are still some gaps in the wavelength coverage especially for high-power and single-frequency emission, particularly in the visible and UV spectral range. With further material development, efficient frequency-conversion configurations and careful cavity architecture design, VECSELs could offer tailored solution for existing applications and pave the way for new ones.

One of the main application areas for lasers is medicine. In Table 6.2, we make a modest attempt to review several medical and life science applications of lasers and discuss their requirements from the perspective of the current achievements of VECSEL technology.

Table 6.2. *A prospective list of medical and other life science applications where VECSELs could be used.*

Application	Short description & laser specifications	What VECSELs can offer
Eye surgery and retinal laser therapy	Laser light is used to coagulate blood vessels e.g. to seal tears, which can lower the risk of vision loss in various eye diseases. • 577 nm (haemoglobin absorption)	VECSELs have a compact footprint and are more affordable than e.g. PDLs. Emission at 577 nm with a good beam quality and several watts of

	• Pulsed operation with ~1 µs pulse, also few tens of milliseconds have been used. The risk of ruptures increases as pulse length decreases. Peak powers of ~2 W have been utilized [98].	output power can be achieved via intracavity frequency doubling. Microsecond pulses have been obtained by directly modulating the pump laser [P1]. Yellow diode lasers producing microsecond pulses are also available and have proved to be effective in retinal therapy [99].
Photodynamic Therapy (PDT)	Laser light is used to activate a photosensitizer to cause a photochemical process that creates free radicals and destroys targeted cells [100]. Routinely used in cancer therapy [101]. • Laser wavelength is dependent on the photosensitizer's absorption spectrum. Typically, photosensitizers have absorption peaks within 630–740 nm range. • Both CW and pulsed operation are used.	VECSELs can easily produce high-power red light via frequency doubling [102]. The wavelength versatility and broad tuning range of VECSELs could provide important benefits for dealing with a wider range of photosensitizers while employing only one laser system. On the other hand, the needs in terms of power level and brightness are met by simpler laser diode technology, whenever available for a certain wavelength.
Selective Photothermolysis (PT)	Laser light is directed to a certain tissue target, e.g. a blood vessel. The target absorbs the light producing enough heat to cause controlled damage. Often used to treat cutaneous vascular diseases such as PWSs [103], and PT is also the method behind tattoo removal. • 577 nm (haemoglobin absorption), 585–595 for deeper penetration. • Pulsed operation with few ms pulses to avoid unwanted damage [103, 104].	The preferred yellow emission is already available as a commercial VECSEL product (Genesis Taipan 577 commercialized by Coherent, delivers multi-watt output power [105]). Longer yellow wavelengths are demonstrated in this thesis and integrated into a laser system designed for medical use. In addition, medical laser company Asclepion has designed a table-top yellow laser for dermatology based on semiconductor laser technology [106].
Photoacoustics (PA)	Imaging method in which laser light is absorbed by tissue causing it to heat up. This temperature change induces sound waves which can be detected to form an image [107]. • Pulsed NIR lasers (1064 nm) are often used for deeper penetration, but visible wavelengths can be better for more targeted absorption. • Pulse duration is in the nanosecond range, repetition rate in tens of Hz and typical pulse energy is a few tens of mJ [108].	The development of VECSEL technology continuously aims for higher power and shorter pulses. However, we should note that unlike with the solid-state systems the fast carrier dynamics in VECSEL gain mirrors does not allow for energy accumulation between pulses. Cavity damping schemes have led to the generation of ns pulses with peak powers of 57 W [109].
Stimulated Emission Depletion	Aims at microscopy imaging on a smaller scale than the diffraction limit. Two laser beams are overlapped; the first laser beam	VECSELs are power scalable and they can emit continuous yellow-orange radiation and be wavelength tuned to

(STED) Microscopy	excites fluorophores in a sample and the second depletes fluorescence around the excited spot through stimulated emission. • Absorption spectrum of the fluorophores determines the laser wavelength. Common green and yellow fluorescent proteins require excitation with blue laser and depletion with yellow/orange laser (~560–600 nm). • Both lasers can be pulsed (picosecond range) or the depleting laser can be CW for simplicity and lower cost. • Few hundred mW of CW power is needed on the sample which translates to a few W of laser power [110].	match a fluorophore's absorption peak. Therefore, they would be suitable to operate as the depletion laser in STED microscopy. Other advantages are low cost for a high-power source, small footprint and reliability. Preliminary experiments were performed using a yellow VECSEL as the depleting laser in collaboration with UCL during this thesis work [111].
Flow Cytometry	Cells (or other particles) are passed through laser light one at a time and the resulting forward scatter, side scatter and fluorescence light are collected by detectors and analysed to determine multiple characteristics of cells [112, 113]. • Several visible wavelengths are required e.g. blue, green, yellow and red. • Tens of mW of CW output power is sufficient and	VECSELs can reach the visible spectrum via frequency doubling and a power scale of tens of mW is easily achievable. A possible advantageous feature is the relatively broad tuning range (~10–20 nm) for visible wavelengths. Diode and solid state lasers can also offer low-cost average power emission in the visible range.
NIR Laser Surgery	Laser light is absorbed to an extent that it vaporizes tissue leading to tissue ablation. The advantage over a conventional scalpel is that, since it is a thermal effect, the laser cut tissue is burnt and hence less bleeding occurs. Can be used to e.g. remove cancerous [114] tissue or resurface skin. • Water absorbs light increasingly from about 800 nm until 11 µm and there is a high peak around 2.9 µm [115]. Hence, IR lasers are optimal for tissue ablation. • High-power, usually pulsed, lasers are needed.	VECSELs emitting at 2 µm are mature. Power-wise they cannot yet match the currently used lasers in NIR laser surgery (such as Er:YAG laser and CO2), but average power in the range of 10 W could already be used in nano-surgery. Main advantages over solid-state systems are compactness and overall simple solution.
Multiphoton microsocpy	Based on nonlinear excitation in which light effect is confined to a volume smaller than in the case of one-photon fluorescence. This provides benefits in terms of phototoxicity and allows optical sectioning of the sample with 3D reconstruction [116]. • NIR/IR laser preferred for deep penetration, low scattering and lower	Modelocked VECSELs possess high repetition rate (1 GHz range) providing better factor of merit with lower average power, and their wavelength can be tailored to match a wide range of targets [117, 118]. In addition, they exhibit a high amplitude stability and are potentially lower cost systems

	phototoxicity, but laser wavelength dependent on fluorophore's absorption. • Ultrashort pulse duration (femtosecond range) necessary. Low power is sufficient (milliwatt range).	compared to established ultrafast solid state lasers.

Bibliography

[1] M. Guina, A. Rantamäki and A. Härkönen, “Optically pumped VECSELs: review of technology and progress,” *Journal of Physics D: Applied Physics,* vol. 50, no. 38, p. 383001, 2017.

[2] M. Zaret, G. Breinin, H. Schmidt, H. Ripps, I. Siegel and L. Solon, “Ocular lesions produced by an optical maser (laser),” *Science,* vol. 134, no. 3489, p. 1525–1526, 1961.

[3] O. Tan, J. Carney, R. Margolis, Y. Seki, J. Boll, R. Anderson and J. Parrish, “Histologic responses of portwine stains treated by argon, carbon dioxide, and tunable dye lasers: a preliminary report,” *Archives of Dermatology,* vol. 9, no. 122, p. 1016–1022, 1986.

[4] M. Mainster, “Continuous-wave and Micropulse 577 nm Yellow–orange Laser Photocoagulation: A Laser for All Reasons,” *Retina Today,* 2010.

[5] N. Farahani, M. Schiebler and L. Bentolila, “Stimulated Emission Depletion (STED) Microscopy: from Theory to Practice,” in *Microscopy: Science, Technology, Applications and Education*, Badajoz, Spain, Formatex Research Centre, 2010.

[6] C. E. Max, S. S. Olivier, H. W. Friedman, J. An, K. Avicola, B. V. Beeman, H. D. Bissinger, J. M. Brase, G. V. Erbert, D. T. Gavel, K. Kanz, M. C. Liu, B. Macintosh, K. P. Neeb, J. Patience and K. E. Waltjen, “Image improvement from a sodium-layer laser guide star adaptive optics system,” *Science,* vol. 277, no. 5332, p. 1649–1652, 1997.

[7] M. Enderlein and W. G. Kaenders, “Sodium guide star (r)evolution,” *Optik & Photonik,* vol. 11, no. 5, p. 31–35, 2016.

[8] Y. Feng, L. Taylor and D. Calia, “25 W Raman-fiber-amplifier-based 589 nm laser for laser guide star,” *Optics Express,* vol. 17, no. 21, pp. 19021-19026, 2009.

[9] D. J. Wineland, R. E. Drullinger and F. L. Walls, “Radiation pressure cooling of bound resonant absorbers,” *Physical Review Letters,* vol. 40, no. 25, p. 1636–1642, 1978.

[10] I. K. Kominis, T. W. Kornack, J. C. Allred and M. V. Romalis, “A sub femtotesla multichannel atomic magnetometer,” *Nature,* vol. 422, p. 596–599, 2003.

[11] S. Bize, P. Laurant, M. Abgrall, H. Marion, I. Maksimovic, I. Cacciapuoti, J. Grunert, C. Vinn, F. Pereira dos Santos, P. Rosenbusch, P. Lemonde, G. Santarelli, P. Wolf, A.

Clarion, A. Luiten, M. Tobar and C. Salomon, “Cold atom clocks and applications,” *Journal of Physics B,* vol. 38, no. 9, p. 449–478, 2005.

[12] H. Häffner, C. F. Roos and R. Blatt, “Quantum computing with trapped ions,” *Physics Reports,* vol. 469, no. 4, p. 155–203, 2008.

[13] S. C. Burd, D. T. C. Allcock, T. Leinonen, J.-P. Penttinen, D. H. Slichter, R. Srinivas, A. C. Wilson, R. Jördens, M. Guina, D. Leibfried and D. J. Wineland, “VECSEL systems for the generation and manipulation of trapped magnesium ions,” *Optica,* vol. 3, no. 12, p. 1294–1299, 2016.

[14] M. A. Ansari and E. Mohajerani, “Mechanisms of laser-tissue interaction: I. optical properties of tissue,” *Journal of Lasers in Medical Sciences,* vol. 2, no. 3, p. 119–125, 2011.

[15] M. M. Jawad, S. T. Abdul, A. A. Zaidan, B. B. Zaida, A. W. Naji and I. T. Abdul Qader, “An overview of laser principle, laser-tissue interaction mechanisms and laser safety precautions for medical laser uses,” *Internationa Journal of Pharmacology,* vol. 7, no. 2, p. 149–160, 2011.

[16] A. J. Welch and M. J. C. (. van Gemert, Optical-Thermal Response of Laser-Irradiated Tissue, Dordrecht, Heidelberg, London, New York: Springer, 2011.

[17] M. H. Niemz, Laser-tissue interactions, Berlin, Heidelberg: Springer-Verlag, 2007.

[18] S. Jacques, “Optical absorption of melanin,” [Online]. Available: https://omlc.org/spectra/melanin/index.html. [Accessed July 2018].

[19] S. Prahl, “Optical absorption of hemoglobin,” 1999. [Online]. Available: https://omlc.org/spectra/hemoglobin/index.html. [Accessed July 2018].

[20] D. J. Segelstein, *The complex refractive index of water,* University of Missouri-Kansas City, 1981.

[21] H.-P. Berlien, G. J. Müller, H. Breuer, N. Krasner, T. Okunata and D. Sliney, Applied Laser Medicine, Berlin Heidelberg: Springer-Verlag, 2003.

[22] V. V. Tuchin, Tissue Optics, Light Scattering Methods and Instruments for Medical Diagnostics, Third Edition, SPIE Press Book, 2015.

[23] J. Popp, V. V. Tuchin, A. Chiou and S. (. Heinemann, Handbook of Biophotonics: Volume 2: Photonics for Health Care, Weinheim: Wiley VCH, 2011.

[24] J. Popp, V. V. Tuchin, A. Chiou and S. (. Heinemann, Handbook of Biophotonics: Volume 1: Basics and Techniques, Weinheim: Wiley VCH, 2011.

[25] C. Raulin, S. Karsai and Eds, Laser and IPL technology in dermatology and aesthetic medicine, Berlin, Heidelberg: Springer, 2011.

[26] P. S. Tsai, P. Blinder, B. J. Migliori, J. Neev, Y. jin, J. A. Squier and D. Kleinfeld, “Plasma-mediated ablation: an optical tool for submicrometer surgery on neuronal and vascular systems,” *Current Opinion in Biotechnology,* vol. 20, no. 1, p. 90–99, 2009.

[27] R. R. Anderson and J. Parrish, “Selective photothermolysis: precise microsurgery by selective absoprtion of pulsed radiation,” *Science,* vol. 220, no. 4596, p. 524–527, 1983.

[28] Z. Husain and T. S. Alster, “The role of lasers and intense pulsed light technology in dermatology,” *Clinical, Cosmetic and Investigational Dermatology,* vol. 9, p. 29–40, 2016.

[29] R. Steiner, “Laser-Tissue Interactions,” in *Laser and IPL Technology in Dermatology and Aesthetic Medicine*, Springer Science & Business Media, 2011, p. 23–36.

[30] J. S. Waibel, “Pulsed Dye Laser,” in *Laser treatment of vascular lesions,* , vol. 1, S. Bard and D. J. Goldberg, Eds., New York, S. Karger AG, 2014, p. 48–73.

[31] H. McCoppin and D. J. Goldberg, “Laser treatment of facial telangiectasia: an update,” *Dermatologic Surgery,* vol. 36, no. 8, p. 1221–1230, 2010.

[32] J. S. Dover and K. A. Arndt, “New approaches to the treatment of vascular lesions,” *Lasers in Surgery and Medicine,* vol. 26, no. 2, p. 158–162, 2000.

[33] S. W. Lanigan, “Laser treatment of vascular lesions,” in *Laser Dermatology*, D. J. Goldberg, Ed., Berlin, Springer, 2015, p. 13–35.

[34] J. B. Green, K. Serowka, N. Saedi and J. Kaufman, “Potassium-Titanyl-Phosphate (KTP) laser,” in *Laser treatment of vascular lesions*, vol. 1, S. Bard and D. J. Goldberg, Eds., New York, S. Karger AG, 2014, p. 74–82.

[35] A. R. Styperek, “Argon, krypton and copper lasers,” in *Laser treatment of vascular lesions*, vol. 1, S. Bard and D. J. Goldberg, Eds., New York, S. Karger AG, 2014, p. 26–47.

[36] A. L. Technologies, “QuadroStarPRO YELLOW,” [Online]. Available: https://www.asclepion.com/asclepion_product/quadrostar-pro-yellow/. [Accessed July 2018].

[37] Q. Systems, “Discovery Aesthetics: 585,” [Online]. Available: http://www.quantasystem.com/en/aesthetics/585/. [Accessed July 2018].

[38] Advalight. [Online]. Available: http://advalight.com/. [Accessed July 2018].

[39] N. Basov, O. Bogdankevich and A. Grasyuk, "9B4 - Semiconductor lasers with radiating mirrors," *Journal of Quantum Electronics,* vol. 2, no. 9, p. 594–597, 1966.

[40] W. Jiang, S. Friberg, H. Iwamura and Y. Yamamoto, "High powers and subpicosecond pulses from an external-cavity surface-emitting InGaAs/InP multiple quantum well laser," *Applied Physics Letters,* vol. 58, no. 8, p. 807–809, 1991.

[41] H. Le, S. Cecca and A. Mooradian, "Scalable high-power optically pumped GaAs laser," *Applied Physics Letters,* vol. 58, no. 18, p. 1967–1969, 1991.

[42] M. Kuznetsov, F. Hakimi, R. Sprague and A. Mooradian, "High-power (> 0.5-W CW) diode-pumped vertical-external-cavity surface-emitting semiconductor lasers with circular TEM00 beams," *Photonics Technology Letters,* vol. 9, no. 8, p. 1063–1065, 1997.

[43] M. Kuznetsov, F. Hakimi, R. Sprague and A. Mooradian, "Design and characteristics of high-power (> 0.5-W CW) diode-pumped vertical-external-cavity surface-emitting semiconductor lasers with circular TEM00 beams," *Journal of Selected Topics in Quantum Electronics,* vol. 5, no. 3, p. 561–573, 1999.

[44] O. Okhotnikov, Semiconductor Disk Lasers: Physics and Technology, New York: Wiley, 2010.

[45] J. Berger, D. Anthon, A. Caprara, J. Chilla, S. Govorkov, A. Lepert, W. Mefferd, Q.-Z. Shu and L. Spinelli, "20 Watt CW TEM00 intracavity doubled optically pumped semiconductor laser at 532 nm," in *SPIE Proceedings 8242, VECSELs II*, San Francisco, USA, 2012.

[46] F. Zhang, B. Heinen, M. Wichmann, C. Möller, B. Kunert, A. Rahimi-Iman, W. Stolz and M. Koch, “A 23-watt single-frequency vertical-external-cavity surface-emitting laser,” *Optics Express,* vol. 22, no. 11, p. 12817–12822, 2014.

[47] U. Keller and A. Tropper, "Passively modelocked surface-emitting semiconductor lasers," *Physics Reports,* vol. 429, no. 2, p. 67–120, 2006.

[48] C. Symonds, J. Dion, I. Sagnes, M. S. M. Dainese, L. Leroy and J. Oudar, “High performance 1.55 µm vertical external cavity surface emitting laser with broadband integrated dielectric-metal mirror,” *Electronics Letters,* vol. 40, no. 12, p. 734–735, 2004.

[49] A. Rantamäki, E. Saarinen, J. Lyytikäinen, K. Lahtonen, M. Valden and O. Okhotnikov, “High power semiconductor disk laser with a semiconductor-dielectric -metal compound mirror,” *Applied Physics Letters,* vol. 104, no. 10, p. 101110, 2014.

[50] H. Kahle, C. Mateo, U. Brauch, P. Tatar-Mathes, R. Bek, M. Jetter, T. Graf and P. Michler, “Semiconductor membrane external-cavity surface-emitting laser (MECSEL),” *Optica,* vol. 3, no. 12, p. 1506–1512, 2016.

[51] V. Iakovlev, J. Walczak, M. Gębski, A. Sokół, M. Wasiak, P. Gallo, A. Sirbu, R. Sarzała, M. Dems, T. Czyszanowski and E. Kapon, “Double-diamond high-contrast-gratings vertical external cavity surface emitting laser,” *Journal of Physics D: Applied Physics,* vol. 47, no. 6, p. 065104, 2014.

[52] S. Ranta, T. Hakkarainen, M. Tavast, J. Lindfors, T. Leinonen and M. Guina, "Strain compensated 1120nm GaInAs/GaAs vertical external-cavity surface-emitting laser grown by molecular beam epitaxy," *Journal of Crystal Growth,* vol. 335, no. 1, p. 4–9, 2011.

[53] M. Schmid, S. Benchabane, F. Torabi-Goudarzi, R. Abram, A. Ferguson and E. Riis, "Optical in-well pumping of a vertical-external-cavity surface-emitting laser," *Applied Physics Letters,* vol. 84, no. 24, p. 4860, 2004.

[54] R. Bedford, M. Kolesik, J. Chilla, M. Reed, T. Nelson and J. Moloney, “Power-limiting mechanisms in VECSELs,” in *SPIE Proceedings 5814, Enabling Photonics Technologies for Defense, Security, and Aerospace Applications*, Orlando, USA, 2005.

[55] A. Haug, “Auger recombination in direct-gap semiconductors: band-structure effects,” *Journal of Physics C: Solid State Physics,* vol. 16, no. 21, p. 4159–4172, 1983.

[56] A. Tropper and S. Hoogland, "Extended cavity surface-emitting semiconductor lasers," *Progress in Quantum Electronics,* vol. 30, no. 1, p. 1–43, 2006.

[57] N. Schulz, M. Rattunde, C. Ritzenthaler, B. Rösener, C. Manz, K. Köhler, J. Wagner and U. Brauch, "Resonant optical in-well pumping of an (AlGaIn)(AsSb)-based vertical-external-cavity surface-emitting laser emitting at 2.35µm," *Applied Physics Letters,* vol. 91, no. 9, p. 091113, 2007.

[58] T.-L. Wang, Y. Kaneda, J. Yarborough, J. Hader, J. Moloney, A. Chernikov, S. Chatterjee, S. Koch, B. Kunert and W. Stolz, "High-Power Optically Pumped Semiconductor Laser at 1040 nm," *IEEE Photonics Technology Letters,* vol. 22, no. 9, p. 661–663, 2010.

[59] Z. Liau, "Semiconductor wafer bonding via liquid capillarity," *Applied Physics Letters,* vol. 77, no. 5, p. 651–653, 2000.

[60] A. Maclean, A. Kemp, S. Calvez, J. Kim, T. Kim, M. Dawson and D. Burns, "Continuous tuning and efficient intracavity second-harmonic generation in a semiconductor disk laser with an intracavity diamond heatspreader," *IEEE Journal of Quantum Electronics,* vol. 44, no. 3, p. 216–225, 2008.

[61] M. Guina, E. Kantola, T. Leinonen and A. Rantamäki, “Semiconductor Disk Lasers,” in *Semiconductor laser and diode-based light sources for biophotonics*, IET Books, To be published.

[62] A. Rantamäki, J. Lindfors, M. Silvennoinen, K. J., M. Tavast and O. Okhotnikov, “Low temperature gold-to-gold bonded semiocnductor disk laser,” *Photonics Technology Letters,* vol. 25, no. 11, p. 162–5, 2013.

[63] J. Perez, A. Laurain, L. Cerutti, I. Sagnes and A. Garnache, “Technologies for thermal management of mid-IR Sb-based surface emitting lasers,” *Semiconductor Science and Technology,* vol. 25, no. 4, p. 045021, 2010.

[64] S. Govorkov and L. Spinelli, “Optically-pumped surface-emitting semiconductor laser with heat-spreader compound mirror-structure”. US Patent Patent 8,611,383 17, December 2013.

[65] B. Heinen, T.-L. Wang, M. Sparenberg, A. Weber, B. Kunert, J. Hader, S. Koch, J. Moloney, M. Koch and W. Stolz, “106 W continuous-wave output power from vertical-external-cavity surface-emitting laser,” *Electronics Letters,* vol. 48, no. 9, p. 516–517, 2012.

[66] E. Kantola, T. Leinonen, J.-P. Penttinen, V.-M. Korpijärvi and M. Guina, "615 nm GaInNAs VECSEL with output power above 10 W," *Optics Express,* vol. 23, no. 16, p. 20280–20287, 2015.

[67] E. Saarinen, A. Härkönen, S. Suomalainen and O. Okhotnikov, “Power scalable semiconductor disk laser using multiple gain cavity,” *Optics Express,* vol. 14, no. 26, p. 12868–12871, 2006.

[68] L. Fan, M. Fallahi, J. Hader, A. Zakharian, J. Moloney, R. Bedford, W. Stolz and S. Koch, “Multichip vertical-external-cavity surface-emitting lasers: a coherent power scaling scheme,” *Optics Letters,* vol. 31, no. 24, p. 3612–3614, 2006.

[69] C. Borgentum, J. Bengtsson, A. Larsson, F. Demaria, A. Hein and P. Unger, “Optimization of a broad gain element for a widely tunable high-power semiconductor disk laser,” *Photonics Technology Letters,* vol. 22, no. 13, p. 978–980, 2010.

[70] J. Paajaste, S. Suomalainen, R. Koskinen, A. Härkönen, M. Guina and M. Pessa, "High-power and broadly tunable GaSb-based optically pumped VECSELs emitting near 2μm," *Journal of Crystal Growth,* vol. 311, no. 7, p. 1917–1919, 2011.

[71] A. Khiar, M. Rahim, M. Fill, F. Felder, F. Hobrecker and H. Zogg, “Continuosly tunable monomode mid-infrared vertical external cavity surface emitting laser on Si,” *Applied Physics Letters,* vol. 97, no. 15, p. 151104, 2010.

[72] P. Klopp, U. Griebner, M. Zorn and M. Weyers, "Pulse repetition rate up to 92 GHz or pulse duration shorter than 110 fs from a mode-locked semiconductor disk laser," *Applied Physics Letters,* vol. 98, no. 7, p. 071103, 2011.

[73] D. Waldburger, S. Link, M. Mangold, C. Alfieri, E. Gini, M. Golling, B. Tilma and U. Keller, “High-power 100 fs semiconductor disk lasers,” *Optica,* vol. 3, no. 8, p. 844–52, 2016.

[74] S. Yellen, R. Waters, Y. Chen, B. Soltz, S. Fischer, D. Fekete and J. Ballantyne, “20 000 h InGaAs quantum well lasers,” *Electronics Letters,* vol. 26, no. 25, p. 2038–2048, 1990.

[75] W. Horn, “HIgh power diode lasers for industrial applications,” *Laser Technik Journal,* vol. 4, no. 3, p. 62–65, 2007.

[76] M. Jetter, B. Roman, H. Kahle and P. Michler, “MECSEL: new concept for optically pumped semiconductor disk lasers with versatile wavelength,” in *SPIE Proceedings 10682, Semiconductor Lasers and Laser Dynamics VIII*, Starsbourg, France, 2018.

[77] M. Guina, T. Leinonen, A. Härkönen and M. Pessa, "High-power disk lasers based on dilute nitride heterostructures," *New Journal of Physics,* vol. 11, no. 12, p. 125019, 2009.

[78] V.-M. Korpijärvi, T. Leinonen, J. Puustinen, A. Härkönen and M. Guina, "11 W single gain-chip dilute nitride disk laser emitting around 1180 nm," *Optics Express,* vol. 18, no. 25, p. 25633–25641, 2010.

[79] V.-M. Korpijärvi, E. Kantola, T. Leinonen, R. Isoaho and M. Guina, “Monolithic GaInNaAsSb/GaAs VECSEL operating at 1550 nm,” *Journal of Selelected Topics in Quantum Electronics,* vol. 21, no. 6, p. 480–484, 2015.

[80] V. Iakovlev, T. Leinonen, A. Sirbu, E. Kapon and M. Guina, “33 W continuous output power of 1275 nm semiconductor disk laser,” *Optics Express,* vol. 25, no. 6, p. 7008–7013, 2017.

[81] J. Rautiainen, J. Lyytikäinen, A. Sirbu, A. Mereuta, A. Caliman, E. Kapon and O. Okhotnikov, "2.6 W optically-pumped semiconductor disk laser operating at 1.57-µm using wafer fusion," *Optics Express,* vol. 16, no. 26, p. 21 881–21 886, 2008.

[82] M. Rahim, F. Felder, M. Fill and H. Zogg, "Optically pumped 5 µm IV-VI VECSEL with Al-heat spreader," *Optics Letters,* vol. 33, no. 24, p. 2008, 3010-3012.

[83] M. Rahim, M. Fill, F. Felder, D. Chappuis, M. Corda and H. Zogg, “Mid-infrared PbTe vertical external cavity surface emitting laser on Si-substrate with above 1 W output power,” *Applied Physics Letters,* vol. 95, no. 24, p. 241107, 2009.

[84] J. Armstrong, J. Bloemnergen, J. Ducing and P. Pershan, “Interactions between light waves and nonlinear dielectric,” *Physical Review,* vol. 127, no. 6, p. 1918–1939, 1962.

[85] R. W. Boyd, Nonlinear optics, 2nd ed., San Diego, Ca: Academic Press, 2003.

[86] R. L. Sutherland, Handbook of Nonlinear Optics, 2nd ed., New York: Marcel Dekker, Inc., 2003.

[87] V. G. Dmitriev, G. G. Gurzadyan and D. N. Nikogosyan, Handbook of nonlinear optical crystals, 3rd ed., Berlin: Springer, 1999.

[88] M. Houe and P. Townsend, “An introduction to methods of periodic poling for second-harmonic generation,” *Journal of Physics D,* vol. 28, no. 9, p. 1747–1763, 1995.

[89] C. Xu, H. Okayama and Y. Ogawa, “Photorefractive damage of LiNbO3 quasiphase matched wavelength converters,” *Journal of Applied Physics,* vol. 87, no. 7, p. 3203–3208, 2000.

[90] Q.-Z. Shu, A. Caprara, J. Berger, D. Anthon, H. Jerman and L. Spinelli, “Intracavity-tripled optically-pumped semiconductor laser at 355 nm,” in *SPIE Proceedings 7193, Solid State Lasers XVIII*, San Jose, USA, 2009.

[91] Smith and A., “AS-Photonics: SNLO,” 2018. [Online]. Available: http://www.as-photonics.com/snlo. [Accessed September 2018].

[92] I. O. f. Standarization, “ISO homepage,” [Online]. Available: https://www.iso.org/home.html. [Accessed August 2018].

[93] E. Comission, “Medical Devices,” [Online]. Available: https://ec.europa.eu/growth/single-market/european-standards/harmonised-standards/medical-devices_en. [Accessed August 2018].

[94] Y. Kapicioglu, G. Sarac and H. Cenk, “Treatment of erythematotelangiectatic rosacea, facial erythema, and facial telangiectasia with a 577-nm pro-yellow laser: a case series,” *Lasers in Medical Science,* ePub ahead of print 31 July 2018.

[95] E. A. Tanghetti, “Split-face randomized treatment of facial telangiectasia comparing pulsed dye laser and an intense pulsed light handpiece,” *Lasers in Surgery and Medicine,* vol. 44, p. 97–102, 2012.

[96] N. Uebelhoer, M. Bogle, B. Stewart, K. Arndt and J. A. Dover, “split-face comparison study of pulsed 532-nm KTP laser and 595-nm pulsed dye laser in the treatment of facial

telangiectasias and diffuse telangiectatic facial erythema," *Dermatologic Surgery,* vol. 33, no. 4, p. 441–448, 2007.

[97] B. Kwiek, M. Ambroziak, K. Osipowicz, K. C. and M. Rozalski, "Treatment of previously treated facial capillary malformations: results of single-center retrospective objective 3-dimensional analysis of teh efficacy of large spot 532 nm lasers," *Dermatologic surgery,* vol. 44, no. 6, p. 803–813, 2018.

[98] C. Sramek, L. Leung, Y. Paulus and D. Palanker, "Therapeutic window of retinal photocoagulation with green (532-nm) and yellow (577-nm) lasers," *Ophthalmic Surgery, Lasers and Imaging Retina,* vol. 43, no. 4, p. 341–347, 2012.

[99] J. D. Walker, "Initial experience with a yellow diode laser," *Retina: Advanced Ocular Care,* p. 34–36, 2011.

[100] S. Brown, E. Brown and I. Walker, "The present and future role of photodynamic therapy in cancer treatment," *The Lancet Oncology,* vol. 5, no. 8, p. 497–508, 2004.

[101] T. Dougherty, C. Gomer, B. Henderson, G. Jori, D. Kessel, M. Korbelik, J. Moan and Q. Peng, "Photodynamic therapy," *Journal of the National Cancer Institute,* vol. 90, no. 12, p. 889–905, 1998.

[102] S. Ranta, A. Härkönen, T. Leinonen, L. Orsila, J. Lyytikäinen, G. Steinmeyer and M. Guina, "Mode-locked VECSEL emitting 5 ps pulses at 675 nm," *Optics Letters,* vol. 38, no. 13, p. 2289–2291, 2013.

[103] K. Kelly, B. Choi, S. McFarlane, A. Motosue, B. Jung, M. Khan, J. Ramirez-San-Juan and J. Nelson, "Description and analysis of treatments for port-wine stain birthmarks," *Archives of Facial Plastic Surgery,* vol. 7, no. 5, p. 287–294, 2005.

[104] C. Dierickx, J. Casparian, V. Venugopalan, W. Farinelli and R. Anderson, "Thermal relaxation of port-wine stain vessels probed in vivo: the need for 1-10-millisecond laser pulse treatment," *Journal of Investigative Dermatology,* vol. 105, no. 5, p. 709–714, 1995.

[105] Coherent Inc., "Genesis Taipan HD-Series; High-Definition, High-Power Optically Semiconductor Lasers (OPSL)," [Online]. Available: https://cohrcdn.azureedge.net/assets/pdf/Genesis_Taipan_HD_Series_Datasheet_2016.pdf. [Accessed 25 09 2017].

[106] "QuadroStarPRO YELLOW," Asclepion, [Online]. Available: http://www.asclepion.com/asclepion_product/quadrostar-pro-yellow/. [Accessed January 2018].

[107] L. Wang and S. Hu, "Photoacoustic tomography: in vivo imaging from organelles to organs," *Science,* vol. 335, no. 6075, p. 1458–1462, 2012.

[108] M. Xu and L. Wang, "Photoacoustic Imaging in Biomedicine," *Review of Scientific Instruments,* vol. 77, no. 4, p. 041101, 2006.

[109] V. Savitski, J. Hastie, S. Calvez and M. Dawson, "Cavity-dumping of a semiconductor disk laser for the generation of wavelength-tunable micro-Joule nanosecond pulses," *Optics Express,* vol. 18, no. 11, p. 11933–11941, 2010.

[110] A. Honigmann, C. Eggeling, M. Schulze and A. Lepert, "Biophotonics: Super-resolution STED microscopy advances with yellow CW OPSL," *Laser Focus World,* vol. 48, no. 1, 2012.

[111] E. Bailey, R. Marsh, S. Culley, E. Kantola, M. Guina and A. Bain, "Time and polarization resolved CW STED photodeselection in molecular probes," in *SPIE Proceedings 8950*, San Francisco, USA, 2014.

[112] M. Brown and C. Wittwer, “Flow cytometry: principles and clinical applications in hematology,” *Clinical Chemistry,* vol. 46, no. 8, p. 1221–1229, 2000.

[113] S. Cho, J. Godin, C.-H. Chen, W. Qiao, H. Lee and Y.-H. Lo, “Review Article: Recent advancements in optofluidic flow cytometer,” *Biomicrofluidics,* vol. 4, no. 4, p. 043001, 2010.

[114] N. Fried and K. Murray, “High-power thulium fiber laser ablation of urinary tissues at 1.94 µm,” *Journal of Endourology,* vol. 19, no. 1, p. 25–31, 2005.

[115] A. Welch and M. Van Gemert, Eds., Optical-thermal response of laser-irradiated tissue, vol. 2, Springer, 2001, p. 45.

[116] C. Xu, W. Zipfel, J. B. Shear, R. M. Williams and W. W. and Webb, “Multiphoton fluorescence excitation: new spectral windows for biological nonlinear microscopy,” *Proceedings of National Academy of Sciences of the United States of America,* vol. 90, no. 20, p. 10763–10768, 1996.

[117] R. Aviles-Espinosa, G. Filippidis, C. Hamilton, G. Malcolm, K. J. Weingarten, T. Südmeyer, Y. Barbarin, U. Keller, S. I.C.O Santos, D. Artigas and P. and Loza-Alvarez, “Compact ultrafast semiconductor disk laser: targeting GFP based nonlinear applications in living organisms,” *Biomedical Optics Express,* vol. 2, no. 4, p. 739–747, 2011.

[118] F. F. Voigt, F. Emaury, P. Bethge, D. Waldburger, S. M. Link, S. Carta, A. van der Bourg, F. Helmchen and U. and Keller, “Multiphoton in vivo imaging with a femtosecond semiconductor disk laser,” *Biomedical Optics Express,* vol. 8, no. 7, p. 3213–3231, 2017.

[119] K. Kato, “Temperature-tuned 90 degree phase-matching properties of LiB3O5,” *IEEE Journal of Quantum Electronics,* vol. 30, no. 12, p. 2950–2952, 1994.

P1

Publication 1

E. Kantola, T. Leinonen, S. Ranta, M. Tavast, and M. Guina, “High-efficiency 20 W yellow VECSEL,” *Optics Express*, vol. 22, no. 6, p. 6372–6380, 2014.

© 2014 Optical Society of America. Reprinted with kind permission.

High-efficiency 20 W yellow VECSEL

Emmi Kantola,* Tomi Leinonen, Sanna Ranta, Miki Tavast and Mircea Guina

Optoelectronics Research Centre, Tampere University of Technology, Korkeakoulunkatu 3, FIN-33101 Tampere, Finland

emmi.kantola@tut.fi

Abstract: A high-efficiency optically pumped vertical-external-cavity surface-emitting laser emitting 20 W at a wavelength around 588 nm is demonstrated. The semiconductor gain chip emitted at a fundamental wavelength around 1170-1180 nm and the laser employed a V-shaped cavity. The yellow spectral range was achieved by intra-cavity frequency doubling using a LBO crystal. The laser could be tuned over a bandwidth of ~26 nm while exhibiting watt-level output powers. The maximum conversion efficiency from absorbed pump power to yellow output was 28 % for continuous wave operation. The VECSEL's output could be modulated to generate optical pulses with duration down to 570 ns by directly modulating the pump laser. The high-power pulse operation is a key feature for astrophysics and medical applications while at the same time enables higher slope efficiency than continuous wave operation owing to decreased heating.

© 2014 Optical Society of America

OCIS codes: (140.3460) Lasers; (140.3480) Lasers, diode-pumped; (140.3515) Lasers, frequency doubled; (140.3538) Lasers, pulsed; (140.3600) Lasers, tunable; (140.5960) Semiconductor lasers.

References and links

1. O.T. Tan, J. M Carney, R. Margolis, Y. Seki, J. Boll, R. R. Anderson, and J. A. Parrish, "Histologic responses of portwine stains treated by argon, carbon dioxide, and tunable dye lasers: a preliminary report," Arch Dermatol. **122**(9), 1016-1022 (1986).
2. M.A. Mainster, "Continuous-wave and micropulse 577 nm yellow–orange laser photocoagulation: a laser for all reasons," Retina Today, 1-8 (2010).
3. N. Farahani, M. J. Schibler, and L. A. Bentolila, "Stimulated emission depletion (STED) microscopy: from theory to practice," In Microscopy: Science, Technology, Applications and Education, A. Méndez-Vilas, J. Díaz, Eds., Formatex Research Center: Badajoz, Spain, **2**, 1539-1547 (2010).
4. M.A. Mainster, "Wavelength selection in macular photocoagulation. Tissue optics, thermal effects, and laser systems," Ophthalmology **93**(7), 952-958 (1986).
5. C. E. Max, S. S. Oliver, H. W. Friedman, J. An, K. Avicola, B. W. Beeman, H. D. Bissinger J. M. Brase, G. V. Erbert, D. T. Gavel, K. Kanz, M. C. Liu, B. Macintosh, K. P. Neeb, J. Patience, and K. E. Waltjen, "Image improvement from sodium-layer laser guide star adaptive optic system," Science **277**(5332), 1649-1652 (1997).
6. L. Toikkanen, A. Härkönen, J. Lyytikäinen, T. Leinonen, A. Laakso, A. Tukiainen, J. Viheriälä, M. Bister, and M. Guina, "Optically pumped edge-emitting GaAs-based laser with direct orange emission," Photon. Technol. Lett. **26**(4), 384-386 (2014).
7. Y. Yao, Q. Zheng, D. P. Qu, K. Zhou, Y. Liu, and L. Zhao, "All-solid-state continuous-wave frequency doubled Nd:YAG/LBO laser with 1.2 W output power at 561 nm, " Laser Phys. Lett. **7**(2), 112-115 (2010).
8. M. Kuznetsov, F. Hakimi, R. Sprague, and A. Mooradian, "Design and characteristics of high power (>0.5-W CW) diode-pumped vertical-external-cavity surface-emitting semiconductor lasers with circular TEM_{00} beams," J. Select. Topics Quantum Electron. **5**(3), 561-573 (1999).
9. B. Rudin, A. Rutz, M. Hoffmann, D.J.H.C. Maas, A.-R. Bellancourt, E. Gini, T. Südmeyer, and U. Keller, "Highly efficient optically pumped vertical-emitting semiconductor laser with more than 20 W average output power in a fundamental transverse mode," Opt. Lett. **33**(22), 2719–2721 (2008).
10. T.-L. Wang, Y. Kaneda, J.M. Yarborough, J. Hader, J.V. Moloney, A. Chernikov, S. Chatterjee, S.W. Koch, B. Kunert, and W. Stolz, "High-power optically pumped semiconductor laser at 1040 nm," Photon. Technol. Lett. **22**(9), 661-663 (2010).
11. J. Hastie, S. Calvez, M. Dawson, T. Leinonen, A. Laakso, J. Lyytikäinen, and M. Pessa, "High power CW red VECSEL with linearly polarized TEM_{00} output beam," Opt. Express **13**, 77-81 (2005).
12. S. Ranta, M. Tavast, T. Leinonen, N. Van Lieu, G. Fetzer, and M. Guina, "1180 nm VECSEL with output power beyond 20 W," Electron. Lett. **49**(1), 59-60 (2013).
13. N. Schulz, M. Rattunde, C. Manz, K. Koehler, C. Wild, J. Wagner, S.-S. Beyertt, U. Brauch, T. Kuebler, and A. Giesen, "Optically pumped GaSb-based VECSEL emitting 0.6 W at 2.3 μm," Photon. Technol. Lett. **18**(9), 1070-1072 (2006).
14. M. Rahim, F. Felder, M. Fill, and H. Zogg, "Optically pumped 5 μm IV-VI VECSEL with Al-heat spreader," Opt. Lett. **33**(24), 3010-3012 (2008).
15. L. Fan, M. Fallahi, A. Zakharian, J. Hader, J. Moloney, R. Bedford, J. Murray, W. Stolz, and S. Koch, "Extended tunability in a two-chip VECSEL," Photon. Technol. Lett. **19**(8), 544-546 (2007).

16. C. Borgentum, J. Bengtsson, A. Larsson, F. Demaria, A. Hein, and P. Unger, "Optimization of a broadband gain element for a widely tunable high-power semiconductor disk laser," Photon. Technol. Lett. **22**(13), 78-980 (2010).
17. N. Hempler, J.-M. Hopkins, A. Kamp, N. Schulz, M. Rattude, J. Wagner, M. Dawson, and D. Burns, "Pulsed pumping of semiconductor disk lasers", Opt. Express **15**(6), 3247-3256 (2007).
18. T. Leinonen, V.-M. Korpijärvi, A. Härkönen, and M. Guina, "7.4W yellow GaInNAs-based semiconductor disk laser," Electron. Lett. **47**(20), 1139-1140 (2011).
19. M. Fallahi, L. Fan, Y. Kaneda, C. Hessenius, J. Hader, H. Li, J. V. Moloney, B. Kunert, W. Stolz, S. W. Koch, J. Murray, and R. Bedford, "5-W yellow laser by intracavity frequency doubling of high-power vertical-external-cavity surface-emitting laser," Photon. Technol. Lett. **20**(20), 1700-1702 (2008).
20. J. Rautiainen, I. Krestnikov, J. Nikkinen, and O. G. Okhotnikov, " 2.5 W orange power by frequency conversion from dual-gain quantum-dot disk laser," Opt. Lett. **35**(12), 1935-1037 (2010).

1. Introduction

Practical and cost-effective yellow lasers are needed in many important medical applications including dermatology, eye surgery and novel imaging methods. In these applications, overall results can be improved, damage to healthy tissue decreased, or resolution increased by implementing a laser that can be tuned to a preferred wavelength and work in pulsed operation instead of continuous wave [1-3]. The yellow spectral range is particularly interesting in medicine due to increased interaction with hemoglobin in blood, which has high absorption peaks in this range. In addition, some of the most common fluorescent markers often used in fluorescence based medical imaging have their depletion wavelength in the yellow range [3]. For medical applications pulsed operation is often preferred due to increased efficiency and decreased damage to healthy tissue; for example in photocoagulation based eye surgery the ideal pulse width is in the order of 1 μs [4]. Furthermore, the availability of reliable yellow lasers able to operate in pulsed mode would impact scientific application areas, such as astronomy, where lasers emitting narrow linewidth at the sodium absorption line (589nm) can be used to create a laser guide star for earth-based telescopes [5].

The yellow spectral range cannot be reached via direct emission from semiconductor lasers, which is the preferred laser technology when taking into account compactness, cost, efficiency, reliability, and wavelength coverage. The shortest wavelength in the orange region recently demonstrated for direct emission is 599 nm yet the efficiency of the GaInP material system used in this case is rather modest [6]. Alternative yellow laser solutions make use of amplification and frequency conversion in solid-state systems [7] but the complexity, price, and often their limitations in power and wavelength coverage, render them unsuitable for a wide exploitation. A much more attractive path to generate yellow radiation has emerged with the development of vertical-external-cavity surface-emitting lasers (VECSELs), also known as semiconductor disk lasers (SDLs) [8]. These are compact, power scalable laser sources that are able to maintain good beam quality even when emitting output powers in excess of several watts to several tens of watts [9,10]. Owing to the wavelength versatility of semiconductor gain region they can cover an extremely large emission spectrum by direct emission from 670 nm up to 5000 nm [11-14], yet not without gaps, and can be tuned over tens of nanometers [15,16]. Moreover, unlike the solid state disk lasers, owing to the lower carrier lifetimes the output of VECSELs/SDLs can be modulated on a time scale of a few hundreds of nanosecond by directly modulating the pump laser that at the same time can alleviate the need for advanced cooling [17]. VECSELs emitting in the 1140-1260 nm range can be efficiently converted to yellow region using intra-cavity nonlinear crystals [18] however their output powers and their conversion efficiency has been rather modest compared to VECSELs operating at 1064/532 nm. This is to large extent due to the fact that longer wavelength gain regions bring more challenges compared to standard InGaAs/GaAs gain mirrors used for 960-1060 nm window.

In this article, we demonstrated a frequency doubled yellow VECSEL emitting 20 W output power with moderate cooling. The measured output power is an improvement of over 12 W over the previously reported yellow VECSEL [18]. Furthermore, the conversion efficiency from absorbed pump power to yellow output power has been improved from 17 % to 28 %. For GaInAs QW gain material the previous state of the art results were 5 W of 589 nm radiation with ~16 % conversion efficiency [19]. Frequency doubled yellow radiation has also been demonstrated with QDs, but with significantly lower output power and even lower efficiency (~5 %) compared to QW structures [20].

Besides the CW operation, we have also implemented a pulse modulation scheme using direct modulation of the pump lasers. The demonstrated pulse duration in the range of 1µs is a good fit to requirements pertinent to medical and guide star applications. Even if the pulse duration is rather long, it could still ease the thermal load and provided further means to increase the power and improve the overall system efficiency.

2. Experimental setup

The semiconductor gain mirror was grown by molecular beam epitaxy (MBE) with an active region that incorporated 10 GaInAs/GaAs/GaAsP quantum wells grown on top of a 25.5-pair AlAs/GaAs distributed Bragg reflector (DBR). The structure is illustrated in a more detailed manner in Fig. 1. The gain structure was designed to be anti-resonant at 1180 nm. For efficient thermal management, the gain mirror was diced into 2.5 mm x 2.5 mm chips that were capillary bonded to a wedged (2°) intra-cavity CVD diamond heat spreader, which was attached to a water-cooled copper mount with indium foil. The outer surface of the heat spreader was antireflection coated for the designed 1180 nm emission. The operation of the gain material at the fundamental wavelength has already been tested and the results were published in [12]. A maximum output power of 23 W at ~1180 nm was obtained with a 97 % reflecting output coupler.

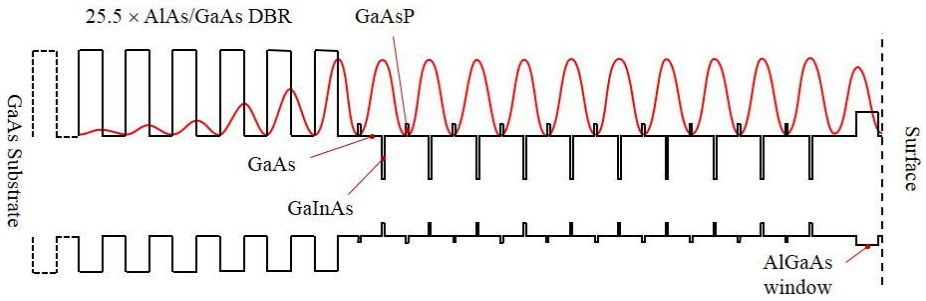

Fig. 1. Schematic illustration of the semiconductor layer structure.

The VECSEL cavity was formed by the gain mirror, a folding mirror (RoC = 75 mm) and a flat end mirror in a V-shaped configuration with the first arm having a length of 102 mm and the second 47 mm. A 1.5 mm thick birefringent filter (BRF) and a 100 µm thick etalon were placed along the first arm of the cavity to achieve wavelength tuning and linewidth narrowing. For efficient second harmonic generation, a 10 mm non-critically phase matched lithium triborate crystal (NCPM LBO) (and later a 10 mm critically phase matched (CPM) LBO crystal) was inserted near the flat end mirror where the mode waist was situated. The crystal facets were flat and had an antireflection coating for the fundamental as well as for the yellow radiation. Phase matching was achieved via temperature tuning the crystal with a TEC operated copper oven. The cavity configuration is shown in Fig. 2.

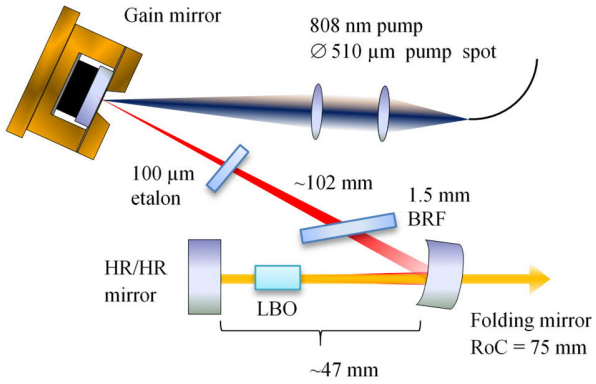

Fig. 2. Schematic illustration of the frequency doubled VECSEL.

All the cavity mirrors were highly reflective for the fundamental radiation. The flat end mirror was also highly reflective for the yellow radiation, however the folding mirror was highly transmissive (R < 5%) for the yellow radiation. Hence the yellow radiation was extracted through it. For the CW experiments, the gain mirror was pumped with a 200 W 808 nm diode laser with a focused spot diameter of about 510 µm. The mode diameter on the gain mirror was approximately 400 µm and inside the LBO crystal it was 230-164 µm. For the pulse modulation we used a lower power pump that could be driven up to peak powers of 71 W by current pulses with amplitudes of ~50 A and pulse durations in the range of 1 µs.

3. High power CW operation

At first, the laser was tested for high power continuous wave yellow output. Several etalon and BRF configurations with varying thicknesses were tested in order to find the optimal pair for stable high power operation, which lead to the selection of 1.5 mm thick BRF and 100 µm thick etalon. We also tested a critically phase matched (CPM) LBO, however the highest power was obtained with the NCPM LBO. For the high power operation measurement the mount temperature was estimated to be in the range of 5 to 8°C. The temperature of crystal oven was set to 38.3 °C; this was optimized according to the emission wavelength of the VECSEL to satisfy the phase matching condition for efficient frequency doubling. The power conversion graph generated from the measured laser output is shown in Fig. 3 (a). A maximum of 20 W of frequency doubled output power was measured for absorbed pump power of about 75 W, which was obtained by subtracting measured reflected pump power (5.13 % of incident power) from the incident pump power. The mount temperature at the maximum output power was 8.3 °C. The mount temperature was measured next to the gain chip. The maximum conversion efficiency (absorbed pump power to yellow output) of ~28 % was achieved at 16 W of output power, which is an improvement of 11 percentage points compared to state of the art yellow VECSEL results reported so far [18].

The emission spectrum of the VECSEL, set by the etalon (FSR ~5 nm, bandwidth ~0.37 nm), was centered at 588.1 nm with a linewidth (FWHM) of <0.2 nm, shown in Fig. 3 (b). The beam profile for the yellow radiation was preserved circular, with some distortions, as shown as inset in Fig. 3 (a), through the measurement range. We did a separate measurement for the output beam quality corresponding to 10 W (power level available at the time of measurement due to NCPM LBO crystal degradation, see next page) of output power. The obtained M^2 value was < 1.5 in horizontal and vertical directions. A scanning Fabry-Pérot interferometer was used to measure the mode spectrum for the fundamental wavelength. When the laser was tuned to 589 nm, single-wavelength operation was observed for yellow output power of ~10 W, but the operation was unstable.

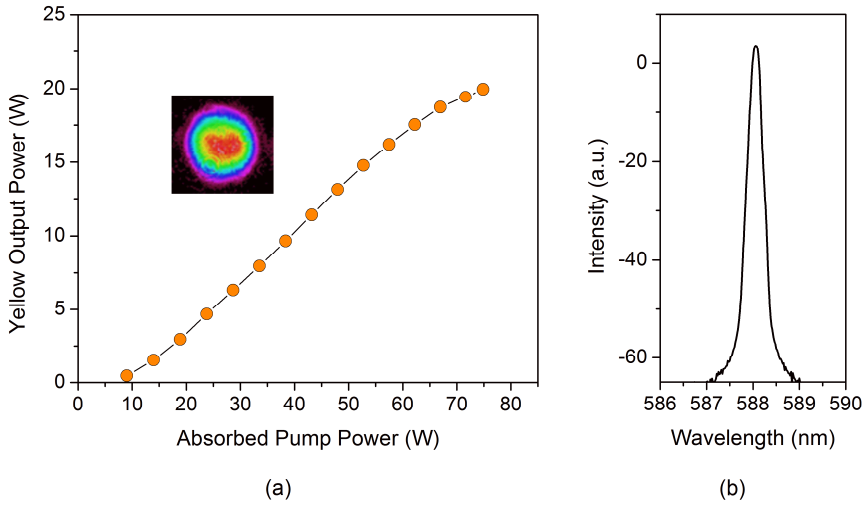

Fig. 3. (a) Output power curve for yellow emission. Inset: Beam profile recorded at maximum power. (b) Yellow spectrum measured at the maximum output power.

Next, the 1.5 mm BRF (placed at Brewster's angle) was rotated around an axis normal to its surface in order to test the tunability of the VECSEL. For this experiment the absorbed pump

power was kept constant at 55 W. The corresponding mount temperatures for the chosen absorbed pump power ranged between 9.2 and 13.5 °C depending on the emission wavelength; the temperature increased towards the edges of the tuning bandwidth due to the reduced gain chip efficiency and consequent increased heat generation. The temperature of the crystal oven was optimized for each wavelength separately. This proved to be challenging because the crystal temperature change was large enough to cause the output power to fluctuate. The 100 µm etalon was taken out each time before the emission wavelength was tuned by rotating the BRF in order to avoid a wavelength jump determined by the FSR of the etalon, and put back in for linewidth narrowing after the laser was tuned to a chosen wavelength.

The tuning spectrum is presented in Fig. 4 with each line having a full width half maximum of ~0.2 nm. The highest output power (15 W) was obtained for emission wavelength of about 588 nm. The tuning bandwidth was ~26 nm ranging from about 576 to 602 nm.

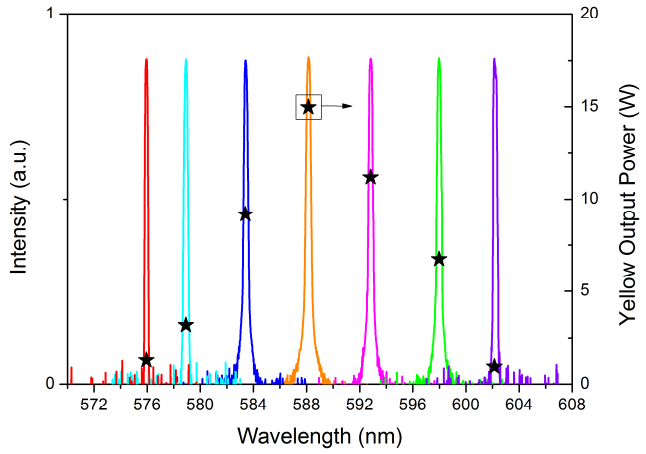

Fig. 4. Spectrum and yellow output power measured at each wavelength tuning point. The spectra curves are rescaled to equal height in order to better reveal their shape for a better comparison. The output power for each wavelength can be read from the right y-axis.

To test the operation at higher temperatures, power curves for different gain mirror mount temperatures were measured. The same cavity configuration was used as described earlier except the nonlinear crystal was changed from 10 mm NCMP LBO to a 10 mm CPM LBO. The change was made, because significant deterioration was observed in the NCPM LBO crystal performance during the course of the experiments and a suitable replacement was not available. We believe the crystal degradation was caused by damaged AR coatings on the facets of the NCPM LBO, which was obvious as observed with an optical microscope. The temperature of the CPM LBO was stabilized with the same copper oven that was used for phase matching with the NCPM LBO. The temperature stabilization was necessary because the stray light of the laser, arising from the parasitic reflections of the gain chip and the BRF, and the pump would have otherwise heated the copper oven of the crystal, and consequently, the crystal above its phase matching temperature (room temperature). The oven temperature was kept constant at 23.1 °C and efficient phase matching was achieved by having the CPM LBO critically cut for type I SHG at 1178 nm and having control of the significant crystal tilts.

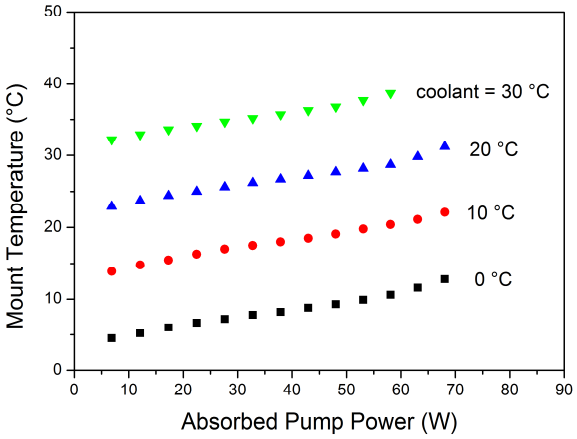

Fig. 5. Evolution of the mount temperature as a function of the absorbed pump power.

The power curves were measured for coolant temperatures of 0, 10, 20 and 30 °C, which corresponded to mount temperatures of 4.5-12.8, 13.9-22.1, 22.9-31.2 and 32.2-38.7 °C, respectively. The dependence of the mount temperature on the absorbed pump power is presented in Fig. 5, which shows that the heat load generated by the increasing pump power led to an increase in the mount temperature of the gain mirror. Whereas, the resulting output power for each temperature setting against absorbed pump power is plotted in Fig. 6. We could not achieve the 20 W of output power that was obtained with the NCPM LBO, because of the CPM LBO crystal properties. The two crystals were ordered from different manufacturers, which can already cause a difference of several Watts in the output as observed while testing two NCPM LBOs from different manufacturers with same specifications. In addition, NCPM LBO is expected to yield higher efficiency because it does not suffer from the phenomena of spatial walk-off and is less sensitive to a slight misalignment of the beams. Furthermore, the acceptance angle of the CPM LBO is smaller than that of the NCPM LBO, which could have an impact on the conversion efficiency. The highest output power of 14.6 W was achieved for lowest mount temperature as expected due to the better luminous efficiency of the semiconductor material as the temperature is decreased. Similarly, the output power is expected to drop for the higher mount temperatures, as is observable from Fig. 6. However, for lower pump powers, the output power was higher for some elevated mount temperatures, which can be seen as overlapping of curves in Fig. 6. This phenomenon was most likely caused by better alignment of the laser wavelength with the gain and with the CPM LBO crystal phase matching condition.

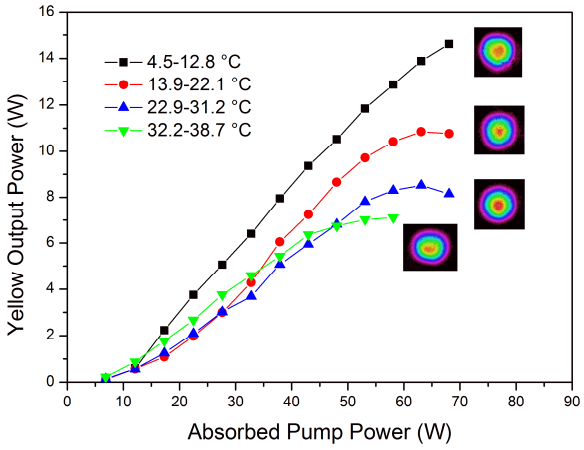

Fig. 6. Output power characteristics for different gain mirror mount temperatures. Insets: Beam profiles recorded at each maximum output power.

4. Pulsed operation

Heating of the gain chip structure by the incident pump power causes thermal rollover and clearly limits the CW operation, as can be seen from the above power curves. In order to overcome the thermal effects and improve conversion efficiency the yellow laser was tested in pulsed mode. The same cavity configuration was used as for the elevated mount temperature experiments, but a pulsed laser was employed for pumping. The LBO crystal temperature was kept near room temperature and the chip mount temperature was measured to be 21 °C throughout the measurements. The pump laser was driven with a driver capable of producing pulse widths up to ~1.5 µs. Two Si biased detectors were used to monitor the light pulses generated by the pump laser and the VECSEL. The pulse waveforms for the pump laser, as well as the yellow output at the maximum operation of the pump laser, are shown in Fig. 7. The respective FWHM pulse widths are 1.64 µs and 1.08 µs. A time delay of 0.66 µs was measured between the pump pulse and the yellow pulse. The reason for the delay is not clear. We suspected that the time delay could be caused by the need for the gain chip to heat up and consequently reach sufficiently low detuning for lasing. However, the delay did not change even when the coolant water temperature was raised to 60°C as would have been expected based on the assumption. This implies that the heating of the gain chip does not play a noticeable role in the pulse on-set delay.

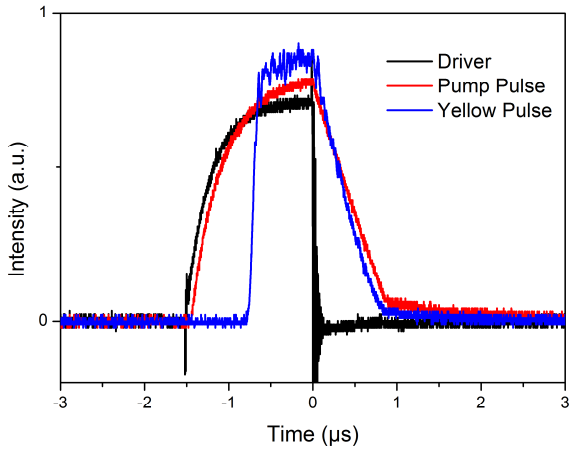

Fig. 7. Pulse shapes for the pump laser driver (black trace), pump laser output (red) and VECSEL output (blue) recorded at maximum pump laser operation for 1.5 µs pulse width setting.

For comparison, power curves for two different pulse widths were measured. First the driver was set to produce 1.5 µs pulses and then to 1.0 µs. The repetition rate was kept at 10 kHz. The peak power of the pulses was calculated by measuring the average power of the output and FWHM pulse width of the pulse waveforms. The peak power measurements for the two different pulse widths are shown in Fig. 8 (a). The CW power curve (average power) is also shown in Fig. 8 (a) for comparison. It can be clearly seen that in pulsed operation higher powers can be achieved due to decreased heating of the semiconductor gain chip. The CW operation shows thermal rollover at around 60 W of absorbed pump power, but the pulsed operation shows a linearly increasing trend, limited by the available peak pump power. Furthermore, the optical-to-optical conversion efficiency of the CW operation at maximum output power was 14 % whereas for the pulsed operation the conversion efficiencies were 20 % and 21 %, for the 1.08 µs and 0.57 µs pulses respectively. The maximum average output power measured for CW operation was 8.5 W and the maximum peak power measured in the pulsed mode was 14.1 W for the 0.57 µs pulse width and 13.8 W for the longer, 1.08 µs pulse width. The maximum average output powers for the pulsed operation were 81 mW and 149 mW, respectively. The pulse width was limited by the long rise time of the driver; at shorter pulse widths the current was cut which decreased the peak pump power. Yellow spectrum for the 0.57 µs pulse is shown in Fig. 8 (b).

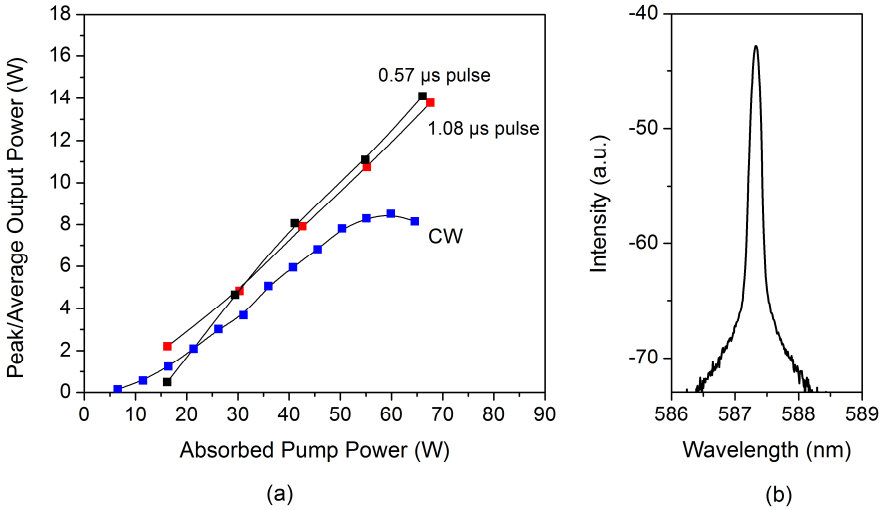

Fig. 8. (a) Output power characteristics for 20 °C (mount temperature of gain mirror) continuous wave (average power) and pulsed operation (peak power) at two different pulse width settings. (b) Output spectrum measured for pulsed operation for 0.57 µs pulse width.

5. Conclusions

High-power efficient operation of a frequency doubled yellow VECSEL has been demonstrated for both CW and pulsed operation. The maximum yellow output power achieved was 20 W for 75 W of absorbed pump power, which yielded an optical-to-optical conversion efficiency of 27 %. The maximum conversion of 28 % was achieved with a slightly lower output power of 16 W. Wavelength selective components inside the laser cavity allowed to narrow the emission linewidth and tune the operation wavelength of the laser; a tuning bandwidth of ~26 nm was measured. A further narrowing of the linewidth into single longitudinal operation with a different choice of etalon would make the laser suitable for guide star application. During the high power measurements, the VECSEL operated also in single wavelength at 589 nm with ~10 W of output power. However, the operation was unstable.

The operation of the laser was also tested at different gain mirror mount temperatures using another, critically phase matched (CPM) LBO crystal. At mount temperature of 12.8 °C the maximum output power achieved was about 15 W, whereas for the highest temperature, 38.7 °C, it was 7 W. The high power operation even at elevated temperature makes it more attractive for implementation into medical equipment, since it will not require high cooling capacity.

The same CPM LBO was used during pulsed operation, where the thermal effects were reduced so that a thermal rollover was not apparent for the available maximum pump power. The maximum output powers achieved with pulse widths of 0.57 and 1.08 µs were 14.1 and 13.8 W respectively, compared to the CW maximum of 8.5 W in this setup. The power curves for the pulsed operation suggest that even higher powers can be achieved for higher peak pump powers. The pulse widths were limited by the modulation capability of the electronics and pump system time, but the ~1 µs long pulses are already suitable for certain medical application e.g. eye surgery.

Acknowledgements

This work was financially supported by the EU FP7 project APACOS (315711) and TEKES project Brightlase (230225). The main author would like to acknowledge TES Foundation and Walter Ahlström Foundation for financial support.

Publication 2

P2

E. Kantola, T. Leinonen, J.-P. Penttinen, V.-M. Korpijärvi, and M. Guina, “615 nm GaInNAs VECSEL with output power above 10 W,” *Optics Express*, vol. 23, no. 16, p. 20280–20287, 2015.

© 2015 Optical Society of America. Reprinted with kind permission.

615 nm GaInNAs VECSEL with output power above 10 W

Emmi Kantola,* Tomi Leinonen, Jussi-Pekka Penttinen, Ville-Markus Korpijärvi and Mircea Guina

Optoelectronics Research Centre, Tampere University of Technology, Korkeakoulunkatu 3, FIN-33101 Tampere, Finland

emmi.kantola@tut.fi

Abstract: A high-power optically-pumped vertical-external-cavity surface-emitting laser (VECSEL) generating 10.5 W of *cw* output power at 615 nm is reported. The gain mirror incorporated 10 GaInNAs quantum wells and was designed to have an emission peak in the 1230 nm range. The fundamental emission was frequency doubled to the red spectral range by using an intra-cavity nonlinear LBO crystal. The maximum optical-to-optical conversion efficiency was 17.5%. The VECSEL was also operated in pulsed mode by directly modulating the pump laser to produce light pulses with duration of ~1.5 µs. The maximum peak power for pulsed operation (pump limited) was 13.8 W. This corresponded to an optical-to-optical conversion efficiency of 20.4%.

© 2015 Optical Society of America

OCIS codes: (140.7300) Visible lasers; (140.3480) Lasers, diode-pumped; (140.3515) Lasers, frequency doubled; (140.3538) Lasers, pulsed; (140.7270) Vertical emitting lasers; (140.5960) Semiconductor lasers.

References and links

1. W.J. Alford, G.J. Fetzer, R.J. Epstein, A. Sandalphon, N. Van Lieu, S. Ranta, M. Tavast, T. Leinonen, and M. Guina, "Optically pumped semiconductor lasers for precision spectroscopic applications," IEEE J. Quant. Electron. **49**(8), 719-727 (2013).
2. S. Ranta, M. Tavast, T. Leinonen, T. Epstein, and M. Guina, "Narrow linewidth 1118/559 nm VECSEL based on strain compensated GaInAs/GaAs quantum-wells for laser cooling of Mg-ions," Opt. Mater. Express **2**(8), 1011-1019 (2012).
3. K. Kuramoto, T. Nishida, S. Abe, M. Miyashita, K. Mori, and T. Yagi, "High power operation of AlGaInP red laser diode for display applications," Proc. SPIE **9348**, 93480H (2015).
4. L. Toikkanen, A. Härkönen, J. Lyytikäinen, T. Leinonen, A. Tukiainen, J.Viheriälä, M. Bister, and M. Guina, "Optically pumped edge-emitting GaAs laser with direct orange emission" IEEE Phot. Tech. Lett. **26**(4), 384-386 (2013).
5. M. Kuznetsov, F. Hakimi, R. Sprague, and A. Mooradian, "Design and characteristics of high-power (>0.5-W CW) diode-pumped vertical-external-cavity surface-emitting semiconductor lasers with circular TEM00 Beams," IEEE J. Sel. Top. Quantum Electron. **5**(3), 561-573 (1999).
6. S. Calvez, J. E. Hastie, M. Guina, O. G. Okhotnikov, and M. D. Dawson, "Semiconductor disk lasers for the generation of visible and ultraviolet radiation," Laser & Photon. Rev., 1-28 (2009).
7. C. Hessenius, P. Y. Guinet, M. Lukowski, J. Moloney, and M. Fallahi, "589-nm single-frequency VECSEL for sodium guidestar applications," Proc. SPIE **8242**, 82420E (2012).
8. J. L. A. Chilla, Q. Shu, H. Zhou, E. S. Weiss, M. K. Reed, and L. Spinelli, "Recent advances in optically pumped semiconductor lasers," Proc. SPIE **6451**, 645108 (2007).
9. J.-Y. Kim, S. Cho, S.-M. Lee, G. B. Kim, J. Lee, J. Yoo, K.-S. Kim, T. Kim, and Y. Park, "Highly efficient green VECSEL with intra-cavity diamond heat spreader," Electron. Lett. **43**(2), (2007).
10. E. Kantola, T. Leinonen, S. Ranta, M. Tavast, and M. Guina, "High-efficiency 20 W yellow VECSEL," Opt. Express **22**(6), 6372-6380 (2014).
11. H. Kahle, R. Bek, M. Heldmaier, T. Schwarzbäck, M. Jetter, P. Michler, "High optical output power in the UVA range of a frequency-doubled, strain-compensated AlGaInP-VECSEL," Appl. Phys. Express **7**(9), 092705 (2014).
12. M. Guina, T. Leinonen, A. Härkönen, and M. Pessa, "High-power disk lasers based on dilute nitride heterostructures," New J. Phys. **11**, 125019 (2009).
13. V.-M. Korpijärvi, E.L. Kantola, T. Leinonen, R. Isoaho, and M. Guina, "Monolithic GaInNAsSb/GaAs VECSEL operating at 1550 nm," IEEE J. Sel. Top. in Quantum Electron. **21**(6), 1700705 (2015).
14. V.-M. Korpijärvi, T. Leinonen, J. Puustinen, A. Härkönen, and M. Guina, "11 W single gain-chip dilute nitride disk laser emitting around 1180 nm," Opt. Express **18**(25), 25633-25641 (2010).
15. J. Rautiainen, A. Härkönen, V. Korpijärvi, J. Puustinen, L. Orsila, M. Guina, and O. Okhotnikov, "Red and UV generation using frequency-converted GaInNAs-based semiconductor disk laser," in *Conference on Lasers and Electro-Optics/International Quantum Electronics Conference*, OSA Technical Digest (CD) (Optical Society of America, 2009), paper CMRR7.

1. Introduction

High-power red lasers are useful for many applications, including laser projection, spectroscopy and medicine. For example, there is an increasing need for single-frequency high-brightness lasers emitting in the long visible wavelength range for quantum optics applications [1,2]. In addition, laser projection relies on lasers emitting >10 W of red, green and blue light. Currently, laser diodes emitting around 640 nm are used as the red light sources in display technology [3]. However, the human eye is more sensitive to shorter red wavelengths, therefore a laser emitting closer to 620 nm would allow higher lumen efficacy. Decreasing the wavelength of laser diodes below 640 nm has proved difficult and would result in severe power and lifetime limitations [4], hence other light sources should be considered.

Frequency doubled vertical-external-cavity surface-emitting lasers (VECSELs) have emerged as compact and wavelength versatile laser platforms generating high-brightness radiation in the visible wavelength range [5,6]. Their external cavity enables efficient frequency conversion by placing a nonlinear crystal inside the laser cavity and thus allows the exploitation of the high intra-cavity field. Furthermore, wavelength selective components (e.g. birefringent filters and etalons) can also be added inside the cavity for narrowing the spectral linewidth and achieving single-frequency operation [7]. Frequency doubled VECSELs have already been extensively reported in the green spectral range [8,9] and high powers have also been demonstrated in the yellow-orange range [10]. However, there are only a few reports on the red spectral range, 610–630 nm, due to the difficulty associated with semiconductor material fabrication for direct emission, as well as for frequency doubled emission. The highest power reported for an AlGaInP quantum well gain mirror is 1.2 W with direct emission at a longer wavelength of 665 nm [11]. GaInAs material system is a good candidate for frequency doubled VECSELs at the shorter visible wavelength range, but it suffers from high lattice strain at wavelengths longer than 1100 nm. This makes it difficult to grow quantum wells emitting in the 1220–1260 nm range needed for frequency doubling to 610–630 nm.

Using semiconductor gain mirrors based on GaInNAs, a wavelength emission range covering 1.1 µm to 1.5 µm can be achieved [12,13]. Compared to GaInAs material systems, the addition of nitrogen decreases the lattice strain, as well as the band gap, enabling the fabrication of gain mirrors at longer wavelengths. So far, most of the efforts on developing GaInNAs-based VECSELS have been focused on demonstrating fundamental emission at 1180 nm and subsequent doubling to 590 nm with power levels above 10 W [14]. In contrast, the developments of red VECSELs based on GaInNAs gain mirrors have been scarce with the best reported power being 4.6 W at 610 nm [15].

In this article, we report on achieving output power of more than 10 W for a red frequency doubled continuous wave (*cw*) VECSEL utilizing GaInNAs quantum wells. We also report pulsed operation of such VECSEL by directly modulating the pump laser. High peak power operation with lower average power would especially benefit medical applications, because damage to healthy tissue can be decreased by decreasing the average power and thus the thermal load on the tissue.

2. Gain mirror design and fabrication

The gain mirror wafer was grown by molecular beam epitaxy on a GaAs substrate. The gain mirror structure was designed to be resonant at 1230 nm and comprised 10 GaInNAs quantum wells (QWs) surrounded by GaAs barrier layers. The QWs were located at the anti-nodes of the standing optical wave formed inside the active region (see Fig. 1 for an illustration of the structure). The thickness of a QW was 7 nm and the corresponding In and N compositions were 31% and 0.5%, respectively. A 50-nm-thick GaInP window layer terminated the active region and served as a carrier barrier layer preventing surface recombination. Clustering within the QW layers was limited by using a growth temperature of 375 °C. After the growth, the wafer was annealed for 4 minutes at ~700 °C to improve the material quality and diced into 3 x 3 mm^2 chips. For efficient heat extraction, the gain chip was capillary bonded to a 300-µm-thick CVD diamond heat spreader. The diamond was nominally flat, but it became apparent during measurements that the surfaces were not parallel causing beam distortion. Furthermore, the diamond was attached to a liquid-cooled copper mount via indium foil. The

outer surface of the diamond was coated with an anti-reflective coating for the pump radiation (808 nm) and the fundamental lasing wavelength (1230 nm).

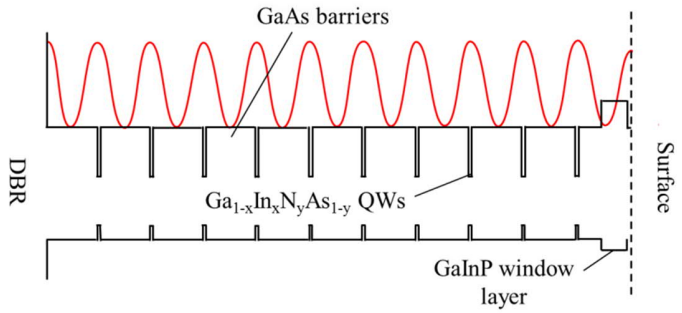

Fig. 1. Schematic illustration of the active region of the gain chip. The In and N compositions were x ~ 35% and y ~ 0.5%, respectively.

3. Laser characterization

3.1 Experimental setup

The VECSEL was built into a V-shaped configuration formed by the gain mirror and two curved dielectric mirrors (external mirrors), as shown in Fig. 2. The folding mirror had a radius of curvature (RoC) of 50 mm and the cavity end mirror had a RoC of 25 mm. The gain mirror was optically pumped using an 808 nm diode laser delivering a maximum *cw* power of ~120 W. The pump radiation was focused to a ~400 µm diameter spot ($1/e^2$) on the gain mirror using a 200-µm fiber and converging lenses. The total length of the cavity was ~147 mm with the first arm having a length of 89 mm. The mode diameter on the gain mirror was 240 µm tangential and 300 µm sagittal. The elliptical shape of the mode was a straight consequence of the ~30° folding angle of the V-shaped cavity.

For efficient intra-cavity frequency doubling, both external cavity mirrors need to be highly reflective (HR) for the fundamental lasing wavelength of 1230 nm. We measured the infrared transmittance of the HR cavity end-mirror (RoC = 25 mm) in order to determine the intra-cavity power. For this measurement, the VECSEL cavity incorporated a HR folding mirror and a partially reflective mirror (output coupler) as the cavity end-mirror. The HR cavity end-mirror (also HR for the red spectral range) was then placed in front of the VECSEL's output beam. A power head meter was used to measure the output power through the HR mirror as well as when the HR mirror was removed from the beam path. The percentage of infrared radiation transmitted through the HR mirror was calculated by dividing the measured power readings. The transmittance of the mirror is wavelength sensitive; hence, this process was repeated for several wavelengths around 1230 nm. The VECSEL was wavelength tuned by placing a 1.0-mm-thick birefringent filter inside the cavity (see Fig. 2 for a detailed illustration of the cavity setup). The transmittance of the long-wave-pass filter (used to filter red radiation leaking through the HR cavity end-mirror) was measured in a similar way. The transmittances of these optical components as a function of wavelength are shown in Fig. 3.

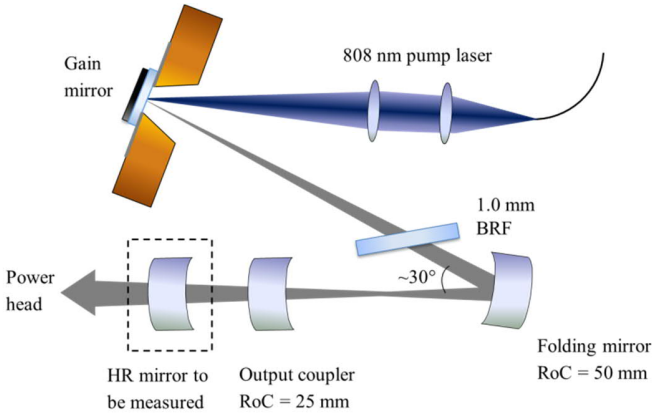

Fig. 2. Illustration of the VECSEL configuration used for measuring the transmittance of the HR cavity end-mirror and long-wave-pass filter ($\lambda > 900$ nm). The HR cavity end-mirror is represented by the mirror inside the dashed box and is not part of the VECSEL cavity.

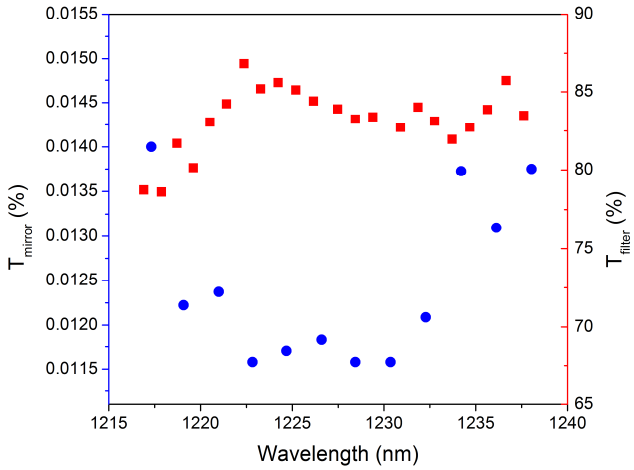

Fig. 3. Transmittance of the HR cavity end-mirror, T_{mirror}, and the long-wave-pass filter, T_{filter} , ($\lambda > 900$ nm) as a function of wavelength.

For frequency doubling measurements, the output coupler in Fig. 2 was replaced by the HR mirror which was characterized as illustrated in Fig. 3. In addition, a 100-µm-thick etalon was added to the cavity for linewidth narrowing and wavelength control, and the 1.0-mm-thick BRF was kept in place for the same reason. The red spectral range was achieved by inserting a nonlinear lithium triborate (LBO) crystal inside the cavity, near the mode waist (~70–80 µm in diameter). The crystal was 10 mm long and specified for Type I second harmonic generation (SHG) cut for non-critical phase matching (NCPM). Phase matching is vital for efficient frequency conversion and it was achieved by temperature stabilizing the crystal with a copper oven to a temperature optimized for frequency doubling at 1230 nm. This was achieved by observing the frequency doubled output power while changing the temperature of the crystal's oven. The temperature that resulted in the highest output power was 20.1 °C. The frequency doubled radiation was extracted from the cavity through the folding mirror, which was highly reflecting for the fundamental wavelength but had low reflectivity (< 5%) for the red spectral range. The cavity configuration is shown in Fig. 4. In addition, a short-wave pass filter was used between the folding mirror and the power head to filter out infrared radiation leaking through the folding mirror. Whereas, a long-wave pass filter was used between the HR cavity end-mirror and a power head to filter out the red light leaking through the cavity end-mirror.

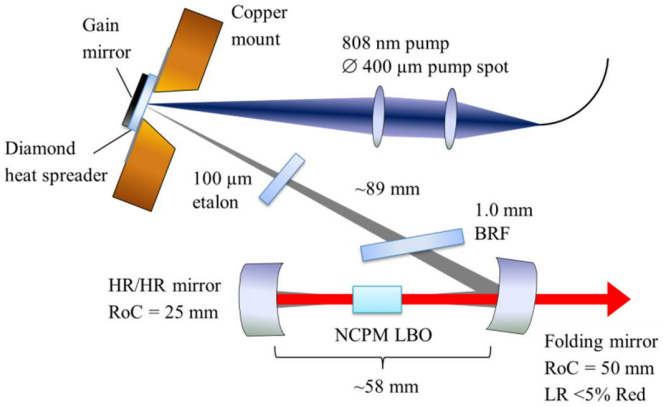

Fig. 4. Schematic illustration of the frequency doubled red VECSEL.

3.2 Continuous wave operation

At first, the VECSEL was operated in continuous wave mode. The cooling liquid was set to a temperature of 1 °C, which corresponded to mount temperatures of 5–8 °C during operation. The maximum frequency doubled output power of 10.5 W was achieved for an absorbed pump power of 59.7 W. This corresponded to an optical-to-optical (absorbed pump power to red output power) conversion efficiency of 17.5%. Absorbed pump power was measured by subtracting the amount of 808 nm pump power reflected from the surface of the gain mirror. The amount of pump radiation reflected from the gain mirror surface was 4.2%. The emission wavelength of the VECSEL was centered at 615 nm (inset of Fig. 5) and exhibited a FWHM linewidth of 0.4 nm. The beam profile (inset of Fig. 5) was recorded with a CCD camera showing an elliptical shape horizontally, which might be a consequence of multi-transversal mode operation potentially caused by the larger pump spot diameter in comparison to the mode diameter. The output spectrum and the beam profile were recorded at 7 W of output power. The output power curve is shown in Fig. 5.

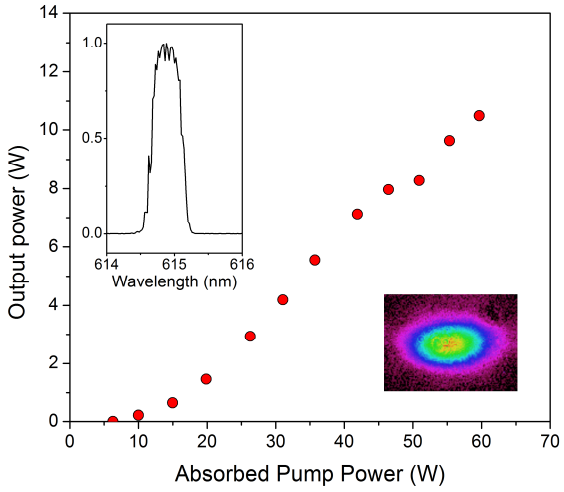

Fig. 5. Output power curve for red emission (output power vs. absorbed pump power). Insets: Output spectrum for red emission and lateral beam profile measured at 7 W.

The intra-cavity power of the VECSEL was determined by measuring the infrared radiation leaking through the HR cavity end-mirror, whose transmission was determined earlier. The intra-cavity power was then estimated by dividing the measured infrared power with the transmission of the mirror. Furthermore, the single-pass conversion efficiency of the LBO crystal was calculated using the measured red output power and the intra-cavity power results. The calculation assumed that there are no losses for the red light inside the cavity, and all of the red light escapes the cavity. At the highest output power, the intra-cavity power was estimated to be 640 W. The maximum single-pass conversion efficiency of 0.8% was obtained

for a red output power of 9.6 W. An almost equal conversion efficiency value was obtained for the highest red output power. Results of the intra-cavity power and single-pass conversion efficiency calculations are shown in Fig. 6.

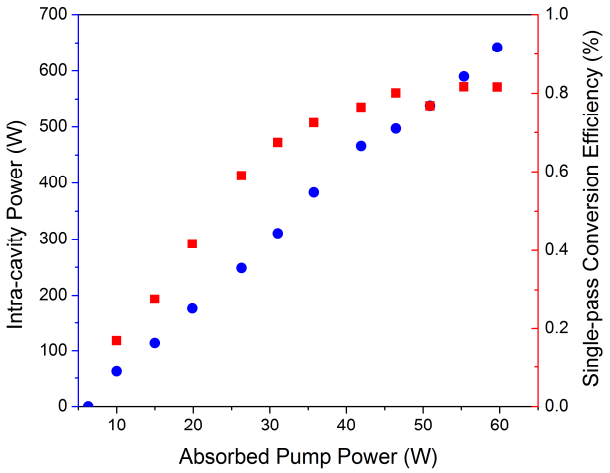

Fig. 6. Intra-cavity power (blue circles) and single-pass conversion efficiency (red squares) of the nonlinear crystal (LBO) vs. absorbed pump power.

3.3 Pulsed operation

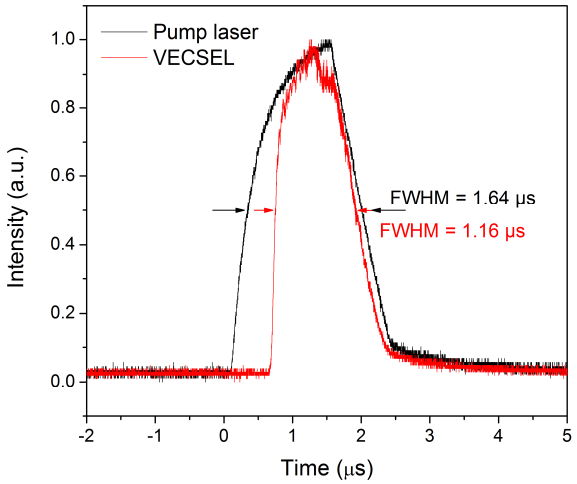

Fig. 7. Pulse waveforms for the pulsed pump laser (black trace) and the red VECSEL output (red) recorded at maximum frequency doubled output for 1.5 µs pulse width setting.

The VECSEL was also pumped in pulsed mode. This reduces the thermal load on the chip and leads to higher conversion efficiency. The same cavity configuration was used for the pulsed measurements as for *cw* measurements except the *cw* 808 nm pump laser was switched to a pulsed 808 nm pump laser. The pump laser was pulsed using a driver capable of producing current pulses up to 1.5 µs. When the driver was set to produce 1.5 µs pulse widths, the pump laser produced peak powers up to 70.6 W. Si-based detectors were used to record the light pulses generated by the pump laser and the VECSEL. The pulse waveforms measured at the maximum output power are shown in Fig. 7 for the pump laser and the VECSEL. The cooling liquid of the gain mirror's mount was set to near room temperature at 20 °C. Owing to the decreased thermal load on the gain mirror, the mount temperature remained at 20 °C throughout the pulsed measurements. For comparison, the VECSEL's output power was also measured in *cw* mode while the mount temperature was near 20 °C. In this case, the cooling liquid was set to 16 °C. Fig. 8 shows the output power curves for both, the pulsed and *cw* operation, as well as the VECSEL's output spectrum. The maximum output power achieved in *cw* mode was 8.0 W, whereas in pulsed mode the maximum peak output power was 13.8 W

for a pulse width of 1.16 µs. Furthermore, thermal rollover was reached for the *cw* operation, whereas in pulsed mode the maximum peak output power was pump power limited. The maximum average output power for the pulsed operation was 161 mW and the maximum optical-to-optical conversion efficiency (absorbed peak pump power to peak output power) was 20.4%.

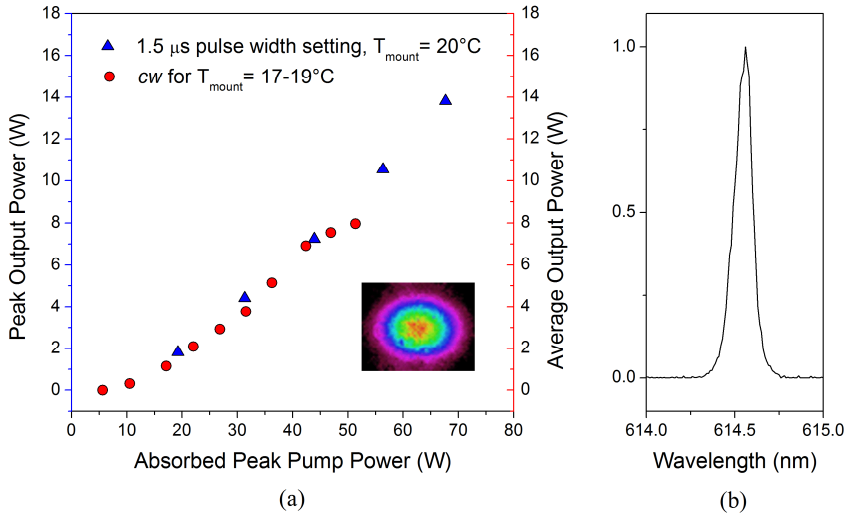

Fig. 8. (a) Output power curves for continuous wave (red circles) and pulsed mode (blue triangles) when the mount temperature was ~20 °C. (b) Output spectrum for the red VECSEL measured at the maximum pulsed pump power.

4. Conclusions

A high-power GaInNAs VECSEL emitting at 615 nm, operating in continuous wave and pulsed modes, has been demonstrated. The VECSEL emitted fundamental radiation in the 1230 nm range and was frequency doubled to ~615 nm via an intra-cavity nonlinear LBO crystal. A maximum of 10.5 W was reached in *cw* mode with an optical-to-optical conversion efficiency of 17.5% for a mount temperature of 8 °C. The single-pass conversion efficiency of the LBO crystal was estimated to be 0.8%. In pulsed mode, the VECSEL generated a maximum of 13.8 W of peak output power for pulse duration of 1.16 µs. In this case the optical-to-optical conversion efficiency was 20.4% and the mount temperature stayed at 20 °C throughout the measurements. The maximum peak output power in pulsed mode was pump power limited; hence, even higher peak output powers are expected with a better pulsed pump laser. The *cw* power measurements were limited by thermal rollover.

Acknowledgments

This work was financially supported by the Academy of Finland project Qubit (decision #278388) and TEKES project ReLase (40016/14). The authors would like to acknowledge Jari Nikkinen for the deposition of the AR-coating on the diamond heat spreader. The main author would also like to acknowledge Walter Ahlström and Ulla Tuominen Foundations for financial support.

Publication 3

P3

E. Kantola, J.-P. Penttinen, S. Ranta, and M. Guina, “72-W VECSEL emitting at 1180 nm for laser guide star adaptive optics,” *Electronics Letters*, vol. 54, no. 19, p. 1135–1137, 2018.

Reproduced by kind permission of the Institution of Engineering & Technology.

72-W vertical-external-cavity surface-emitting laser with 1180-nm emission for laser guide star adaptive optics

E. Kantola✉, J.-P. Penttinen, S. Ranta and M. Guina

We report a high-power optically-pumped vertical-external-cavity surface-emitting laser emitting at around 1180 nm. The free-running laser produced 72 W of output power at a heatsink temperature of 0°C and 53 W near room temperature (20°C). The GaAs-based gain mirror was bonded to a 2-mm-thick diamond attached to a TEC-cooled copper mount in order to enable efficient heat extraction for high-power operation. Moreover, the spectrum of the laser was narrowed down to 0.06 nm by employing a combination of a birefringent filter and an etalon inside the cavity which yielded a maximum of 19 W at a heatsink temperature of 20°C. The demonstration opens a new perspective for the realisation of sodium laser guide star adaptive optics employing frequency doubling of 1180 nm radiation.

Introduction: High-power vertical-external-cavity surface-emitting lasers (VECSELs) emitting in the 1160–1200 nm infrared range have attracted attention due to their ability to generate yellow-orange radiation through second harmonic generation (SHG) [1]. In general, VECSELs are recognised for their power scaling abilities and excellent beam quality, as well as for a broad wavelength coverage enabled by material engineering. The highest power measured from a VECSEL exceeds 100 W at an emission wavelength of 1028 nm [2], and the wavelength coverage extends from ultraviolet (via SHG) to 5 µm, though not without gaps due to material challenges [3]. The 1100–1200 nm range, for example, imposes challenges due to the strain arising from the large lattice mismatch between GaInAs quantum wells and GaAs. This strain can be alleviated by adding small amounts of nitrogen into the crystal, making the so-called diluted nitride structures [4]. Below 1200 nm, the strain can also be compensated by careful optimisation of the growth parameters, i.e. employing strain compensation layers [5]. Furthermore, the external cavity allows for an inclusion of wavelength selective intracavity components which enable narrow-linewidth emission (below MHz range) [6] and high-power frequency-doubling through nonlinear crystals [1, 7]. Single-frequency operation at >20 W of output power has already been demonstrated by Zhang *et al.* at a fundamental wavelength of 1013 nm [8]. These features make VECSELs well suited for applications requiring high-power and high beam quality at specific wavelengths not easily addressed with standard techniques.

Adaptive optics is often employed on earth-based telescopes to correct for the distortion of images caused by the variations in the index of refraction of air due to atmospheric turbulence. As part of the adaptive optics system, a reference object – a so-called guide star – is needed [9]. Unfortunately, there are not many naturally occurring guide stars in the sky, but one can be created artificially by exciting sodium atoms in the atmosphere with a laser. This process sets demanding specifications for the excitation laser. The wavelength needs to match the sodium D_2 line and emit high-power, which translates to >20 W of continuous wave radiation at the challenging yellow wavelength of 589 nm with a linewidth <250 MHz [10].

In this Letter, we demonstrate a VECSEL emitting 72 W of continuous wave emission at around 1180 nm at a heatsink temperature of 0°C, which is the highest power reported to date for this wavelength range. The laser operated at multi-transverse and -longitudinal modes with a full-width-at-half-maximum (FWHM) of 5.5 nm. With the laser guide star-target in mind, we modified the cavity for single transverse mode operation and narrowed the spectrum to 0.06 nm with the available birefringent filter (BRF) and etalon. In this configuration, a maximum output power of 19 W was demonstrated near room temperature (20°C). With appropriate shielding from mechanical and acoustical vibrations and thermal stabilisation of the intracavity elements, we believe that high-power single-frequency operation with similar output power is attainable. Furthermore, frequency conversion to the desired 589-nm yellow wavelength can be achieved either with internal [1, 7] or external cavity doubling [11].

Experimental setup: The VECSEL consisted of a semiconductor gain mirror and a partially transmissive dielectric mirror (i.e. output coupler). The top-emitting gain mirror was grown by molecular beam epitaxy and comprised a 26-pair AlAs/GaAs distributed Bragg reflector and an active region. The active region incorporated 10 GaInAs quantum wells located at the antinodes of the optical standing wave. The compressively strained quantum wells were embedded between GaAs barrier layers and GaAsP strain compensation layers. The active region was terminated with a GaInP window layer to prevent surface recombination, and the active region thickness was matched to make the gain mirror microcavity resonant at the signal wavelength.

Efficient heat extraction is vital for high-power VECSELs. To this end, the gain mirror was capillary bonded from the front surface to a 2-mm-thick diamond heat spreader, which was further bonded to a large temperature stabilised copper heatsink with indium. The copper heatsink arrangement employed four 200-W thermoelectric coolers to keep the heatsink temperature stable even at low temperatures. An antireflection coating was deposited on the diamond heat spreader to minimise losses for the signal and pump wavelengths.

An I-shaped laser cavity was formed between the gain mirror and the output coupler, shown in Fig. 1. For the free-running demonstration, we used a 109-mm-long cavity and a 3% transmissive output coupler with a radius of curvature of 150 mm. The gain mirror was pumped with a commercially available 808-nm diode laser. The pump light was delivered through a 200-µm core fibre and focused onto the surface through a lens arrangement at an angle of ~30°. A relatively large top-hat spot size of 950 µm in diameter (4σ value) was used in this experiment to provide lateral power scaling.

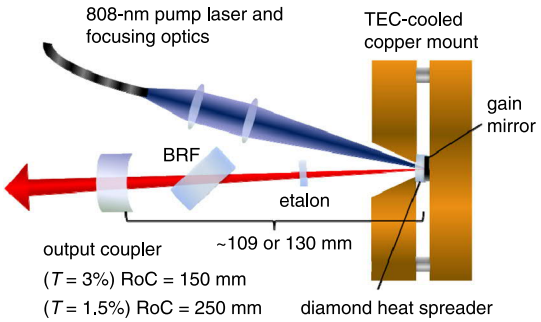

Fig. 1 *Cavity illustration of the 1180-nm VECSEL. The BRF and etalon were employed only in the longer cavity (l = 130 mm, RoC = 250 mm) for narrowing the spectrum*

In addition to the high-power free-running demonstration, we employed a second cavity to demonstrate the feasibility of the laser for narrow linewidth operation. In this setup, a 5-mm-thick quartz BRF and a 250-µm-thick YAG etalon were inserted into the cavity to narrow the spectrum. The length of the cavity was increased to 130 mm in order to make room for the BRF and the etalon. At the same time, the output-coupling mirror was changed to lower coupling (1.5%) to compensate for the losses produced by the new intracavity components, and the radius of the curvature increased to 250 mm to provide a larger mode size on the gain mirror. Moreover, the pump lens arrangement was adjusted to produce a smaller spot diameter (550 µm) for supporting fundamental transverse mode (TEM_{00}) operation.

Results: Fig. 2 shows the output power of the free-running VECSEL as a function of the incident pump power at heatsink temperatures of 0, 10 and 20°C. The incident pump power is defined as the total power incident on the diamond heat spreader and does not take into account the reflections from the diamond surfaces (estimated to be 5% with antireflection coating). The highest power of 72 W was measured at the heatsink temperature of 0°C. This corresponded to 257 W of incident pump power, 29% optical-to-optical conversion efficiency and 38% slope efficiency. To the best of our knowledge, this is the highest power reported at this wavelength range. During the 72-W operation, the spectrum of the laser was centred at 1185.5 nm and the FWHM was measured to be 5.5 nm, shown as an inset in Fig. 2. At heatsink temperatures of 10 and 20°C, the maximum output powers were 62 and 53 W, respectively.

For reference, we measured first the output power of the longer cavity with a 3% transmissive output coupler without any wavelength selective elements. A maximum of 25 W was measured at a heatsink temperature of 20°C. After the output coupler was changed to 1.5% coupling, we placed the BRF and the etalon inside the cavity and fixed the lasing

wavelength to ~1178 nm. A maximum of 19 W of output power was measured at 20°C, and the FWHM linewidth of the uncovered table-top laser was 0.06 nm (Fig. 3). The resolution of the spectrum analyser was 0.01 nm. The beam profile was measured with a charge-coupled-device camera and showed single transverse mode operation (shown as an inset in Fig. 3).

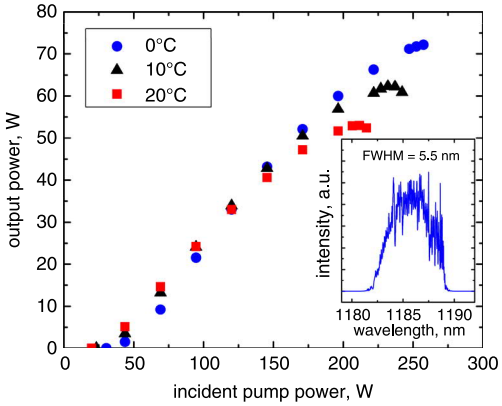

Fig. 2 *Output power curves for heatsink temperatures of 0, 10 and 20°C. Inset: Lasing spectrum recorded at 72 W of output power*

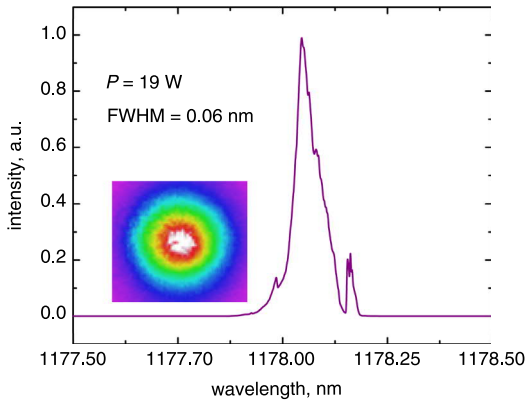

Fig. 3 *Normalised lasing spectrum at the maximum power (19 W) from the cavity including a 5-mm-thick BRF and 250-μm-thick YAG etalon. Inset: Beam profile measured at 19 W of output power*

The purpose of this wavelength narrowing was to demonstrate that high-power operation in single-frequency would be possible in the future with an appropriate mechanical design. In the future work, thicker BRF might be beneficial to further damp the unwanted cavity modes. In an earlier demonstration by Zhang *et al.*, a BRF with a thickness of 10 mm was employed to reach single-frequency operation [8], but in this letter, we were confined to the existing BRF stock in our lab.

Conclusions: We have demonstrated 72W of output power from a free-running VECSEL emitting at around 1180 nm at a heatsink temperature of 0°C. Near room temperature (20°C), the output power reached 53 W in the same configuration. Another cavity arrangement with additional intracavity elements (BRF and etalon) was employed to narrow the lasing spectrum down to 0.06 nm while emitting 19 W of output power near room temperature. The spectrum was narrowed to show that high-power operation is achievable even at more demanding spectral features. With further improvements of the cavity stabilisation, linewidth narrowing, and SHG, we target to demonstrate narrow-linewidth operation at 589 nm with spectral features fulfilling the needs of laser guide star adaptive optics.

Acknowledgments: This work was supported by the Finnish Funding Agency for Technology and Innovation (Tekes) project Photolase (40152/14), TUTLi project ReLase (619/31/2014), Academy of Finland project QUBIT (278388), and Jenny and Antti Wihuri Foundation.

© The Institution of Engineering and Technology 2018
Submitted: *11 July 2018*
doi: 10.1049/el.2018.6225
One or more of the Figures in this Letter are available in colour online.

E. Kantola, J.-P. Penttinen, S. Ranta and M. Guina (*Optoelectronics Research Centre, Tampere University of Technology, Korkeakoulunkatu 3, FIN-33720 Tampere, Finland*)

✉ E-mail: emmi.kantola@tut.fi

J.-P. Penttinen and M. Guina (*Vexlum Ltd, Korkeakoulunkatu 3, FIN-33720 Tampere, Finland*)

References

1 Kantola, E., Leinonen, T., Ranta, S., *et al.*: 'High-efficiency 20 W yellow VECSEL', *Opt. Express*, 2014, **22**, (6), pp. 6372–6380, doi: 10.1364/OE.22.006372
2 Heinen, B., Wang, T.-L., Sparenberg, M., *et al.*: '106 w continuous-wave output power from vertical-external-cavity surface-emitting laser', *Electron. Lett.*, 2012, **48**, (9), pp. 516–517, doi: 10.1049/el.2012.0531
3 Guina, M., Rantamäki, A., and Härkönen, A.: 'Optically pumped VECSELs: review of technology and progress', *J. Phys. D: Appl. Phys.*, 2017, **50**, (38), pp. 1–37, doi: 10.1088/1361-6463/aa7bfd
4 Guina, M., Leinonen, T., Härkönen, A., *et al.*: 'High-power disk lasers based on dilute nitride heterostructures', *New J. Phys.*, 2009, **11**, 125019, doi: 10.1088/1367-2630/11/12/125019
5 Ranta, S., Tavast, M., Leinonen, T., *et al.*: '1180 nm VECSEL with output power beyond 20 W', *Electron. Lett.*, 2013, **49**, (1), pp. 59–60, doi: 10.1049/el.2012.3450
6 Burd, S.C., Allcock, D.T.C., Leinonen, T., *et al.*: 'VECSEL systems for the generation and manipulation of trapped magnesium ions', *Optica*, 2016, **3**, (12), pp. 1294–1299, doi: 10.1364/OPTICA.3.001294
7 Berger, J.D., Anthon, D.W., Caprara, A., *et al.*: '20 Watt CW TEM00 intracavity doubled optically pumped semiconductor laser at 532 nm', *Proc. SPIE*, 2012, **8242**, 824206, doi: 10.1117/12.907511
8 Zhang, F., Heinen, B., Wichmann, M., *et al.*: 'A 23-watt single-frequency vertical-external-cavity surface-emitting laser', *Opt. Express*, 2014, **22**, (11), pp. 12817–12822, doi: 10.1364/OE.22.012817
9 Max, C.E., Olivier, S.S., Friedman, H.W., *et al.*: 'Image improvement from a sodium-layer Laser guide star adaptive optics system', *Science*, 1997, **277**, (5332), pp. 1649–1652, doi: 10.1126/science.277.5332.1649
10 Enderlein, M., and Kaenders, W.G.: 'Sodium guide star (r)evolution', *Opt. Photon.*, 2016, **11**, (5), pp. 31–35, doi: 10.1002/opph.201600038
11 Wilson, A. C., Ospelkaus, C., VanDevender, A.P., *et al.*: 'A 750-mW, continuous-wave, solid-state laser source at 313 nm for cooling and manipulating trapped $^{9}Be^{+}$ ions', *Appl. Phys.*, 2011, **105**, (4), pp. 741–748, doi: 10.1007/s00340-011-4771-1

Publication 4

E. Kantola, A. Rantamäki, I. Leino, J.-P. Penttinen, T. Karppinen, S. Mordon, and M. Guina, “VECSEL-based 590-nm laser system with 8 W of output power for the treatment of vascular lesions,” Journal of Selected Topics in Quantum Electronics, vol. 25, no. 1, 2019.

© 2019 IEEE. Reprinted with kind permission.

P4

VECSEL-based 590-nm laser system with 8 W of output power for the treatment of vascular lesions

Emmi Kantola, Antti Rantamäki, Iiro Leino, Jussi-Pekka Penttinen, Toni Karppinen, Serge Mordon, and Mircea Guina

***Abstract*—We report a compact high-power yellow laser system for the treatment of cutaneous vascular lesions, such as telangiectasia and port wine stains. The system is based on optically-pumped vertical-external-cavity surface-emitting lasers (VECSELs), which have emerged as an attractive alternative to solid-state and dye lasers due to their enhanced functionality and broad wavelength coverage. The reported system is capable of delivering up to 8 W of output power at ~590 nm and includes a handheld scanner for an easy delivery of light onto skin. The scan area can be varied from a single spot (1.4-mm diameter) up to 49 spots covering an area of 1 cm2. Additional features include adjustable fluence (0–52 J/cm2), scan patterns (line, square, hexagon) and pulse length (10–100 ms). The system has been qualified for and is currently used in a clinical trial concerning the treatment of facial telangiectasia (ClinicalTrials.gov Identifier: NCT03472859). Preliminary results of the test are reported indicating reduced treatment time for the yellow system and power reserve that could lead to further increase of the area treated in a single scan.**

***Index Terms*—Yellow lasers, VECSELs, semiconductor disk lasers, telangiectasia, vascular lesions.**

I. Introduction

LASERS have played an important part in the treatment of vascular lesions since the 1960s when Dr. Leon Goldman first suggested ruby lasers for the treatment of various cutaneous disorders [1]. Carbon dioxide and argon lasers soon followed the ruby laser and the first patients with port wine stains were treated with an argon laser in the 1970s [2]. Since then, there has been significant advances in laser technology and it is finally catching up with the needs of the dermatology community, particularly in terms of the emission wavelength.

The treatment of vascular lesions with laser light is based on the technique of selective photothermolysis published by Anderson and Parrish in 1983 [3]. In the paper, they explain how microvessels, or indeed any other target tissue, can be selectively treated while minimizing the thermal damage to the surrounding tissue by choosing the appropriate wavelength of light. In the treatment of vascular lesions, the aim is to destroy unwanted microvessels by targeting oxyhemoglobin inside the vessels. The oxyhemoglobin absorbs the light energy converting it to heat, which is then transferred to the vessel wall resulting in the desired thermal damage [4]. At the same time, the absorption by other chromophores, most notably melanin, should be minimized in order to only selectively target the microvessels.

Oxyhemoglobin has high absorption peaks at 418, 542 and 577 nm, as well as increased absorption in the near infrared region above 800 nm, as seen from the solid red curve in Figure 1. The absorption is highest around 418 nm, but this region also has higher absorption by melanin (dotted brown and orange curves) than the longer 542-nm and 577-nm regions. Melanin absorption continues to decrease towards the longer wavelengths of light, which makes longer yellow wavelengths, such as 585–590 nm, better suited for the treatment of deeper vessels [5]. On the other hand, the increasing water absorption (dashed curve) above 600 nm limits the use of infrared lasers for the treatment of vascular lesions. Deeper penetration can also be achieved with higher fluence, but this increases the risk of collateral damage due to increased heating.

In addition to wavelength, the pulse duration of the laser light should also be optimized according to the target chromophore. The determination of the appropriate pulse duration relies on the concept of thermal relaxation time (TRT). TRT is the time needed for a chromophore to dissipate half of its heat gained from the laser light and, ideally, the pulse duration should match the TRT of the chromophore. If the pulse is shorter than the TRT it might not produce enough heat for effective treatment, whereas very short pulses can

Manuscript received Month day, 2018. This work was supported by the Finnish innovation center TEKES under the Finnish Distinguished Professor project Photolase (#40152/14).

E. Kantola, J.-P. Penttinen and M. Guina are with the Optoelectronics Research Centre in Tampere University of Technology, 33720 Tampere, Finland (corresponding author email: emmi.kantola@tut.fi).

A. Rantamäki was with the Optoelectronics Research Centre. He is currently working for Corelase, Tampere (antti.rantamaki@corelase.fi).

I. Leino was with the Optoelectronics research Centre. He is now with the Finnish company Brighterwave (email: iiro.leino@brighterwave.com).

T. Karppinen is with the Department of Dermatology in Tampere University Hospital and with Epilaser Oy, Tampere, Finland.

S. Mordon is with the The French National Institute of Health and Medicine Research, INSERM U1189 ONCO-THAI, 59037 Lille Cedex, France (email: serge.mordon@inserm.fr) and with the Optoelectronics Research Centre in Tampere University of Technology as Finland Distinguished Professor (email: serge.mordon@tut.fi).

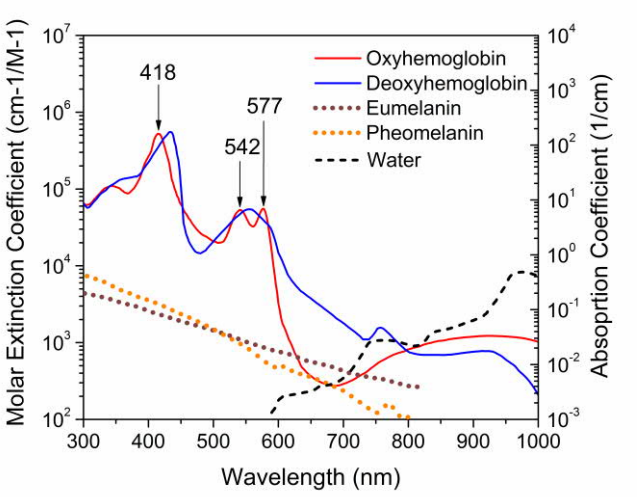

Fig. 1. Absorption curves for the main tissue components [6-9].

cause vessel rupture that leads to visible purpura [10]. Then again, pulses that are longer than the TRT produce excessive heat at the target resulting in collateral damage on the surrounding tissue. TRT depends on the size of the vessels, being longer for larger vessels, and hence longer pulse durations should be used for thicker vessels. For example, for 0.1–1 mm vessels the pulse duration should be in the range of 1–100 ms [11].

In summary, oxyhemoglobin inside microvessels can be most effectively targeted by choosing the most appropriate wavelength of light and by applying the correct pulse duration for the targeted vessel thickness. The wavelength selection minimizes absorption by other chromophores and the correct pulse length assures effective treatment without subjecting the surrounding tissue to excessive heat. These two concepts set the targets for the laser development. The high hemoglobin absorption peak at 577 nm would make it a tempting choice for the treatment of cutaneous vascular lesions. However, currently used yellow lasers, such as pulsed dye lasers, have opted for a longer wavelength of 585–590 nm in order to increase the penetration depth and decrease the melanin absorption while still maintaining high hemoglobin absorption. In terms of fluence, the typical values used in the treatment of vascular lesions by a yellow laser range between 5 and 20 J/cm^2.

In this paper, we report on a yellow laser system based on vertical-external-cavity surface-emitting laser (VECSEL) technology and designed for the treatment of vascular lesions. It offers an attractive alternative for the existing expensive and cumbersome yellow lasers on the market. The developed laser system can produce up to 8.6 W of continuous wave laser light around 585-590 nm (the wavelength can also be extended to 615 nm and beyond [12]) with 10–100 ms pulses and 0–52 J/cm^2 fluence in a desired pattern. The yellow light is directed to the target with a handheld scanning device.

TABLE I
CURRENTLY AVAILABLE LASERS FOR THE TREATMENT OF VASCULAR LESIONS

Laser	Technology	Wavelength (nm)	Pulse length (ms)
KTP	Frequency-doubled solid-state laser	532	1–200
Copper vapour	Metal-vapor laser	578	50–200
Pulsed Dye Laser (PDL)	Dye laser	585, 590, 595, 600	0.45–1.5
Alexandrite	Solid-state laser	755	3
Diode	Semiconductor laser	800, 810, 930	1–250
Nd:YAG	Solid-state laser	1064	1–100

II. TECHNOLOGY

A. *Available laser systems*

Table I lists the currently available and studied vascular lesion lasers on the market also indicating their emission wavelength and pulse length [11,13]. The golden standard for the treatment of vascular lesions is the pulsed dye laser. It has been used to treat vascular lesions since 1985 and offers a versatile solution for a variety of conditions [5]. The main features include a typical emission wavelength of 585 or 595 nm, pulse durations in the 10–40 ms range and spot sizes ranging from 3 mm up to about 10 mm. In addition, a dynamic cooling device is often used in parallel to reduce discomfort and to allow the use of higher fluence. The earlier versions of the pulsed dye laser had a much shorter pulse duration of ~0.45 ms but a longer pulse was later employed to reduce purpura and vessel rupture. The newer versions also employ the so-called dual wavelength approach to target methemoglobin [14]. The pulsed dye laser is the first laser that has been designed according to the theory of selective photothermolysis and therefore is not associated with severe adverse effects [5]. However, the drawbacks include large size, circular beam pattern, and high acquisition and annual maintenance costs.

Other commercially available and traditional options for the treatment of vascular lesions include the green KTP laser and the yellow copper bromide laser. The KTP laser operates at a shorter wavelength and therefore has a higher melanin absorption, which leads to an increased risk of dyspigmentation [15]. Whereas, the yellow copper bromide laser is commonly associated with adverse side effects, such as scarring and hypo- and hyperpigmentation [16]. In the 1980s, the blue-green emitting argon laser (along with the ruby laser) was the most frequently used laser to treat vascular lesions, but since then it has been replaced with longer wavelength lasers. Lasers emitting beyond the yellow spectral region, i.e. in the red and near-infrared, have also been considered due to their ability to penetrate deeper in the skin. Such lasers include the red Alexandrite, diodes and Nd:YAG. However, they are used only to target large vessels, deeply located in the skin.

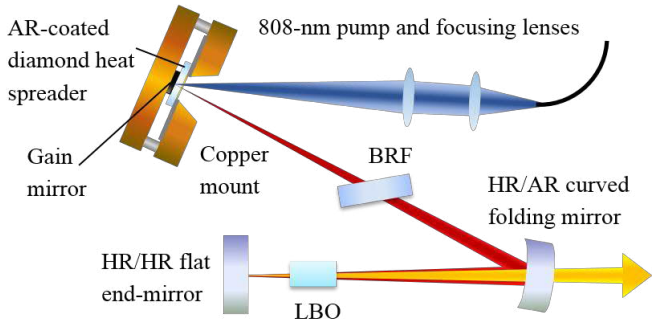

Fig. 2. Schematic illustration of the VECSEL cavity inside the module.

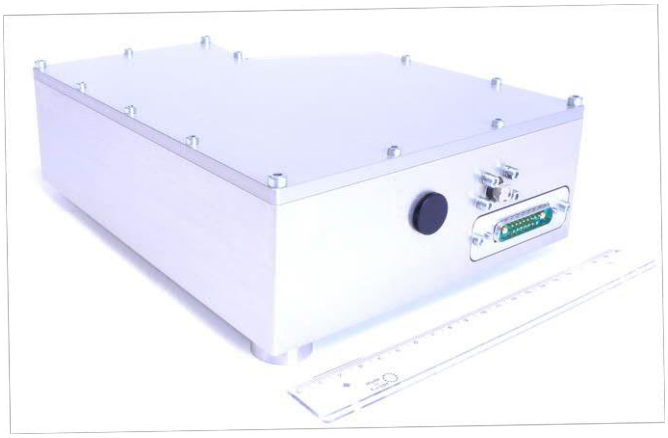

Fig. 3. Photo of the VECSEL module accompanied by a 20-cm long ruler.

In addition, new types of yellow lasers are emerging in the medical market as fully functional medical systems [17-19]. This suggests that laser technology is finally catching up with the demands of the medical field, and it is now possible to tailor laser features to specific medical applications, for example, with semiconductor technology.

B. Frequency doubled VECSELs

Vertical-external-cavity surface-emitting lasers (VECSELs), also known as Semiconductor Disk Lasers (SDLs), are surface emitting semiconductor lasers recognized for their power scaling abilities and excellent beam quality [20]. They combine the most beneficial features of semiconductor and solid-state lasers: wavelength tailoring through material engineering and functionality enabled by external cavity architectures. These features allow for a broad coverage of lasing wavelengths in the infrared and, via second harmonic generation with nonlinear crystals, in the visible and UV spectral ranges [21,22]. For example, 20 W of yellow light with good beam quality has been reported from a lab setup [23]. Furthermore, by adding wavelength selective components inside the external laser cavity, VECSELs can be designed to emit narrow linewidth [24] and have a wavelength tuning range up to tens of nanometers [25]. It is also easy to produce light pulses down to a few hundred nanoseconds from a

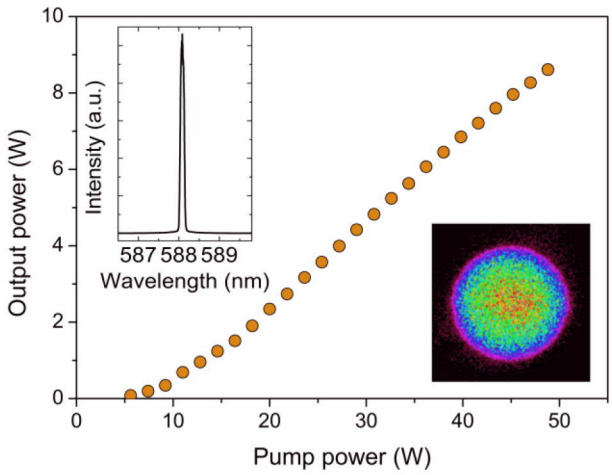

Fig. 4. Output power characteristics of the yellow VECSEL module delivered through a multi-mode fiber with a 200 µm diameter of the core. Emission spectrum and beam profile shown as insets.

VECSEL by directly modulating the pump laser [26]. Even shorter, picosecond or some hundreds of femtoseconds pulses are possible by employing semiconductor saturable absorber mirrors (SESAMs) [27,28].

Typically, a VECSEL is comprised of a semiconductor gain mirror, one or more external mirrors and a pump laser (see Fig. 2). The gain mirror itself incorporates a highly reflective mirror (often a Distributed Bragg Reflector, DBR) and a semiconductor gain region, and is usually grown by molecular beam epitaxy (MBE) or Metalorganic Vapour Phase Epitaxy (MOVPE). The gain region includes several quantum well (QW) or quantum dot layers separated by barrier layers. The purpose of the barrier layers is three-fold; they are used to compensate for the strain that QWs can impose on the structure, absorb pump light efficiently and confine the pump-generated carriers to the specific QWs for recombination. Lasing is achieved by optically pumping the gain mirror with a suitable pump laser. Inexpensive, commercially available diode lasers can often be utilized, since VECSELs have a broad absorption range thanks to the semiconductor material characteristics.

Optical pumping enables high power operation with circular beam profiles, but it also induces significant heating in the gain mirror because only a portion of it is converted into useful photons. This heating can be detrimental to the operation of a VECSEL; hence, thermal management is vital. To this end, a conductive heat spreader element between the gain mirror and a heat sink is typically employed. Diamond heat spreaders are most commonly used due to their high thermal conductance and wide transmission window. Several reviews have been published on the technology and progress of VECSELs, the most recent in 2017 providing also a comprehensive overview on wavelength coverage, thermal management and power capabilities [29]. We should also note that this technology has been commercialized by Coherent, Inc. for medical application, in particular with focus on the 577-nm wavelength and ophthalmic photocoagulation treatments. The output

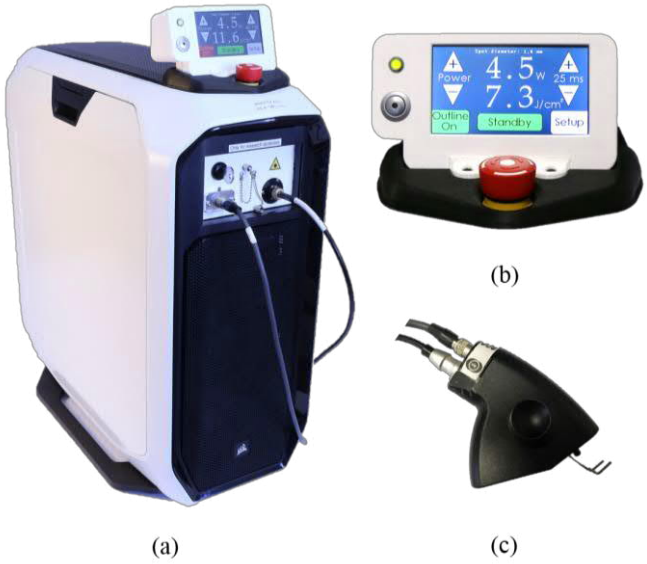

Fig. 5. Photo of the VECSEL module (a), the touch-screen on top with varied treatment parameters (b), and the MedArt handheld scanner (c).

power of their commercial system is 3–6 W at 577 nm, while for 590 nm it is much lower, typically below 1 W [30].

III. VECSEL-BASED YELLOW LASER SYSTEM

A. Laser Module Design and Processing

The semiconductor gain mirror used for the yellow laser system was grown by MBE and designed to emit infrared radiation in the 1180-nm range. The gain region incorporated 10 GaInAs QWs that were surrounded by GaAs barriers and GaAsP strain compensation layers. It was grown on top of a 25.5-pair AlAs/GaAs DBR, which acted as one of the laser cavity mirrors. The QWs were placed at the antinodes of the optical standing wave to enhance the gain, and the material has a resonant structure i.e. the standing wave profile has a node at the semiconductor-air-interface.

A small chip (2.5 mm x 2.5 mm) was diced from the gain structure and capillary bonded onto an intracavity diamond heat spreader of good optical quality. The synthetic single-crystal diamond heat spreader was used to extract the heat generated by the optical pumping in the gain mirror. To stabilize the temperature of the gain mirror, the diamond was further attached to a TEC-cooled copper plate set at room temperature. The top surface of the diamond was antireflection coated for the 1180-nm emission and the 808-nm pump laser.

The external cavity of the VECSEL was built into a V-shaped configuration defined by the gain mirror and two external dielectric mirrors. The external cavity allowed for an easy inclusion of intracavity components while still keeping the laser module compact. It also enabled to take advantage of the high intracavity power (typically 600–800 W) by inserting a nonlinear crystal for converting the infrared radiation to yellow via frequency doubling. For this purpose, a lithium triborate (LBO) crystal was placed near the mode waist of the cavity. In addition, a birefringent filter (BRF) was utilized to fix the wavelength and polarization for the LBO crystal.

The gain mirror was pumped with a commercial 808-nm diode laser. The pump light was delivered via an optical fiber from the pump laser module and focused on the gain mirror surface using lenses. Fig. 2 shows a schematic illustration of the VECSEL cavity including the pump laser.

TABLE II
TECHNICAL SPECIFICATIONS OF THE VECSEL-BASED YELLOW LASER SYSTEM

Technical Specifications	
Basic features	
Wavelength	585 ±5 nm
Power	up to 8.6 W in cw
Size	64 x 26 x 60 cm^3
Weight	approx. 30 kg
Treatment parameters	
Spot size	1.4 mm diameter
Pulse length	10–100 ms
Fluence	0–52 J/cm^2
Scan patterns	Line, square, hexagon
Scan area	From single spot up to 1 cm^2
Spot spacing	Low, medium and high density

B. Laser Module Characterization

The VECSEL cavity was assembled and sealed inside an airtight aluminum housing (with dimensions of 22 x 16 x 8 cm^3), shown in Fig. 3. All the cavity components were glued on a baseplate for a robust finish. The most critical cavity components, such as the LBO crystal, also had their own TEC-cooling. Dielectric mirrors were used to steer the yellow output beam through a collimation lens and towards a fiber port. The dielectric mirrors also act as wavelength filters to remove residual fundamental radiation from the output beam. In addition, a beam pick-off was placed in front of the fiber port to direct a small portion of the output beam into a photodiode for monitoring the output power. The collimated output beam was then coupled into a multimode fiber with a core diameter of 200 µm. The spectral features, listed in Table II, were characterized using a spectrum analyzer. The system output power as a function of the incident 808-nm pump power is shown in Fig. 4. The maximum continuous wave output power achieved was 8.6 W at 588 nm.

An important aspect of the device characterization is also lifetime. Throughout the testing of the system and preliminary clinical trials, we have accumulated more than 100 hours of operation time without any sign of degradation of the laser characteristics. What is also important is that similar gain

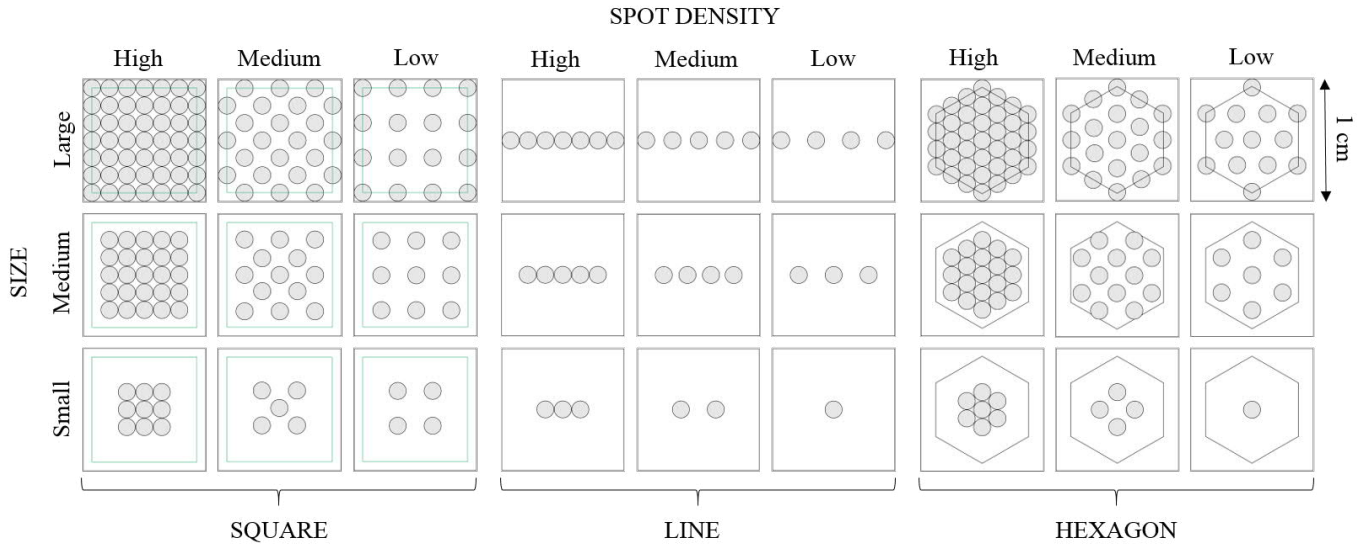

Fig. 6. Illustrations of the handheld scanners scan patterns (courtesy of MedArt A/S).

material has been tested in a lifetime measurement system involving multiple open-air cavities and exhibited more than 1000 continuous operation hours to date.

C. System Features

The VECSEL module was then integrated into a laser system designed for medical applications, shown in Fig 5a. The system includes the VECSEL module, the pump laser and custom-built electronics. The system is turned on with a main power switch in the back panel and a turn-key switch in the front panel. The key switch enables the system usage and activates a 30-second warm-up period, after which the laser is in "Standby"-state and can be ramped up to a wanted power level.

The treatment parameters are controlled using a touch-screen on top of the system, shown in Fig. 5b. The varied parameters are laser power and pulse length with typical ranges of 0–7 W and 10–100 ms, respectively. These parameters, along with the spot size of the output beam, determine the treatment fluence, which is automatically calculated and displayed on the touch-screen. The current system produces a spot size of 1.4 mm in diameter allowing us to reach treatment fluences up to 52 J/cm^2, which is sufficient for treating vascular lesions. The output beam exhibits good beam quality and is shown as an inset in Fig.4. However, it should be noted that compared to the pulsed dye laser, the 1.4-mm spot size is relatively small. In our system, this shortcoming is overcome by employing a handheld scanner, which directs the fiber-coupled light onto skin in a pre-defined pattern. Using such a scheme with a typical pulse duration of 25 ms (i.e. 25 ms dwell time on each treatment spot), an area of about 1 cm^2 can be covered in less than a second. In addition, the use of a scanner also brings flexibility enabling a diverse choice for treatment areas via programming.

The handheld scanner, shown in Fig 5c (from MedArt A/S, Denmark) [31], has three different settings that can be varied by pressing the buttons on the side of the scanner: scan pattern, scan area size and spot density. The available scan patterns include a single spot, line, square and hexagon profiles. Compared to the pulsed dye laser, which usually provides only circular beam spot profiles, these settings offer the user the freedom to select the most appropriate pattern for each situation. The scanner also includes a metallic distance piece attached to the front of the scanner to indicate the correct treatment distance of 27 mm. The scan patterns are listed in Table II and illustrated in Fig. 6.

The laser is turned on by pushing the grey button next to the touch-screen (see Fig. 5b), which then ramps up the laser to a chosen power value. At this point, no light is yet emitted, since the output of the laser is still blocked by a laser shutter. In this "Ready"-state, the user can still adjust all the main treatment variables. The treatment is started by pressing the foot pedal that is connected to the system; the foot pedal opens the laser shutter and initiates the operation of the laser scanner. Once the scanner has covered the predetermined treatment area, the shutter is automatically closed. Thus, the system output is not modulated in the transition periods when the scanner moves from one spot to another. This is possible since the transition time of the scanner from one spot to another is only 1 ms, which is considerably smaller than the dwell time on each spot. Consequently, the fluence introduced during the transition periods is negligible when compared to the treatment fluence.

Several safety measures have been implemented to the system in order to prevent any accidental light emission when the system is on. These features require that the handheld scanner and the output fiber be connected to the system before the shutter can be opened by the foot pedal. Moreover, the system also has to be at the target power level to enable light emission; if the output power is not within 0.1 W of the target,

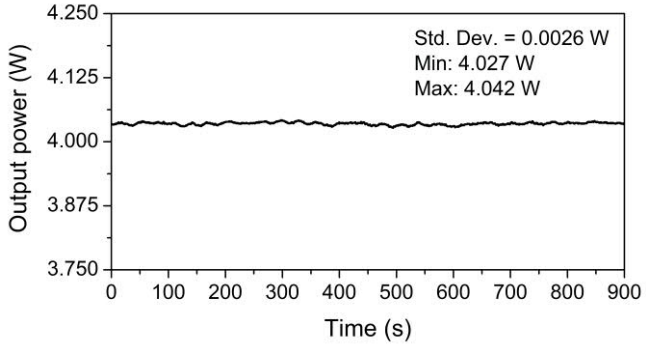

Fig. 7. Output power stability shown as a function of time. The yellow system was set to emit ~4 W of output power and a power meter was used to collect data for 15 minutes.

light is not emitted even if the foot pedal is pressed. The power stability was also tested by measuring the output power of the system through the handheld scanner for 15 minutes, which corresponds to a typical treatment time (Fig. 7). The system was set to emit ~4 W (typical treatment output power); the corresponding standard deviation of the output power was only 2.6 mW. Finally, the system is also equipped with an interlock that can be connected to a trigger signal which turns the laser off if unauthorized personnel enter the treatment area.

Altogether, the air-cooled system weighs about 30 kg and is portable. Since it has been being built in a computer housing that stands upright (see Fig. 5a), it can be set on a table without occupying any more space than a regular computer. The technical specifications of the system are listed in Table II.

IV. Clinical trials

The yellow laser system was qualified for a clinical trial to be used as an investigational device. The trial is a split-face study that compares the efficacy of the yellow system and a traditional green KTP laser in the treatment of dilated blood vessels (telangiectasia) on the cheeks. The trial protocol was approved by the local Ethical Committee (Tampere University Hospital, Reg. No. R17111) and was commenced in early 2018. Preliminary results show that there is not a statistically significant difference between the efficacies of the two lasers assessed by the physicians. Fig. 8 shows the before and after images of a patient's cheek. The left cheek was treated with the KTP laser and the right cheek with the yellow system. More than 75% clearance of telangiectasia was observed after two treatments for this patient.

Secondary object of the trial is also to qualitatively assess the usability of the yellow system. So far, the treating physicians have reported that the treatments are performed approximately five times faster with the yellow laser system than with the KTP laser (due to the fast scanning ability), but patients have experienced more pain with the yellow system, presumably linked to higher absorption and heat generation. The experienced pain limits the treatment fluence that can be used with the yellow laser and, hence, might affect the treatment outcome. However, this issue could be solved in the

Fig. 8. Before (left) and after (right) images of a patient taken with Visia Imaging System. The left cheek (top line) was treated with the traditional KTP laser and the right cheek (bottom line) with the VECSEL-based yellow system. Two treatments with both lasers were performed at approximately 1-2 month interval.

future by adding a cooling device to the system. Different cooling devices are already in use in similar dermatologic lasers. Another perspective is that given the existing power reserve, we could maintain the required fluence even with an increased spot size. Thus the treatment time could be further reduced by increasing the scanning area. The full scale results of the trial will be published in a medical journal once the study is completed and the statistical analysis has been performed.

V. Conclusions

In this paper, we have described a yellow lasers system designed and developed for the treatment of vascular lesions. The system employs an intracavity frequency-doubled VECSEL and produces up to 8.6 W of continuous wave light at around 590 nm delivered through a multimode-fiber. The illumination of the treatment area is done with a handheld scanner with selectable scan patterns. The scan area can be varied from a single spot (1.4-mm diameter) up to 49 spots covering an area of 1 cm^2. A touch-screen system interface allows for an easy control of the treatment parameters, such as pulse length, adjustable in the range of 10–100 ms, and fluence that can be tailored in the range of 0–52 J/cm^2.

Finally, the efficacy of the yellow system is evaluated in a split-face study against traditional green KTP laser to compare their efficacy in the treatment of facial telangiectasia. The trial is registered under ClinicalTrials.gov webpage with identifier number NCT03472859. Preliminary results of the clinical trials indicate that treatments can be performed approximately five time faster with the yellow system than with the KTP laser

and the available excess output power would enable even faster treatment times if the spot size is increased.

ACKNOWLEDGMENT

The authors thank dermatologist Dr. Ari Karppinen (Epilaser Oy) for valuable discussions on the system features and for helping to design and perform the clinical trial. The authors also want to thank Pascal Deleporte (INSERM ONCOTHAI, Lille, France) for his help in designing the system housing. E. Kantola acknowledges support given by Jenny and Antti Wihuri Foundation.

REFERENCES

[1] L. Goldman, R. G. Wilson, P. Hornby, and R. G. Meyer, "Radiation from a Q-switched ruby laser. Effect of repeated impacts of power output of 10 megawatts on a tattoo of a man," *J Invest Dermatol.*, vol. 44, pp. 69–71, 1965.

[2] L. Goldman, R. Dreffer, R .J. Rockwell, and E. Perry, "Treatment of portwine marks by an argon laser," *J Dermatol Surg.*, vol. 2, no. 5, pp. 385–388, 1976.

[3] R. R. Anderson and J. A. Parrish, "Selective photothermolysis: precise microsurgery by selective absorption of pulsed radiation," *Science*, vol. 220, no. 4596, pp. 524–527, 1983.

[4] Z. Husain and T. S. Alster, "The role of lasers and intense pulsed light technology in dermatology," *Clin Cosmet Investig Dermatol.*, vol. 9, pp. 29–40, Feb 2016.

[5] J. S. Waibel, "Pulsed dye laser," in *Laser treatment of vascular lesions*, vol 1, S. Bard and D.J. Goldberg, Ed. New York: S. Karger AG, 2014, pp. 48–73.

[6] H. Buiteveld, J. M. H. Hakvoort, and M. Donze, "The optical properties of pure water," in *SPIE Proceedings on Ocean Optics XII*, edited by J. S. Jaffe, vol. 2258, pp. 174–183, 1994.

[7] L. Kou, D. Labrie, and P. Chylek, "Refractive indices of water and ice in the 0.65–2.5 μm spectral range," *Appl. Opt.*, vol. 32, pp. 3531–3540, 1993.

[8] S. Jacques. Optical absorption of melanin [Online]. Available: https://omlc.org/spectra/melanin/index.html

[9] S. Prahl. (1999, Dec 15). Optical absorption of hemoglobin [Online]. Available: https://omlc.org/spectra/hemoglobin/index.html

[10] H. McCoppin and D. J. Goldberg, "Laser treatment of facial telangiectasia: an update," *Dermatol Surg*, vol. 36, pp. 1221–1230, 2010.

[11] J. S. Dover and K. A. Arndt, "New approaches to the treatment of vascular lesions," *Lasers Surg Med*, vol. 26, pp. 158–162, 2000.

[12] E. Kantola, T. Leinonen, J.-P. Penttinen, V.-M. Korpijärvi, and M. Guina, "615 nm GaInNAs VECSEL with output power above 10 W," *Opt. Express*, vol. 23, no. 16, pp. 20280-20287, 2015.

[13] S. W. Lanigan, "Laser Treatment of Vascular Lesions," in *Laser Dermatology*, D. Goldberg, Ed. Berlin: Springer, 2013, pp. 13–35.

[14] A. M. Chapas, K. Eickhorst, R.G. Geronemus, "Efficacy of early treatment of facial port wine stains in new-borns: a review of 49 cases," *Lasers Surg Med*, vol. 39, pp. 563–568, 2007.

[15] J. B. Green, K. Serowka, N. Saedi, and J. Kaufman, "Potassium-Titanyl-Phosohate (KTP) laser," in *Laser treatment of vascular lesions*, vol 1, S. Bard and D.J. Goldberg, Ed. New York: S. Karger AG, 2014, pp. 74–82.

[16] A. R. Styperek, "Argon, krypton, and copper lasers," in *Laser treatment of vascular lesions*, vol 1, S. Bard and D.J. Goldberg, Ed. New York: S. Karger AG, 2014, pp. 26–47.

[17] Asclepion Laser Technologies. QuadroStarPRO YELLOW [Online]. Available: https://www.asclepion.com/asclepion_product/quadrostar-pro-yellow/

[18] Quanta Systems. Discovery Aeasthetics: 585 [Online]. Available: http://www.quantasystem.com/en/aesthetics/585/

[19] Advalight. [Online]. Available: http://advalight.com/

[20] M. Kuzentsov. "VECSEL semiconductor lasers: a path to high-power, quality beam and UV to IR wavelength by design" in *Semiconductor disk lasers: physics and technology*. O. Okhotnikov, Ed. Weinheim: WILEY-VCH Verlag GmbH & Co. KGaA, 2010, pp. 1–58.

[21] J. Berger, D. Anthon, A. Caprara, J. Chilla, S. Govorkov, A. Lepert, W. Mefferd, Q.-Z. Shu, and L. Spinelli, "20 Watt CW TEM00 intracavity doubled optically pumped semiconductor laser at 532 nm," in *Proceedings of SPIE*, vol. 8242, pp. 824206, 2012.

[22] H. Kahle, R. Beck, M. Heldmaier, T. Schwazbäck, M. Jetter, and P. Michler, "High optical output power in the UVA range of a frequency-doubled, strain-compensated AlGaInP-VECSEL," *Appl. Phys. Express*, vol. 7, 2014.

[23] E. Kantola, T. Leinonen, S. Ranta, M. Tavast and M. Guina, "High-efficiency 20 W yellow VECSEL," *Opt. Express*, vol. 22, no. 6, pp. 6372–6380, 2014.

[24] C. Hessenius, P. Y. Guinet, M. Lukowski, J. Moloney, and M. Fallahi, "589-nm single-frequency VECSEL for sodium guidestar applications," in *Proceedings of SPIE*, vol. 8242, 2012.

[25] S. Ranta, M. Tavast, T. Leinonen, N. Van Lieu, G. Fetzer, and M. Guina, "1180 nm VECSEL with output power beyond 20 W," *Electron. Lett.*, vol 49., no. 1, pp. 59–60, Jan 2013.

[26] E. Kantola, T. Leinonen, J.-P. Penttinen, V.-M. Korpijärvi, and M. Guina, "615 nm GaInNAs VECSEL with output power above 10 W," *Opt. Express*, vol. 23, no. 16, Jul 2015.

[27] U. Keller, K. J. Weingarten, F. X. Kartner, D. Kopf, B. Braun, I. D. Jung, R. Fluck, C. Honninger, N. Matuschek, and J. Aus der Au, "Semiconductor staurable absorber mirrors (SESAM's) for femtosecond to nanosecond pulse generation in solid state lasers," *J. Sel. Top. Quantum Electron.*, vol 2, no. 3, 1996.

[28] B. W. Tilma, M. Mangold, C. A. Zaugg, S. M. Link, D. Waldburger, A. Klenner, A. S. Mayer, E. Gini, M. Golling, and U. Keller "Recent advances in ultrafast semiconductor disk lasers," *Light: Science & Applications*, vol. 4, e310, Jul 2015.

[29] M. Guina, A. Rantamäki, and A. Härkönen, "Optically pumped VECSELs: review of technology and progress," *J. Phys. D: Appl. Phys.*, vol. 50, 2017.

[30] Coherent. Continuous wave (cw) solid-state lasers [Online]. Available: https://www.coherent.com/lasers/main/cw-solid-state-lasers

[31] MedArt [Online]. Available: https://medart.dk

Emmi Kantola was born in Rovaniemi, Finland. She received her MPhys (Hons) degree in physics with astrophysics from the University of Kent, Canterbury, England, in 2011. She joined the Optoelectronics Research Centre, Tampere University of Technology, Tampere, Finland, in 2012 for doctoral studies, and since then she has been working with high-power vertical-external-cavity surface-emitting lasers. Her research interests include high-power VECSELs and their application to medicine and quantum optics.

Antti Rantamäki joined the Optoelectronics Research Centre, Tampere University of Technology, Tampere, Finland, in 2008. He received his M.Sc. and D.Sc. degrees from the Tampere University of Technology in 2010 and 2015, respectively. His research concerned optically pumped vertical-external-cavity surface-emitting lasers. He is currently working at Corelase Oy, Tampere, Finland.

Iiro Leino, born in 1984, is originally from Iitti, Finland. He studied in Tampere University of Technology (TUT) and in 2010 he received his B.Sc. in communication electronics, majoring in electronics. In 2012, he got his M.Sc. from signal processing and communications engineering, majoring in embedded systems.

From 2011 to 2012, he was a research assistant in Electronics Department at Printed Electronics Research Group studying laser sintering. From 2012 to 2016, he was a project researcher in Optoelectronics Research Centre (ORC). Starting from 2017, he has been working as a product development engineer in Brighterwave Oy, Tampere, Finland. His main task and interest now is creating augmented reality devices.

Jussi-Pekka Penttinen was born in Valkeakoski, Finland in 1989. He received his B.Sc and M.Sc. (Tech) degrees in advanced engineering physics (photonics) from the Tampere University of Technology, Tampere, Finland, in 2012 and in 2015.

From 2010 to 2015, he was as a Research Assistant with Optoelectronics Research Centre. Since 2015, he has been a Project Researcher with ORC, and since September 2017, he has also acted as a Co-Founder and CEO of Vexlum Ltd, a VECSEL-laser company located in Korkeakoulunkatu 3, 33720 Tampere, Finland. His current research interests focus on the development of high-power VECSELs with wavelengths on demand for applications in medical and quantum technology.

Toni Karppinen was born in Kauhava, Finland in 1984. He received his M.D. degree from the University of Tampere in 2012, PhD in photodermatology in 2017 and specialist degree in Dermatology and Allergology in 2018.

Since 2012, he has been involved in studies about the effects of ultraviolet radiation (vitamin D, mood, addiction, circadian rhythm) and photodynamic therapy (effectiveness, cost-effectiveness). Today he runs a national register study investigating the skin cancer risk related to narrow-band ultraviolet B phototherapy. He has almost 10-year experience in dermatological laser treatments in Epilaser Oy and he joined the yellow laser project in 2015 to plan the clinical trial. Also his future research interests include dermatological lasers.

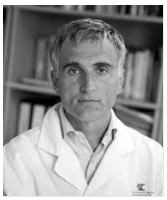

Prof. Serge R. Mordon, PhD, works in Lille, France for the French National Institute of Health and Medical Research (INSERM). He is the director of INSERM ONCOTHAI (Image Assisted Laser Therapies Assisted for Oncology) and the director of the Photomedicine Center (Lille University Hospital).

Since 1981, he has been involved in the medical applications of lasers, particularly in Dermatology and Plastic Surgery. More recently, he has focused his research on Focal Laser Ablation and Photodynamic Therapy. He is an internationally recognized expert in laser-tissues interaction and laser applications in medicine. He has authored over 600 articles and book chapters.

Prof. Mordon is the author of sixteen issued patents. Since 2012, he holds a Master Degree in Strategy and Organization Management (University of Paris). He is the President of The French Medical Laser Society and Board Member of several professional societies. He is an associate editor of the editorial board for the journal, Lasers in Surgery and Medicine. In 2015, he has been nominated Finland Distinguished Professor. In 2018, he has been nominated Fellow Member of the European Alliance of Medical and Biological Engineering and Science (EAMBES).

Prof. Mircea Guina obtained his MSc degree in optoelectronics at the "Politehnica" University of Bucharest in 1997, and his PhD degree in physics from the Tampere University of Technology (TUT) in 2002. In 2008 he was appointed professor at TUT where he is currently the head of the Optoelectronics Research Centre. He conducts scientific work related to molecular beam epitaxy and the development of novel optoelectronic devices for a wide range of applications. His current projects are concerned with the development of uncooled lasers for hybrid integration on Si-photonics platform, the development of high power lasers for medicine and quantum technology, development of light sources for LIDAR and integrated sensors, as well as the development of ultra-high efficiency multijunction solar cells. He has published more than 180 journal papers, several book chapters, and holds 4 international patents.

Prof. Guina is a Topical editor for Optics Letters and the Journal of the European Optical Society. He has an outstanding track record in leading large scale research projects extending from basic science to technology transfer. Recently, he was awarded an ERC Advanced Grant for the development of solar cells with efficiency of more than 50%. He is also a strong advocate of bridging research and entrepreneurial activities and is a co-founder in three start-ups related to laser technologies. Website of Prof. Guina's group: www.tut.fi/orc

Publication 5

T. Karppinen, E. Kantola, A. Karppinen, A. Rantamäki, H. Kautiainen, S. Mordon, and M. Guina, “Treatment of telangiectasia on the cheeks with a compact yellow (585 nm) semiconductor laser and a green (532 nm) KTP laser: a randomized double-blinded split-face trial,” submitted to *Lasers in Medicine and Surgery* on 12.9.2018.

P5

Treatment of telangiectasia on the cheeks with a compact yellow (585 nm) semiconductor laser and a green (532 nm) KTP laser: a randomized double-blinded split-face trial

MD Toni Karppinen [123*], MPhys (Hons) Emmi Kantola[4], MD Ari Karppinen[3], D. Sc. (Tech) Antti Rantamäki[4], Hannu Kautiainen [5], Prof. Serge Mordon[6] and Prof. Mircea Guina[4]

1. *Medical School, University of Tampere, Tampere, Finland*
2. *Department of Dermatology, Tampere University Hospital, Tampere, Finland*
3. *Epilaser Oy, Lempäälä, Finland*
4. *Optoelectronics Research Centre, Tampere University of Technology (TUT), Korkeakoulunkatu 3, 33720 Tampere, Finland*
5. *Unit of Primary Health Care, Helsinki University Central Hospital, and Department of General Practice, University of Helsinki, and Unit of Primary Health Care, Kuopio University Hospital, Helsinki and Kuopio, Finland*
6. *The French National Institute of Health and Medical Research (INSERM), INSERM U1189 – ONCO-THAI, avenue Oscar Lambert 1, 59037 Lille Cedex, France*

Funding acknowledgements: The trial was performed in Epilaser Oy facilities. The development of the new yellow laser was done by the Optoelectronics Research Centre in cooperation with INSERM and funded by the Finnish Funding Agency for Innovation (FiDiPro project Photolase #40152/14 with support funding provided by Modulight Oy, Nanofoot Oy, and Brighterwave Oy).

Conflict of Interest Disclosures: All authors have completed and submitted the ICMJE Form for Disclosure of Potential Conflicts of Interest. A.K. is the CEO of Epilaser Oy, which received compensation for device expenses during the trial. No other conflicts of interest were reported.

[*]Contact author details: toni.karppinen@icloud.com, Suvantokatu 1 E 24, 33100 Tampere, +358-400-214026

ABSTRACT

Objectives: The primary objective of this study was to compare a traditional green KTP laser to a new investigational yellow laser (PhotoLase) in the treatment of facial telangiectasia in terms of the treatment outcomes. The secondary objective was to assess the functionality and reliability of the PhotoLase system from the perspective of the user.

Study Design/Methods: The study was a randomized split-face double-blinded study that compared the treatment efficacy of the 532-nm KTP laser and the investigational 585-nm PhotoLase laser. One or two treatments were given based on the response of the first treatment. The improvement of telangiectasia was graded according to a 7-point Telangiectasia Grading Scale (TGS) by the subjects and blinded physicians. The subjects assessed the amount of pain during the treatments using Visual Analogue Scale (VAS), and evaluated adverse effects 2–3 days after the treatment(s) using a self-assessment form.

Results: At least 50% improvement was seen in 15/18 subjects after the first PhotoLase treatment, and a similar result was observed for KTP, as assessed by the blinded physicians ($p=0.29$). In the subjects' assessment, 7/18 subjects had at least 50% improvement after the first PhotoLase treatment, whereas at least 50% improvement was observed for 10/18 subjects in the KTP side, the difference being significant ($p=0.008$). The amount of pain was higher with PhotoLase compared to KTP (67.7 vs. 34.6, $p<0.001$). There was no difference in the frequency of erythema, crusting or purpura between the devices, but more blistering and less edema were seen after PhotoLase treatment ($p<0.05$). Treatment with PhotoLase was evaluated to be 4.7-fold faster than with KTP and the PhotoLase system was more compact, narrower, lighter and easier to carry than KTP.

Conclusions: The investigational PhotoLase laser enables significantly faster treatments, but the process is somewhat more painful than with KTP, otherwise providing a similar clinical outcome in the treatment of facial telangiectasia.

Keywords: Telangiectasia; KTP laser; green laser; yellow laser; semiconductor disk laser technology; comparative study

INTRODUCTION

Millions of people worldwide are affected by facial telangiectases, small dilated blood vessels with diameters between 0.1 to 1.0 mm. Predisposing conditions include rosacea, photodamage, topical steroid use and genetic factors. Discomfort and psychological distress drive patients to seek help, and telangiectasia treatments are among the most common dermatological laser procedures.[1,2] Treatment of superficial vascular lesions is based on selective photothermolysis, where the target chromophore is the intravascular oxyhaemoglobin in red blood cells. Absorption of laser light heats the chromophore leading to vessel wall damage. Several lasers are used for vascular indications, but the standard lasers are yellow pulsed dye laser (585- or 595-nm) and green potassium-titanyl-phosphate (KTP) laser (532-nm), because their wavelengths are close to the α and β absorption peaks (542 and 577 nm) of oxyhaemoglobin.[3]

The original PDL (577-nm) had a short pulse duration of 0.3 ms, causing frequently post-operative purpura. Modern PDLs, such as Cynergy™ (Cynosure) and VBeam® (Syneron Candela) operate at wavelengths of 585 and 595 nm, respectively, and have micropulse mode and adjustable pulse durations up to 40 ms for less purpura.[2] Spot sizes in Cynergy™ and VBeam® range from 3 to 12 mm. Currently available KTP devices have adjustable pulse durations from 0.05 to 2000 ms and spot sizes from 0.2 to 12 mm. One KTP system, Aura XP (Laserscope), can be equipped with a SmartScan scanner (Laserscope).

The safety and efficacy of PDL and KTP have been demonstrated in numerous studies, and both are suggested as first line treatments for facial telangiectases by the European Society for Laser Dermatology. At least 50–90% improvement can be expected after 1–3 treatments.[3] For facial capillary malformations, PDL is still the gold standard therapy[4], but modern large spot size KTPs seem also effective and can be considered first line regimen.[5,6]

The advantage of the yellow PDL compared to the green KTP is the longer emission wavelength, enabling deeper penetration and treatment of larger vessels. In addition, oxyhaemoglobin has higher absorption for yellow than for green wavelengths. Yellow wavelengths also have lower melanin absorption, allowing treatment of darker skin phototypes with lower risk of epidermal damage.[2]

However, the yellow PDL has some intrinsic disadvantages such as large size and high annual maintenance costs. To address the needs of the dermatologic community a novel laser technology, namely optically pumped semiconductor disk laser (SDL), has emerged to provide a compact and cost-effective alternative for a yellow laser source. SDLs, also known as VECSELs (vertical external-cavity surface-emitting lasers), are recognized for their power scaling abilities, transverse mode control and the ability to tailor the emission wavelength according to specific application needs.[7,8] With the addition of wavelength selective components and suitable laser cavity configurations, SDLs can also be designed to emit narrow linewidth[9] and have a wavelength tuning range up to tens of nanometers.[10] Light pulses down to a few hundred nanometers can be easily achieved by directly modulating the pump laser of an SDL.[11] Another pulsing method, possibly more attractive for medical applications, is to use a continuous wave SDL as a source and guide it through a handheld scanning device capable

of producing different pulse lengths and treatment patterns by moving the laser beam to a different spot. In this case the pulse duration is limited by the mechanical capability rather than by the intrinsic modulation features of the semiconductor, which are much faster.

The primary objective of this pilot study was to compare the efficacy of a yellow laser system based on SDL technology to the traditional green KTP laser in the treatment of facial telangiectasia. This included comparing the treatment outcome and the adverse effects caused by the treatment. The secondary objective was to assess the functionality of the new yellow laser from the point of view of the treating investigators.

MATERIALS AND METHODS

Study Design

The study was a split-face comparative double-blinded study without a separate control group. It was designed to enable a comparison between a traditional green laser and an investigational yellow laser. The split-face design eliminated individual biases and the randomization eliminated possible small variations in the symmetry of the telangiectases on the face. The double-blinded assessment eliminated subjective and objective biases of the investigators and the subjects. The protocol was approved by the Ethics Committee of Tampere University Hospital (Reg. No. R17111). The protocol followed the principles of the Declaration of Helsinki and its amendments.

Devices

The study employed two different laser systems: the traditional green KTP laser (Aura XP, Laserscope) and the investigational yellow laser called PhotoLase. The KTP laser emits 532-nm radiation up to 15 W, and was equipped with a Laserscope SmartScan scanner, which delivered 127 spots with a diameter of 1.0 mm, forming a hexagon pattern and covering an area of ~1.1 cm^2 in 17.5 seconds.

The PhotoLase laser (Fig. 1a) was developed at the Optoelectronics Research Centre (ORC), Tampere University of Technology in collaboration with the French National Institute of Health and Medical Research (INSERM). It emits 585-nm yellow radiation up to 8 W in continuous wave operation, delivered via a multimode optical fiber with a diameter of 200 µm. The device was equipped with a MedArt scanner (Fig. 1b) capable of delivering the laser light in different patterns (single spot, line, square, and hexagon). One scan covered an area of ~1.0 cm^2 in less than a second and included 37 spots with a diameter of 1.4 mm. The pulse duration was adjustable in the range 10–100 ms. Only the hexagon shape (Fig. 1c) was used to enable a more accurate comparison of the two laser systems. The pulse duration was fixed to 25 ms based on pre-clinical tests indicating good clinical end-point. A detailed description of the system can be found in Kantola et al. 2019 (in press).

The study also employed a Canfield Visia Imaging System to assess the effectiveness of the laser treatments. The imaging system produces high quality multi-spectral images with standardized lighting and facial positioning.

Subject inclusion and exclusion criteria

Finnish speaking volunteering adults with symmetrical facial telangiectasia, and a Fitzpatrick's skin phototype I–IV, were included in the study. Exclusion criteria were unbalanced chronic disease, pregnancy, lactation, haemophilic condition, being under guardianship, alcohol or drug abuse and significant tanning less than 6 weeks prior to the study. All volunteers gave their informed consent.

Treatment Protocol

The subjects were randomized to receive KTP treatment on one side of the face and PhotoLase on the contralateral side. The randomization was performed in blocks of two using a web-based validated program (Research Randomizer). The investigators T.K. and A.K. randomized and enrolled all the participants. One to two treatments were performed at 1- to 2-month intervals depending on the recommendation of the investigators and preferences of the subjects. Prior to the first treatment, the investigators assessed each subject and categorized the severity of their telangiectasia into mild, moderate or severe (Fig. 2).

Treatment parameters were selected to achieve the same clinical end-point of vessel disappearance or clot formation within the vessel. Double passes were used when needed. KTP settings were 20–30 J/cm^2 at 10-ms pulse duration and the PhotoLase settings were 5.6–8.1 J/cm^2 at 25-ms pulse duration. No topical anesthesia or cooling was used.

Efficacy Assessments

The primary endpoint of this study was the 7-point Telangiectasia Grading Scale[13], which was assessed by the subjects and the blinded investigators (T.K. and A.K.). The TGS is scored: -1 = condition worsened; 0 = no change; 1 = some improvement (<25%); 2 = intermediate improvement (25–50%), 3 = significant improvement (50–75%); 4 = very significant improvement (>75%); 5 = complete resolution of telangiectasia. The investigators assessed the TGS using the Visia images taken prior and 1–2 months after the treatment(s). The assessment was

performed as a consensus assessment by the investigators T.K. and A.K. Even though T.K. and A.K. also performed the treatments, the efficacy assessments can be regarded blinded, since the Visia images did not show information about which device was used in either side of the face. In addition, the subjects gave their own best assessment of the clinical outcome using a mirror.

Safety Assessments

Assessment of adverse effects was conducted 48–72 hours after the treatment(s) through a self-assessment form given to the subjects. Visual Analogue Scale (VAS, 0–100) was used for pain and a 4-point scale (0=absent, 1=mild, 2=moderate, 3=severe) for erythema, edema, crusting, purpura and blisters.

Sample Size Calculation

The sample size calculation assumes, that a clinically important difference, as measured by a 7-point Telangiectasia Grading Scale (-1–5), is 2. With an alpha error of 0.05, power of 0.80 and a sigma value of 2, we arrived at a sample size of 16 with a sample size calculator comparing two independent samples[13]. Assuming that there will be a few dropouts during the study, a sample size of 20–30 subjects is warranted.

Statistical Analysis

Statistical comparisons between the KTP and PhotoLase treatments were made using the McNemar test, Wilcoxon signed ranks test and permutation test with exact p-values. Stata 15.1 (StataCorp LP; College Station, Texas, USA) statistical package was used for the analysis.

RESULTS

General

Twenty-four subjects participated and completed the study. Six subjects were excluded from the analysis, since their telangiectases were not assessable using the Visia images. The mean age of the subjects was 48 years (range 27–63 years), sixteen (89%) females and two (11%) males. Nine subjects received KTP on the left cheek and PhotoLase on the right cheek, and nine subjects vice versa. Five subjects (28%) received a single treatment and thirteen subjects (72%) received two treatments. The Fitzpatrick's skin phototypes were I, II or III in 6/8/4 subjects, respectively. The baseline telangiectasia grades were I, II, or III in 4/9/5 subjects, respectively, and the grades were symmetrical in all of the subjects.

Safety

The amount of pain, as measured using VAS, was higher with PhotoLase when compared to KTP, 67.7 (SD 22.9) vs. 34.6 (SD 16.9), respectively. There was no difference in the frequency of erythema, crusting or purpura between KTP and PhotoLase, as assessed using a 0–3 scale, 2–3 days after the treatments. More blistering and less edema were seen after PhotoLase treatment ($p < 0.05$, Table 1). A small superficial atrophic scar was noted in two subjects on the PhotoLase side.

Efficacy

In the blinded investigators' assessment, fifteen subjects (83%) had a TGS value of 3 or larger, indicating at least 50% improvement after the first PhotoLase treatment, and a similar result was observed for KTP (p=0.29). In the subjects' assessment, seven subjects (39%) had at least 50% improvement after the first PhotoLase treatment, whereas at least 50% improvement was observed for ten subjects (56%) in the KTP side, the difference being significant (p=0.008).

The potential benefit of the optional second treatment was also assessed by the subjects and the blinded investigators. Based on the subjects' assessment, 11/13 benefited from the second KTP treatment, and 10/13 from the second PhotoLase treatment. The difference between the devices was insignificant (p=0.54). Based on the blinded investigators' consensus assessment, 9/13 subjects benefited from the second KTP treatment, and 8/13 from the second PhotoLase treatment. The difference between the devices was insignificant (p=0.81).

Figs. 3 and 4 show the before and after Visia images of a female subject with moderate telangiectasia. Photographs were taken before and after the treatments. The left side was treated with KTP and the right side with PhotoLase. In this case, the improvement in TGS was 4 on the KTP side and 3 on the Photolase side after the first treatment and 4 on both sides after the second treatment.

Functionality of the investigational device

The secondary objective of the study was to assess the functionality of the investigational device. The evaluation was performed by the investigators (T.K. and A.K.) based on their user-experience during the study. The most obvious difference in functionality was observed in the scanning speeds of the scanners, 17.5 seconds per 1.1 cm^2 for the SmartScan scanner (KTP) and less than one second per 1.0 cm^2 for the MedArt scanner

(PhotoLase). Assuming a mean of three seconds between the scans, this yields a 4.7-fold difference in treatment speed favouring PhotoLase. The SmartScan scanner was also larger, bulkier and heavier. The button that was pressed to initiate the scanning was integrated to the SmartScan scanner, but the MedArt scanner was used with a foot pedal. The investigators favored the hand-button for easier administration of the pulses. The investigational device PhotoLase appeared to be more compact, narrower, lighter and easier to carry compared to the KTP laser. Both laser systems were stable during the trial period and no malfunctions were noted.

DISCUSSION

To our knowledge, this is the first head-to-head study to compare a 585-nm yellow SDL to a traditional 532-nm green KTP laser in the treatment of facial telangiectasia. We were able to recruit the desired number of subjects with full compliance throughout the study period, and both laser systems were shown similarly effective.

Recently Kapicioglu et al. (2018) reported a non-controlled case series using a 577-nm yellow SDL for the treatment of erythematotelangiectatic rosacea, facial erythema and facial telangiectasia. They achieved over 80% cure rate for facial erythema and telangiectasia in 76.6% of subjects after first treatment, whereas we achieved over 50% cure rate in 83.3% of cheeks treated with PhotoLase or KTP. Our parameters for KTP were 20–30 J/cm^2 at 10-ms pulse duration and for PhotoLase 5.6–8.1 J/cm^2 at 25-ms pulse duration. In comparison, Kapiciogly et al. used 16–22 J/cm^2 fluences with the 577-nm laser. There are probably two main reasons for the cure rate difference. Firstly, our trial was conducted in private sector, where typically milder presentations of telangiectasia are treated, compared to hospital conditions. Only 28% of our subjects had severe telangiectasia. Secondly, we chose not to use topical anesthesia or cooling to prevent possible vasoconstriction in the treatment area, which resulted in limitation to use higher PhotoLase fluences due to pain.

Another split-face study by Uebelhoer et al. (2007) compared KTP (Gemini, Laserscope) and 595-nm PDL (VBeam®) for facial telangiectases. The PDL settings were a 10-mm spot, a fluence of 7.5 J/cm^2, a 10-ms pulse duration, optional pulse stacking, and dynamic nitrogen cooling spray. The KTP settings were mostly 10 J/cm^2 at 18 ms and 9 J/cm^2 at 23 ms with 5- and 10-mm spot sizes, respectively, and a sapphire contact cooling. The percentage of improvement was 62% with KTP, and 49% with PDL after the first treatment, being slightly lower than cure rates in our study. Tanghetti et al. (2012) used a 595-nm PDL (V-Star®, Cynosure) for facial telangiectases with Zimmer air cooling and could use fluences as high as 8.1–14.5 J/cm^2 with 10- and 40-ms pulse durations. In their study, about 80% of subjects reached a 50% or higher cure rate with 1–2 treatments, a result that we reported after the first treatment with PhotoLase.

Like the yellow SDLs, modern large spot size KTPs can challenge the gold standard role of PDLs, as shown by Uebelhoer et al. More recently, Kwiek et al. (2017, 2018) showed the efficacy of large spot size KTP (ExcelV®, Cutera) in patients with facial capillary malformations. The settings were a 5- to 10-mm spot size, a fluence of 8–11.5 J/cm^2 and pulse duration 4 to 9 ms. An integrated sapphire glass contact cooling was used. The median improvement was 70.4% after a mean of 7.1 treatments in previously non-treated patients[5], and 59.1% after a mean of 6.2 treatments in previously treated patients[6].

No serious side effects were reported during the present study. More blistering, but less edema was observed for the PhotoLase system compared to KTP. A small superficial atrophic scar resulting from a blister was noted in the PhotoLase side in two subjects, which is an unwanted adverse effect that we want to eliminate in the future. Instead of a fixed pulse duration, we will tailor the pulse duration for the vessel caliber in the future. In addition, epidermal cooling will be included to prevent epidermal damage and to optimize treatment parameters. We are planning to use either an updated scanner with an integrated contact cooling, or air cooling in our future trials.

The 4.7-fold faster treatment time using the MedArt scanner can be considered a major benefit compared to SmartScan scanner. The power reserve of PhotoLase also makes it possible to increase the scanning area of one illumination sequence while still applying sufficient fluence on the treatment area. This would further reduce the time of treatment, especially for larger treatment areas. We acknowledge that the present study would be stronger, if the PhotoLase system was compared to a modern PDL or large spot size KTP. The functionality and speed of modern devices are on a different level than that of Aura XP with SmartScan. Newer KTP devices with large spot size can also treat telangiectases with lower fluencies due to deeper penetration and even distribution of energy, reducing the cooling effect of blood flow.[6] On the other hand, we still consider it fair to compare the clinical outcome of the present devices, since the scanning patterns were similar and the spots sizes were close to each other in terms of diameter.

The strengths of the present study are the randomized split-face design, high-quality Visia images and excellent subject compliance. Some discrepancy can be seen in the subjects' TGS assessment compared to blinded investigators' consensus assessment. We believe that such a difference resulted from the insensitivity of the TGS assessment tool, which has relatively large 25% grading steps. Subjects might easily give different curing scores, if they notice even a slight difference in the erythema between face sides. Experienced clinicians, then again, will not let too small differences distract the overall assessment. Also, the subjects' assessment was based on their

memory, whereas the blinded investigators had high-quality standard and erythema-weighted images to compare the results very systematically.

CONCLUSION

To conclude, we demonstrated non-inferiority of the novel yellow semiconductor disk laser, PhotoLase, in the treatment of facial telangiectasia compared to the traditional green KTP laser. A major benefit of the PhotoLase is the significant decrease of treatment time, which could be further decreased by enlarging the scanning area for single illumination. The PhotoLase system can also be considered more user-friendly in the present setting. However, larger studies with optimized cooling, laser parameter tailoring, and comparison to modern PDL or KTP devices are warranted in the future.

ACKNOWLEDGMENTS

The authors would like to thank M. Sc. (Tech) Iiro Leino (TUT) and Pascal Deleporte (INSERM) for their contributions in the design and assembly of the investigational device PhotoLase. This work was financially supported by the Finnish Funding Agency for Innovation (TEKES) as part of FidiPro project Photolase (#40152/14). E. Kantola would also like to acknowledge Antti and Jenny Wihuri Foundation for their support.

TABLES AND FIGURES

Table 1. The frequency of treatment reactions of the first treatment with KTP and PhotoLase. The intensity of the reactions was scaled: 0=absent, 1=mild, 2=moderate, 3=severe.

Adverse effect	**Treatment reactions 2-3 days after KTP treatment (%)**	**Treatment reactions 2-3 days after PhotoLase treatment (%)**	**P-value**
Erythema			0.87
0	1 (6)	2 (11)	
1	7 (39)	7 (39)	
2	8 (44)	6 (33)	
3	2 (11)	3 (17)	
Crusting			0.55
0	11 (61)	9 (50)	
1	4 (22)	5 (28)	
2	3 (17)	3 (17)	
3	0 (0)	1 (6)	
Edema			0.007
0	2 (11)	3 (17)	
1	1 (6)	7 (39)	
2	5 (28)	6 (33)	
3	10 (56)	2 (11)	
Purpura			0.12
0	11 (61)	14 (78)	
1	3 (17)	3 (17)	
2	1 (6)	1 (6)	
3	1 (6)	0 (0)	
Blistering			0.023
0	15 (83)	10 (56)	
1	3 (17)	3 (17)	
2	0 (0)	3 (17)	
3	0 (0)	2 (11)	

P-values calculated with Wilcoxon signed ranks test.

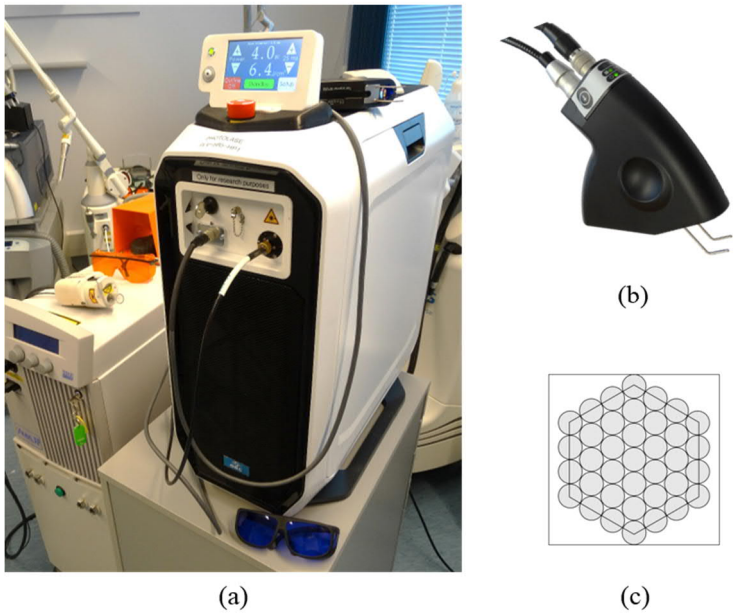

Figure 1. (a) Photo of the investigational yellow laser system, namely PhotoLase. The green KTP laser is also visible in the background. (b) Photo of the handheld scanner used to deliver the yellow laser light from PhotoLase unit (developed by MertArt A/S, Denmark) and (c) an illustration of the hexagon pattern produced by the MedArt scanner (courtesy of MedArt). Other patterns and sizes are also available, but this study only utilized the hexagon to enable comparison with the KTP SmartScan.

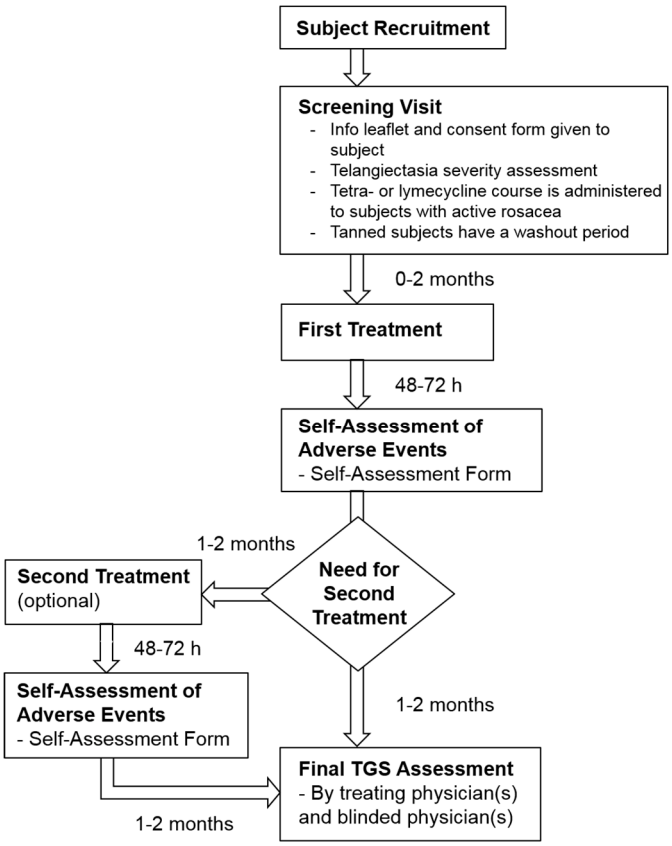

Figure 2. Flowchart of the study.

Figure 3. Regular Visia images of a female subject with moderate baseline telangiectasia. Photographs were taken before and after the first and second treatments. The left side was treated with KTP laser and the right side with PhotoLase laser. In this case, the improvement in TGS was 4 on the KTP side and 3 on the PhotoLase side after the first treatment and 4 on both sides after the second treatment.

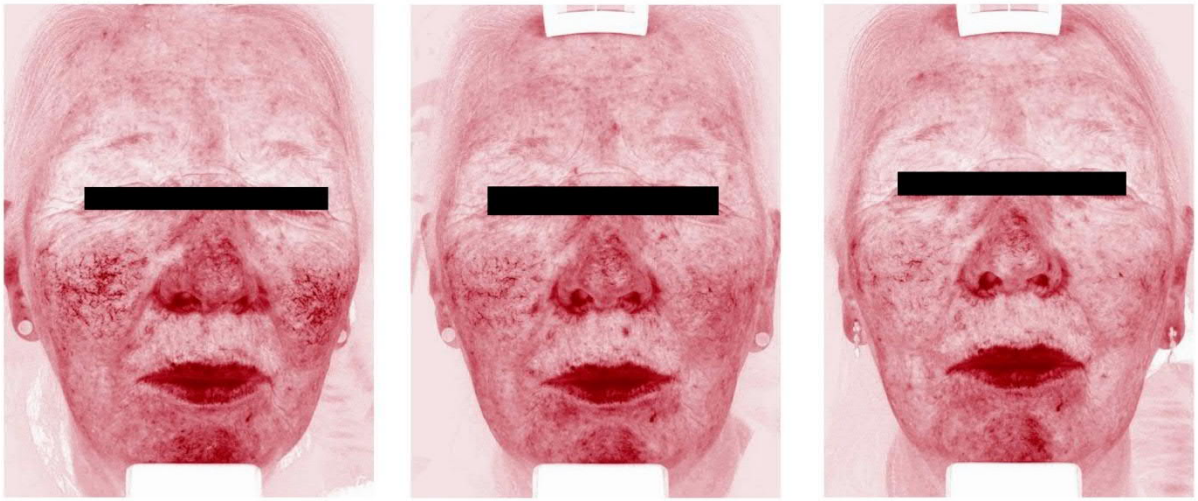

Figure 4. Visia erythema images before and after the first and second treatments. Note the added benefit of the second treatment on both sides of the face.

REFERENCES

1. Gupta G and Bilsland D. A prospective study of the impact of laser treatment on vascular lesions. *Br J Dermatol*. 2001;143:356-359.

2. McCoppin HHH and Goldberg DJ. Laser treatment of facial telangiectases: an update. *Dermatol Surg*. 2010;36:1221-1230.

3. Adamic M, Pavlovic MD, Troilius Rubin A, Palmetun-Ekbäck M, Boixeda P. Guidelines of care for vascular lasers and intense pulsed light sources from the European Society for Laser Dermatology. *J Eur Acad Derm Venereol*. 2015;29:1661-1678.

4. Lee WJ and Chung HY. Capillary Malformations (Portwine Stains) of the Head and Neck. *Otolaryngol Clin N Am*. 2018;51:197-211.

5. Kwiek B, Rozalski M, Kowalewski C, Ambroziak M. Retrospective Single Center Study of the Efficacy of Large Spot 532nm Laser for the Treatment of Facial Capillary Malformations in 44 Patients With the Use of Three-Dimensional Image Analysis. *Lasers Surg Med.* 2017;49:743-749.

6. Kwiek B, Ambroziak M, Osipowicz K, Kowalewski C, Rozalski M. Treatment of Previously Treated Facial Capillary Malformations: Results of Single-Center Retrospective Objective 3-Dimensional Analysis of the Efficacy of Large Spot 532 nm Lasers. *Dermatol Surg.* 2018;44:803-813.

7. Kuznetsov M. VECSEL semiconductor lasers: a path to high-power, quality beam and UV to IR wavelength by design. In: Okhotnikov O, ed. *Semiconductor disk lasers: physics and technology.* Weinheim, Gemany: WILEY-VCH Verlag GmbH & Co. KGaA, 2010.

8. Guina M, Rantamäki A, Härkönen A. Optically pumped VECSELs: review of technology and progress. *J Appl Phys.* 2017;50:383001.

9. Zhang F, Heinen B, Wichmann M, et al. A 23 W single-frequency vertical-external-cavity surface-emitting laser. *Opt Express.* 2014;22:12817-12822.

10. Borgentum C, Bengtsson J, Larsson A, Demaria F, Hein A, Unger P. Optimization of a broadband gain element for a widely tunable high-power semiconductor disk laser. *IEEE Photonic Tech L.* 2010;22:78-980.

11. Kantola E, Leinonen T, Ranta S, Tavast M, Guina M. High-efficiency 20 W yellow VECSEL. *Opt Express.* 2014;22:6372-6380.

12. Kantola E, Rantamäki A, Leino I, et al. VECSEL-based 590-nm laser system with 8 W of output power for the treatment of vascular lesions. In Press. *J Sel Top Quantum Electron.* 2019;25.

13. Tanghetti EA. Split-Face Randomized Treatment of Facial Telangiectasia Comparing Pulsed Dye Laser and an Intense Pulsed Light Handpiece. *Lasers Surg Med.* 2012;44:97-102.

14. Kapicioglu Y, Sarac G, Cenk H. Treatment of erythematotelangiectatic rosacea, facial erythema, and facial telangiectasia with a 755-nm pro-yellow laser: a case series. *Lasers Med Sci.* ePub ahead of print 10 Aug 2018. Doi:10.1007/s10103-018-2606-6.

15. Uebelhoer N, Bogle M, Stewart B, Arndt K, Dover J. A split-face comparison study of pulsed 532-nm KTP laser and 595-nm pulsed dye laser in the treatment of facial telangiectasias and diffuse telangiectatic facial erythema. *Dermatol Surg.* 2007;33:441-8.

Tampereen teknillinen yliopisto
PL 527
33101 Tampere

Tampere University of Technology
P.O.B. 527
FI-33101 Tampere, Finland

ISBN 978-952-15-4270-1
ISSN 1459-2045